LATE OLIGOCENE TO EARLY MIOCENE NORTH-SOUTH EXTENSION IN THE WESTERN GREAT BASIN

by

Scott Robertson Kerstetter

APPROVED BY SUPERVISORY COMMITTEE:

John S. Oldow, Chair

Thomas H. Brikowski, Co-Chair

Prabin Shilpakar

Hejun Zhu

LATE OLIGOCENE TO EARLY MIOCENE NORTH-SOUTH EXTENSION IN THE WESTERN GREAT BASIN

by

SCOTT ROBERTSON KERSTETTER, BS

DISSERTATION

Presented to the Faculty of

The University of Texas at Dallas

in Partial Fulfillment

of the Requirements

for the Degree of

DOCTOR OF PHILOSOPHY IN

GEOSCIENCE

THE UNIVERSITY OF TEXAS AT DALLAS

August 2018

ACKNOWLEDGMENTS

I would like to thank Dr. John Oldow for his advice throughout this research project. I also want to thanks my committee members, Dr. Tom Brikowski, Dr. Prabin Shilpakar, and Dr. Hejun Zhu, for their feedback and comments on the research. Special thanks to David Katopody for assistance in the field and to Dr. Jeff Dunham, Nick Mueller, Sarah Dunn, and Brent Cland for their continued feedback and advice. This research was funded by grants from the National Science Foundation and the Ellison Miles Center for Geological Field Research, and scholarships from Pioneer Natural Resources.

April 2018

LATE OLIGOCENE TO EARLY MIOCENE NORTH-SOUTH EXTENSION IN THE WESTERN GREAT BASIN

Scott Robertson Kerstetter, PhD
The University of Texas at Dallas, 2018

Supervising Professor: John S. Oldow

In the central and southern Walker Lane, a network of six east-northeast east-west, and west-northwest trending half-grabens, spanning an area of 15,000 km2, controlled the spatial distribution and thickness of late Oligocene to early Miocene volcanic and volcaniclastic rocks. The basins range from 10 to 25 km long, are 4 to 7 km wide, and from 0.5 to 1.5 km deep. Internally, the basins are segmented by north-northeast and north-northwest striking transfer faults that accommodated along-axis changes in basin geometry and across-axis dog-leg steps of up to 15 km. The basin-fill consists of synextensional rhyolite tuff, andesite, and volcaniclastic rocks that form asymmetric stratal wedges that thicken to the north and south into basin-bounding extensional faults. In several locations, the bounding faults are overlapped by post-extensional deposits of tuff and andesite that maintain uniform stratigraphic thicknesses throughout the region. The half-grabens controlled deposition of rhyolite tuff ranging in age from 27.4 to 23.75 Ma and andesite dated at 22 to 16.6 Ma. Individual faults were variously sealed by 23.75 Ma rhyolite tuff and 16.1 to 15.7 Ma andesite. Half graben development ceased by the mid-to-late Miocene and the basins were subsequently dissected by Late Miocene to

Quaternary faults. Analysis of 1335 fault-slip measurements collected within late Cenozoic and pre-Cenozoic rocks along major basin-controlling faults indicates the half-grabens formed in a period of regional north-south extension and predated west-northwest extension associated development of Late Miocene and Pliocene to contemporary basins and topography. Locally, east-west and east-northeast striking andesitic dikes intrude the basin-fill sequences and are consistent with emplacement during north-south extension.

TABLE OF CONTENTS

LIST OF FIGURES

CHAPTER 1

SYNOROGENIC DEPOSITION IN AN EAST-WEST TRENDING HALF-GRABEN DURING LATE OLIGOCENE TO EARLY MIOCENE NORTH-SOUTH EXTENSION IN WEST-CENTAL NEVADA

INTRODUCTION

Present-day mountain ranges in the Great Basin (Fig. 1.1) preserve a fragmented history of late Cenozoic extensional structures and related strata that indicate changes in the direction of crustal stretching prior to the onset of contemporary west-northwest extension. Often cited as evidence of changes in the extension direction are the orientations of faults and fault-induced tilts, dike swarms, the stratal geometry of graben-fill sequences, and fissure vents (Zoback and Thompson, 1978; Burke and McKee, 1979; Speed and Cogbill, 1979; Oldow and Steuer, 1985; Hardyman and Oldow, 1991; Oldow and Meinwald, 1992; Oldow and Dockery, 1993; Zoback et al., 1994). Much of the lines of evidence are dissected by extensional and transtensional faulting in the Basin and Range Province and Walker Lane and was therefore buried beneath the modern basins, uplifted and eroded, or simply disrupted by younger faulting (Ekren and Byers, 1976; Zoback and Thompson, 1978; Tincher and Stockli, 2009). Nevertheless, changes in the late Cenozoic extension direction have been proposed using what remaining evidence has been recognized.

The proposed changes in late Cenozoic extension and their supporting evidence vary in orientation and timing suggesting a complex history of extension across the Great Basin. Orientations and ages of late Cenozoic dikes across the Great Basin suggest that changes in extension may have occurred diachronously (Best, 1988). In north-central Nevada, the mid-

Miocene Northern Nevada Rift formed by north-northwest—trending fault systems and swarms of dikes oriented sub-parallel to the rift axis suggest east-northeast extension occurred between 20 and 10 Ma prior to onset of late Miocene to recent west-northwest extension (Zoback and Thompson, 1978; Zoback et al., 1994). The presence of "volcano-tectonic troughs," or half-grabens (Burke and McKee, 1979), that are bound by east-west—striking faults and contain late Eocene to early Miocene volcanic and sedimentary rocks provide evidence an even older period of north-south extension in the northern Great Basin (Best, 1988). The basin-fill takes the form of prismatic wedges that thicken across-strike and is consistent with normal displacement on east-west—striking master faults during north-south extension. Similar east-west—trending half-grabens provide evidence for north-south extension in west-central Nevada (Hardyman and Oldow, 1991). A series of east-northeast and east-west—trending half-grabens contain late Oligocene ignimbrites and early Miocene andesite flows and lahar, and breccia that form asymmetric stratal wedges that thicken southward into east-northeast—striking master faults. In some cases, these basins are intruded by east-west—striking dikes consistent with emplacement during north-south stretching (Oldow and Steuer, 1985; Hardyman and Oldow, 1991; Oldow and Meinwald, 1992; Oldow and Dockery, 1993).

Evidence of changes in the extension direction have gained little traction with the geologic community and may be caused by in the inherent inability of fault, dike or tilt orientations to uniquely define strain axes. Fault geometry and dike orientations are subject to crustal anisotropy and maybe influenced by pre-existing structures (Delaney et al., 1986). The dip direction of faulted strata is controlled by the footwall geometry (Gibbs, 1983). Furthermore, tilted strata only record the dip-slip displacement on the fault and is incapable of recording

strike-slip displacement that is needed in order to calculate the net-slip direction on a given fault. Asymmetric basins that formed in the hanging walls of strike-slip and oblique-slip faults best demonstrate this issue (Beeson et al., 2017).

Strain-rate axes determined from fault-slip inversion (Twiss and Unruh, 1998) can supplement qualitative estimations that employ fault, dike, and stratal dip orientations. The direction of extension can be calculated using the orientation of slickenlines and shear sense on a fault regardless of its attitude and is therefore beyond the influence of crustal anisotropy and reactivated structures. The use of fault-slip inversion to determine extension direction has been validated in modern cases by the use of earthquake focal mechanisms, geodetic studies and strain meters (Oldow, 2003; Ferranti et al., 2009).

In this study we document the existence of a pre-Basin and Range extension direction by the integration basin geometry, synextensional stratal patterns, intrusive rock trends, all supplemented by fault-slip inversion to analyze the kinematic history of faults. We demonstrate a period of north-south extension by recognizing a west-northwest—trending half-graben in the Palmetto Mountains of west-central Nevada. The half-graben formed contemporaneously with extrusion of early Miocene volcanic rocks as is demonstrated by upward decreases in bedding dip in the graben-fill sequences, by thickening of units to the south and north into basin master faults, and by units abruptly changing stratigraphic thickness across faults. Fault-slip analysis demonstrates that the west-northwest—trending half-graben developed during a period of early Miocene north-south extension that occurred prior to contemporary faulting in the central Walker Lane. Faults of the west-northwest—trending half-graben changed kinematics corresponding to changes in the direction of extension and were reactivated during younger deformation events.

GEOLOGIC FRAMEWORK

There is a rectilinear depositional boundary in the west-central Great Basin (Fig. 1.2) that controlled the distribution of the late Cenozoic stratigraphy from the late Oligocene to the present. The boundary features a southern west-northwest—trending margin with dog-legs connected by north-northeast—trending segments of the boundary, and a linear eastern margin that trends north-northeast. The Late Cenozoic rocks are divided into two broad stratigraphic units by an unconformity, a late Oligocene to early Miocene section and mid-Miocene to Quaternary section, both of which vary in spatial distribution, thickness and lithology across the rectilinear depositional boundary (Speed and Cogbill, 1979c; Oldow and Meinwald, 1993; Oldow and Dockery, 1992; Oldow et al., 2009; Tincher and Stockli, 2009). The late Oligocene to early Miocene section is 2 to 3 km thick to the north and west of the rectilinear boundary and is nearly absent to the south and east of the boundary occurring as isolated 10 to 210 m thick exposures (Stewart, 1979; Speed and Cogbill, 1979a; Ekren and Byers, 1985a; 1985b; Proffett and Proffett, 1976). Mid-Miocene to Quaternary rocks occur on both sides of the rectilinear boundary but are have different lithologies despite being age-equivalent. North and west of the boundary, the mid-Miocene to Quaternary stratigraphy consists of approximately equal parts sedimentary and volcanic rocks, and lies on both late Oligocene to early Miocene strata and pre-Cenozoic rocks with angular unconformity (Robinson et al., 1968; Diamond, 1990; Diamond and Ingersoll, 2002; Oldow et al., 2003). South and east of the boundary, the mid-Miocene to Quaternary section is predominately composed of volcanic rocks (Albers and Stewart, 1972; Worthington, 1992).

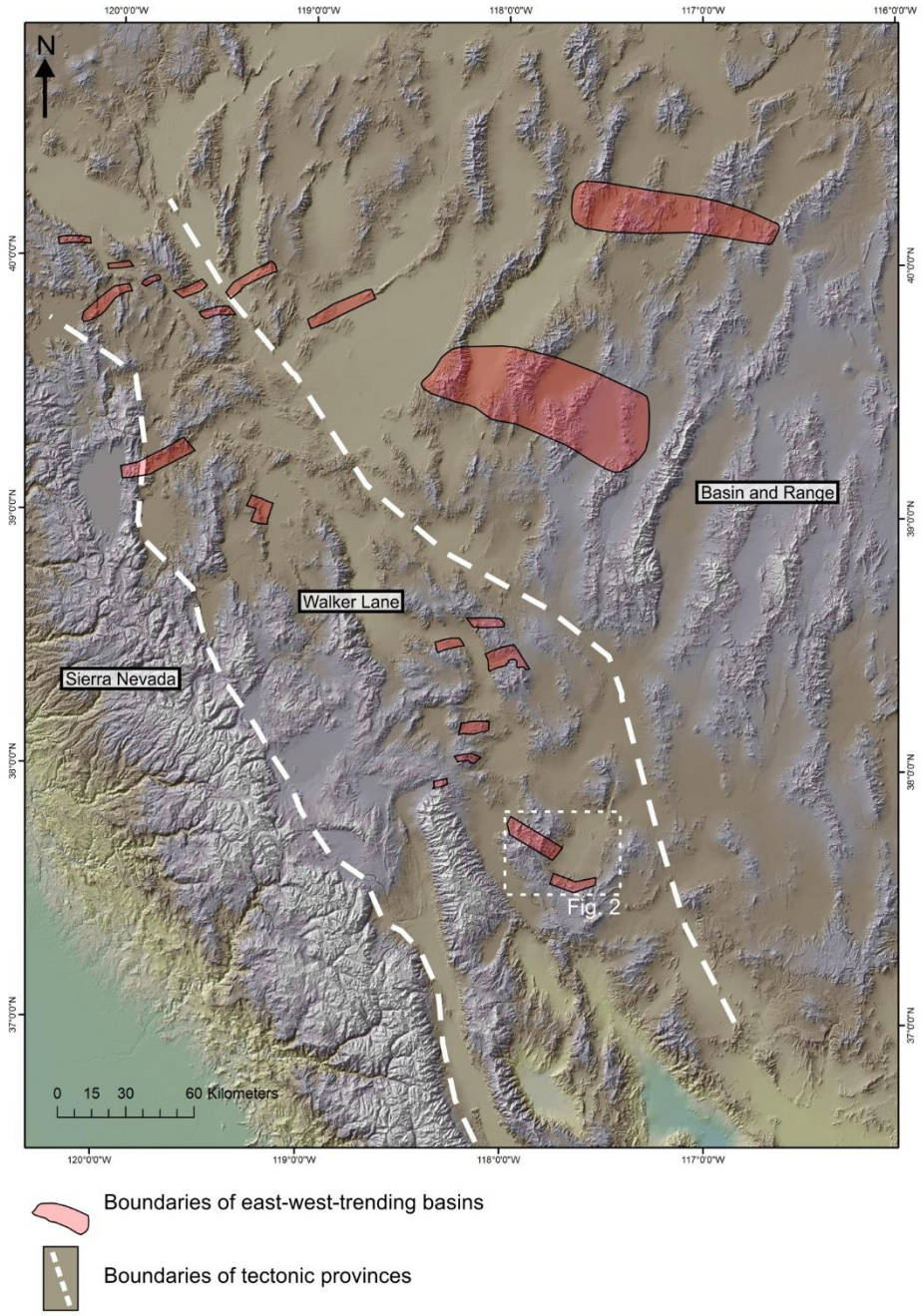

Figure 1.1. Physiographic map of the Great Basin.

The depositional boundary was controlled by segments of a complex network of faults that strike north-northwest, north-northeast, west-northwest and east-northeast. North-

northwest-striking transcurrent faults of the Fish Lake Valley-Owens Valley faults system and the Walker Lane are connected by left-lateral east-northeast—striking faults of the Mina deflection and a system of sinistral west-northwest and dip-slip north-northeast—striking faults (Locke et al., 1940; Ryall and Priestley, 1976; Dokka and Travis, 1990; Wesnousky, 2005; Dunn, 2016). Several contemporary west-northwest, east-northeast and north-northeast—striking faults form a rectilinear boundary that spatially coincides with the late Cenozoic depositional boundary.

Along the north and west side of the depositional boundary, faults with modern displacement previously formed the boundaries of late Oligocene to early Miocene and mid-Miocene to Quaternary basins that have nearly perpendicular axes despite controlling the spatial distribution, thickness and lithologic variability of stratigraphic units throughout the late Cenozoic (Hardyman and Oldow, 1991; Oldow et al., 2009). The late Oligocene to early Miocene section often forms the base of the Cenozoic stratigraphy and rests on pre-Cenozoic rocks (Robinson et al., 1968; Ekren and Byers, 1985a; 1985b). Mid-Miocene to Quaternary rocks overlie the Oligo-Miocene section with angular unconformity and also lie in direct contact with the pre-Cenozoic rocks where the older Cenozoic rocks are stratigraphically omitted across faults (Oldow et al., 2009). Each of these units is typically 100 to 300 m thick except where they abruptly increase thickness into 1.0 to 2.5 km deep basins (Ross, 1961; Albers and Stewart, 1972; Speed and Cogbill, 1979b). Mid-Miocene to Pliocene rocks accumulated in north-northeast—trending half-grabens overlying a detachment that were uplifted and exposed in the present-day mountain ranges or buried beneath triangular, north-northeast, and north-northwest—trending prismatic basins that accumulated Pliocene to Quaternary rocks (Elias,

2005; Ferranti et al., 2009; Oldow et al., 2009). In contrast, late Oligocene to early Miocene rocks accumulated in east-northeast, east-west, and west-northwest—trending basins that are 10 to 25 km long and 4 to 6 km wide (Speed and Cogbill, 1979b; Oldow and Meinwald, 1979; Oldow and Dockery, 1979). Late Oligocene to early Miocene rocks within the basins form asymmetric stratal wedges that thicken southward into basin-bounding faults. The varying trends of the late Oligocene to early Miocene basins spatially correspond to a region that underwent 20° to 30° clockwise vertical-axis rotation since the late Miocene (Petronis et a., 2009). Basins outside the rotational domain have east-northeast trends whereas basins within the rotational domain trend east-west to west-northwest.

Late Oligocene to Early Miocene Rocks

The late Oligocene to early Miocene section consists of volcanic, sedimentary and intrusive rocks associated with a lower unit of late Oligocene tuff and an upper unit of early Miocene andesite (Ferguson, 1927; Robinson et al., 1968; Garside, 1979; Speed and Cogbill, 1979a; Ekren and Byers, 1985a; 1985b; Stewart et al., 1994; Henry and John, 2013). The thickest sections accumulate within east-northeast, east-west, and west-northwest—trending basins and dip southward reaching thicknesses of 1.0 to 2.0 km along the southern margins of asymmetric basins (Speed and Cogbill, 1979b; Oldow and Meinwald, 1992; Oldow and Dockery, 1993). Outside of these basins, the Oligo-Miocene section is flat-lying and varies in thickness from 10 to 200 meters, and in some areas is completely omitted from the stratigraphy (Garside, 1979; Speed and Cogbill, 1979c; Oldow and Steuer, 1985).

The lithologic composition of the late Oligocene to early Miocene section changes from basin to basin such that the basin-fill variously consists of late Oligocene tuff and early Miocene

andesite, Oligocene tuff buried by post-extensional andesite, or only early Miocene andesite (Hardyman and Oldow, 1991). The Oligocene and early Miocene rocks are separated by an unconformity that is most apparent where the lower tuff unit, that normally forms the base of the section, is absent and the early Miocene andesite overlies the pre-Cenozoic rocks (Garside, 1979; Speed and Cogbill, 1979c). Both units vary in thickness in and around the late Oligocene to early Miocene basins and show abrupt changes in thickness across faults (Speed and Cogbill, 1979c; Oldow and Meinwald, 1992; Oldow and Dockery, 1993). The Late Oligocene unit is composed of several unconformity-bound tuffs with ages ranging from 27.4 to 23.7 Ma (Proffett and Proffett, 1976; Speed and Cogbill, 1979a; Petronis et al., 2009; Henry and John, 2013) that have a cumulative thickness of 2 to 3 km but typically vary thickness from 300 to 1000 m as various stratigraphic units are omitted across high-angle normal faults (Speed and Cogbill, 1979c; Hardyman and Oldow, 1991). The early Miocene unit is incorporated into east-west basins to the north with minimum thicknesses of 300 to 500 m (Oldow and Meinwald, 1992; Oldow and Dockery, 1993). In some cases basin development ended during the early Miocene so that the upper part of the andesite overlapped the basins' master faults (Speed and Cogbill, 1979c).

The early Miocene andesite is best exposed in the eastern Excelsior Mountains and the Monte Cristo Range and is composed of lava flows, lahar, tuff and sedimentary rocks, and associated hypabyssal intrusive rocks (Ferguson, 1927; Garside, 1979; Stewart et al., 1994). In these two areas, the andesite section variously overlies Oligo-Miocene ignimbrites, Permian and Cretaceous metasedimentary rocks, and Jurassic and Cretaceous plutons. The andesite contains an angular unconformity that separates the section into lower and upper units that allows the

upper unit to lie directly on the underlying tuff and pre-Cenozoic rocks where the lower unit is missing. The andesite sections in these two areas have similar lithologic compositions but show slight variations in age.

In the eastern Excelsior Mountains (Garside, 1979), the early Miocene andesite section rests unconformably on Oligo-Miocene ignimbrites, Permian and Cretaceous metasedimentary rocks and Cretaceous pluton. The andesite contains a lower section of lava flows that is at least 100 m thick and overlies a 22 Ma tuff and is intruded by a west-northwest—trending hypabyssal pluton and associated vent breccia dated at 18.9 ± 0.8 Ma. The pluton is surrounded by an elongate alteration aureole that has a 5 km long west-northwest—trending axis and is 250 to 1000 m wide and encompasses argillized and silicified parts of the pluton, vent breccia, and the 22 to 19 Ma lower andesite. These units are all unconformably overlain by a 100 m thick upper andesite unit composed of lava flows and minor lahar and is dated at 15.7 ± 0.5 to 16.1 ± 0.7 Ma. The upper andesite unit overlaps the lower andesite unit and Cretaceous metasedimentary rocks on either side of an east-west, high-angle contact that stratigraphically omits the lower andesite.

In the Monte Cristo Range (Stewart et al., 1994), the early Miocene andesite overlies Oligo-Miocene tuffs, Paleozoic metasedimentary rocks, and Jurassic pluton. The lower and upper andesite units in this area are termed the Blair Junction sequence and Gilbert Andesite, respectively, and are separated by a medial 30 m thick sedimentary unit composed of mudstone to fine-grained sandstone. The Blair Junction sequence consists of a volcanic-dominated basal section of lava flows, breccia and lahars and passes upward into a more clastic-dominated middle section of andesitic tuff with interleaved sandstones and conglomerate and an upper unit of coarse-grained flows and breccias. The base of the section is intruded by andesitic intrusive

rocks dated at 22.2 Ma, the tuff in the middle section is dated at 16.6 Ma and the top of the unit is 15.7 Ma. The Gilbert Andesite consists of flows and breccias that cap the hills and ridges in the Monte Cristo Range overlying tilted rocks of the Blair Junction sequence with angular unconformity and is dated at 15 Ma.

Geology of the Clayton Valley Area

Clayton Valley and the surrounding ranges (Fig. 1.3) preserve stratal and fault geometries associated with late Cenozoic deposition and extension along the rectilinear depositional boundary that forms the southern margin of Cenozoic exposures. Pre-Cenozoic rocks are primarily exposed south and north of a west-northwest—trending belt of late Cenozoic rocks that is 25 km wide and 55 km long, but also crop out within the eastern side of the belt (Albers and Stewart, 1972). The southern margin of the late Cenozoic section follows a west-northwest—trending fault-controlled boundary that is punctuated by north-northeast—trending dog-legs (Oldow et al., 2009; Oldow and Geissman, 2013). The southern boundary separates thin, flat-lying Cenozoic strata overlying Paleozoic metasediments and Mesozoic pluton from thick, tilted strata resting on Paleozoic rocks to the north (Oldow et al., 2009). The northern margin of the late Cenozoic outcrop belt is variously depositional and structural. Late Cenozoic strata predominately overlie Paleozoic rocks depositionally but locally the Cenozoic section structurally overlies Mesozoic metamorphic tectonites and Cenozoic intrusive rocks.

A rectilinear system of faults consists of west-northwest—trending strike-slip faults that are through-going and divide the bedrock exposures into 25 to 70 km long and 5 to 10 km wide structural panels that are then crossed and further segmented by north-northeast—striking normal faults that merge with the west-northwest—striking faults (Robinson et al., 1968; 1976; Albers

and Stewart, 1972; Oldow et al., 2009). The fault network contains both present-day structures that bound range fronts and cut across the ranges as narrow anastomosing fault zones, and earlier Cenozoic faults that are cross cut and exposed in the mountain ranges by Pliocene to Quaternary faulting that began around 3 to 5 Ma. A mid-Miocene to Pliocene low-angle detachment fault is cut by Pliocene to Quaternary faults whereas older mid-Miocene to Pliocene high-angle faults merge with the detachment (Oldow et al., 2009).

The west-northwest and north-northeast—trending segments of the rectilinear depositional boundary were controlled by faults that have been active for much of the late Cenozoic. The west-northwest—trending segments of the boundary are controlled by the Icehouse Canyon fault as it extends 25 km west-northwest across the Silver Peak Range and coincides with the 15 km long segment of the Palmetto Mountain fault system that forms southern boundary to Clayton Valley and the low-lying Palmetto foothills. Dog-legs in the southern boundary coincide with contemporary faults that form the western and eastern north-northeast—trending margins of Clayton Valley and do not extend southward past the Palmetto Mountain fault system.

Late Cenozoic Stratigraphy

The late Cenozoic stratigraphic units are separated by an unconformity (Fig. 1.3) that separates the late Oligocene to early Miocene section from the mid-Miocene to Quaternary section consistent with age-equivalent rocks across the western Great Basin (Dover, 1962; Albers and Stewart, 1972). The mid-Miocene to Quaternary section forms a west-northwest—trending exposure belt 20 km wide and 55 km long, and often forms the base of the Cenozoic stratigraphy, resting directly on pre-Cenozoic rocks. The mid-Miocene to Quaternary section

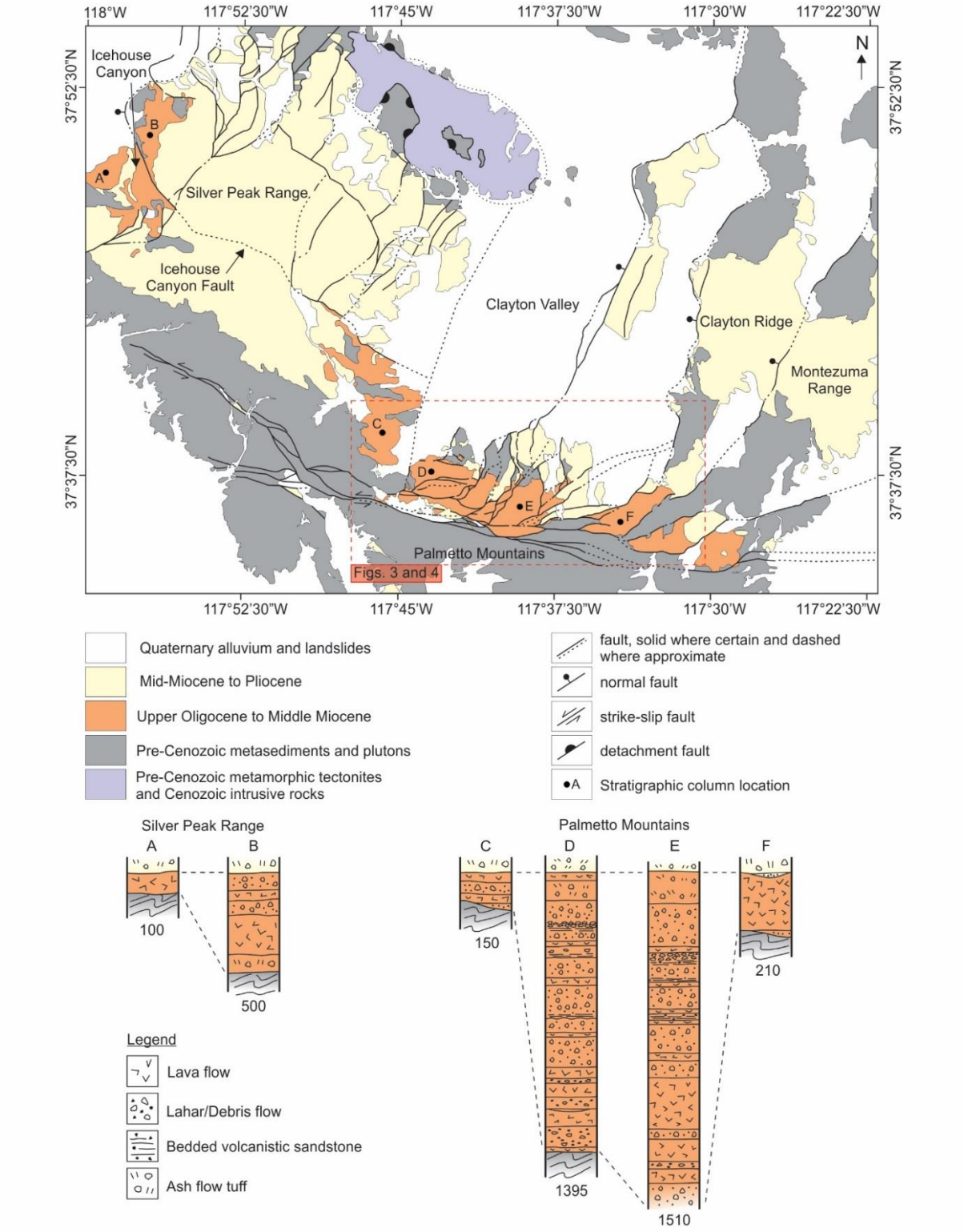

Figure 1.2. Geologic map and stratigraphic columns of the Clayton Valley region.

varies in thickness from 20 m to 3500 m, showing abrupt changes across high-angle faults, and is composed of multiple unconformity-bounded units that each vary in thickness and spatial distribution such that each unit lies in contact with pre-Cenozoic rock at some point (Oldow et al., 2009). The underlying late Oligocene to early Miocene section is more spatially restricted and is localized in and around west-northwest—trending basins that are 10 to 25 km long and 4 to 6 km wide and track the rectilinear depositional boundary through the Palmetto Mountains and central Silver Peak Range (Robinson et al., 1968, Albers and Stewart, 1972).

Late Oligocene to Early Miocene. The late Oligocene to early Miocene section shows abrupt variations in thickness and lithology (Fig. 1.3) across north-northeast and west-northwest—striking faults that bound the elongate andesite basins on all sides and juxtapose the basin-fill sequence with Paleozoic metasedimentary rocks and Mesozoic pluton (Dover 1962; Oldow et al., 2009). The stratigraphic thickness of the late Oligocene to early Miocene succession is preserved by the mid-Miocene to Quaternary succession allowing recognition of growth relationships in the older succession. Despite the limited exposure in the Silver Peak Range, the early Miocene section at Icehouse Canyon (Fig. 1.3) shows an abrupt increase in thickness across the west-northwest—striking Icehouse Canyon fault and is overlain mid to late Miocene tuff, flows and sedimentary rocks on both sides of fault (Oldow et al., 2009). The footwall to the south exposes a 100 m thick section of andesite flows and breccia that rest on Paleozoic metasedimentary rocks over a sub-horizontal contact. Equivalent rocks to the north are 500 m thick and consist of a basal section of conglomerate overlain by late Oligocene rhyolitic tuff, and an upper section of early Miocene andesite lava flows and lahars that pass upward into bedded sedimentary rocks with interleaved lava flows, debris flows and ignimbrites

(Robinson et al., 1968). Although the late Oligocene to early Miocene section shows growth across a west-northwest—trending fault system and is flat-lying on the footwall, the rocks in the hanging wall are tilted up to 30° east by younger north-northeast—trending faults (Robinson et al., 1968; 1976; Elias, 2005; Oldow et al., 2009). The eastern edge of footwall of the Icehouse Canyon fault is bounded near Cow Camp by a north-northeast—striking fault and exposes a 150 m thick section of andesite resting on a shallowly-dipping contact over Paleozoic metasedimentary rocks (Albers and Stewart, 1972). Exposures of early Miocene andesite to the southeast across the fault in the northern Palmetto Mountains are 1395 to 1510 m thick. The abrupt increase in thickness is accommodated by west-northwest and north-northeast—striking faults that bound the andesite on all sides and are in turn overlain by successions of late Miocene tuffs. Here, the basal tuff is absent and the early Miocene andesite rests directly on the Paleozoic substrate. The early Miocene andesite is buried to the east by outcrops of late Miocene tuff and Quaternary alluvial deposits (Dover, 1962). The eastern-most early Miocene andesite crops out at Lida Wash where the unit occupies horses bounded by east-west, east-northeast and northeast—striking faults (Albers and Stewart, 1972). The andesite, composed almost entirely of flows, rests on Paleozoic rocks and is overlain by late Miocene flows giving the unit a thickness of 210 m. On the east side of Clayton Valley, the andesite is stratigraphically omitted across north-northeast—striking faults allowing late Miocene silicic tuffs to rest directly on pre-Cenozoic rocks on Clayton Ridge and Montezuma Range (Albers and Stewart, 1972).

Mid-Miocene to Quaternary. The mid-Miocene to Quaternary section has a complex stratigraphy that shows substantial lateral variation in thickness and lithology (Fig. 1.3) across high-angle faults that caused abundant unconformities, stratigraphic omission and tilting during

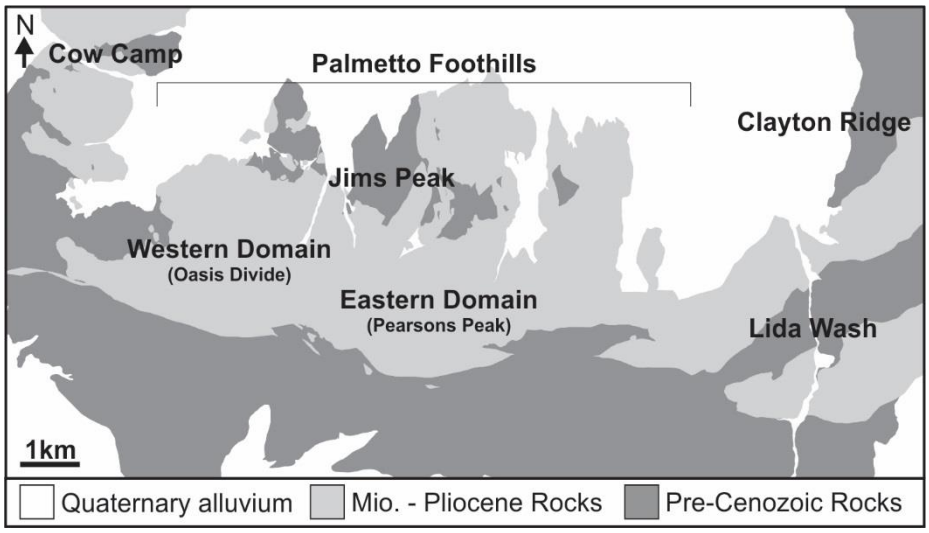

Figure 1.3. Geographic locations in the Palmetto area.

deposition (Oldow et al., 2003; Elias, 2005; Oldow et al., 2009). The Silver Peak Range preserves the most lithologically diverse section and consists of a basal unit of mid-Miocene sedimentary rocks and interleaved tuff (13 to 11 Ma), several medial late Miocene units that are variously composed of silicic tuff, flows and volcaniclastic sedimentary rocks (6.9 to 5.9 Ma), and an upper Plio-Quaternary unit containing sedimentary rocks and basalt flows (4.8 to 3.0 Ma). The mid-Miocene to Quaternary section varies thickness from 20 to 2755 m across the range due to a complex pattern of stratigraphic omission and thickness changes across high-angle faults (Oldow et al., 2009). The western and eastern margins of the Silver Peak Range reveal Paleozoic rocks, Mesozoic pluton, and early Miocene andesite beneath the mid-Miocene to Quaternary section whereas the extensive deposits in the central part of the range completely bury the older Cenozoic units (Robinson et al., 1968; Stewart et al., 1974; Robinson et al., 1976). South of the Icehouse Canyon fault, the unit decreases to 365 m thick which was accomplished by complete omission of entire stratigraphic units from the mid-Miocene to Quaternary section

(Oldow et al., 2009). In the Palmetto Mountains, the mid-Miocene sedimentary section is absent and the unit contains a 65 to 510 m thick section of late Miocene tuff and flows that overlie pre-Cenozoic rocks and early Miocene andesite. The unit rests directly on Paleozoic metasedimentary rocks on Clayton Ridge and islands of bedrock in north-central Clayton Valley reaching a thickness of 300 m and contains late Miocene tuff and tuffaceous sediments (Albers and Stewart, 1972). Farther east on Montezuma Range, the unit is composed of late Miocene tuff intruded by Pliocene rhyolite flows and domes.

Mid-Miocene to Quaternary Basins and Extension

Late Cenozoic faults and stratal geometries preserved in the ranges indicate the region experienced multiple periods of extensional basin formation (Oldow et al., 2009). The spatial variability of mid-Miocene to Quaternary rocks records the superposed development of two basin systems whereas earlier Cenozoic faults and strata are the focus of this paper.

Contemporary faults that formed the modern physiography initiated transtensional deformation around 3 to 5 Ma (Bachman, 1978; Henry and Perkins, 2001; Stockli et al., 2003; Andrew and Walker, 2009; Mueller et al., 2016). Transtensional deformation is accommodated on the orthogonal fault network composed of west-northwest—trending anastomosing fault zones and north-northeast—trending range front faults (Wesnousky, 2005; Oldow, 2008; Dunn et al., 2016). These faults operate under west-northwest extension, oriented N55W to N65W, as determined by geodetic studies, earthquake focal mechanisms, and fault-slip inversion (Oldow, 2003; Ferranti et al., 2009). West-northwest stretching causes coordinated dip-slip displacement on north-northeast—striking faults and left-lateral strike-slip motion on west-northwest—striking faults.

Synextensional strata in the Silver Peak Range indicate that before 3 to 5 Ma and since at least 13 Ma deformation was accommodated by high-angle faults underlain by a shallowly northwest-dipping detachment surface across much of the region and was termed the Silver Peak-Lone Mountain extensional complex (Oldow et al., 2009). The detachment fault separates late Cenozoic rocks, lower Paleozoic sediments and Mesozoic plutons from metamorphic tectonites and Cenozoic plutons. The detachment is currently exposed by a turtleback structure in the Silver Peak Range (Kirsch, 1971) and was deformed into its current configuration by west-northwest—trending folds (Oldow et al., 2008). Prior to folding, motion on the detachment formed a network of north-northeast—trending basins bounded by north-northeast—striking normal faults and west-northwest—striking transfer faults that controlled deposition of eastward thickening prismatic wedges composed of mid to late Miocene volcanic and sedimentary rocks (Oldow et al., 2003; Elias, 2005; Oldow et al., 2009). The mid to late Miocene basin-fill that structurally overlaid the detachment was deformed into gentle, north-northeast—trending folds by localized shortening caused by movement over a detachment with a ramp-flat geometry (Oldow et al., 2009). The transport direction on the detachment is uncertain but is inferred to be northwest oriented given the north-northeast—trending axes of the mid-Miocene to Pliocene basins.

GEOLOGY OF THE PALMETTO AREA

The late Cenozoic depositional boundary in the Palmetto area (Figs. 1.4 and 1.5) separates extensive exposures of early to late Miocene rocks resting on Paleozoic metasediments and unconformably overlain by sparse outcrops of the Pliocene to Quaternary rocks to the north from exposures of Paleozoic metasediments and Mesozoic plutons overlain by sparse early to

late Miocene rocks to the south. Early Miocene rocks have a stratigraphic component, informally referred to as the Pearsons Peak andesite, consisting of lava flows lahars, tuff, sedimentary rocks, and an intrusive component that is composed of east-west—striking dikes and an east-northeast—trending pluton that are emplaced in the base of the early Miocene stratigraphy and Paleozoic sedimentary rocks. The Pearsons Peak andesite itself is further divided into a lower unit composed of lavas, lahars, sedimentary rock and tuff overlain with angular unconformity by an upper andesite composed of lava flows. The late Miocene to Quaternary section is dominated by late Miocene tuffs with subsidiary lava flows and sedimentary rocks that comprise five unconformity-bounded sequences. Three of the four late Miocene units correlate to the formations of the Coyote Hole Group defined by Oldow et al (2009) in the neighboring Silver Peak Range, including the Rhyolite Ridge Tuff, Cave Springs Formation, and the Argentite Canyon Formation whereas the Tuff of Oasis Divide is defined herein. The Pliocene to Quaternary basalts and sedimentary rocks correlate to the Fish Lake Valley assemblage and formation of contemporary basins (Oldow et al., 2009; Katopody et al., in review).

The early Miocene andesite and late Miocene to Quaternary section are separated by an angular unconformity consistent with Cenozoic unconformities mapped across the western Great Basin. The late Miocene to Quaternary section forms laterally extensive sheets that predominately strike north-northwest and dip 20 to 25 degrees east although the upper basalts are relatively flat-lying. Late Miocene to Quaternary rocks depositionally overlie all subunits of the Pearsons Peak andesite as well as on Paleozoic and Mesozoic rocks. The early Miocene Pearsons Peak andesite is exposed along a 4 km wide exposure belt that has a west-northwest

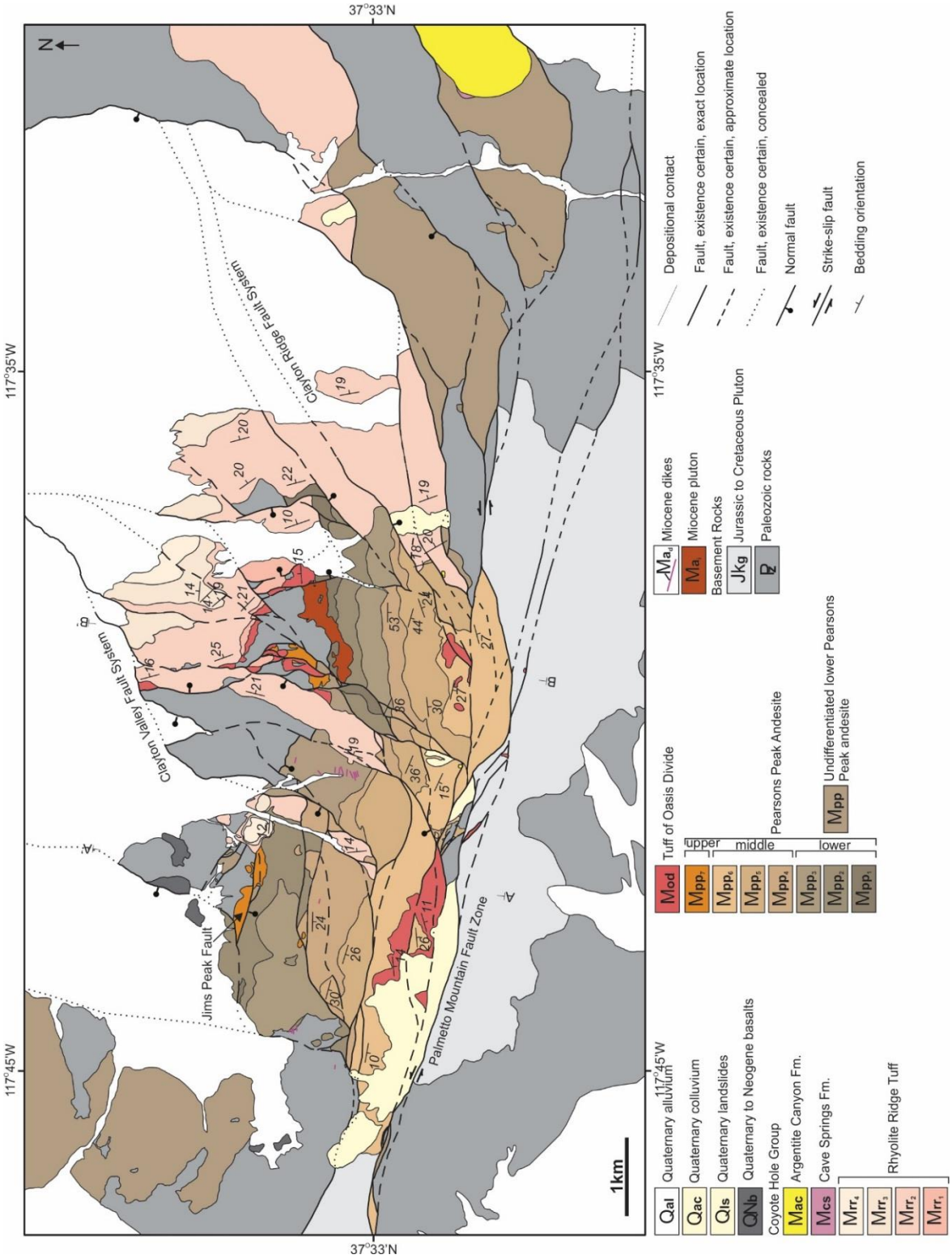

Figure 1.4. Geologic Map of the Palmetto area.

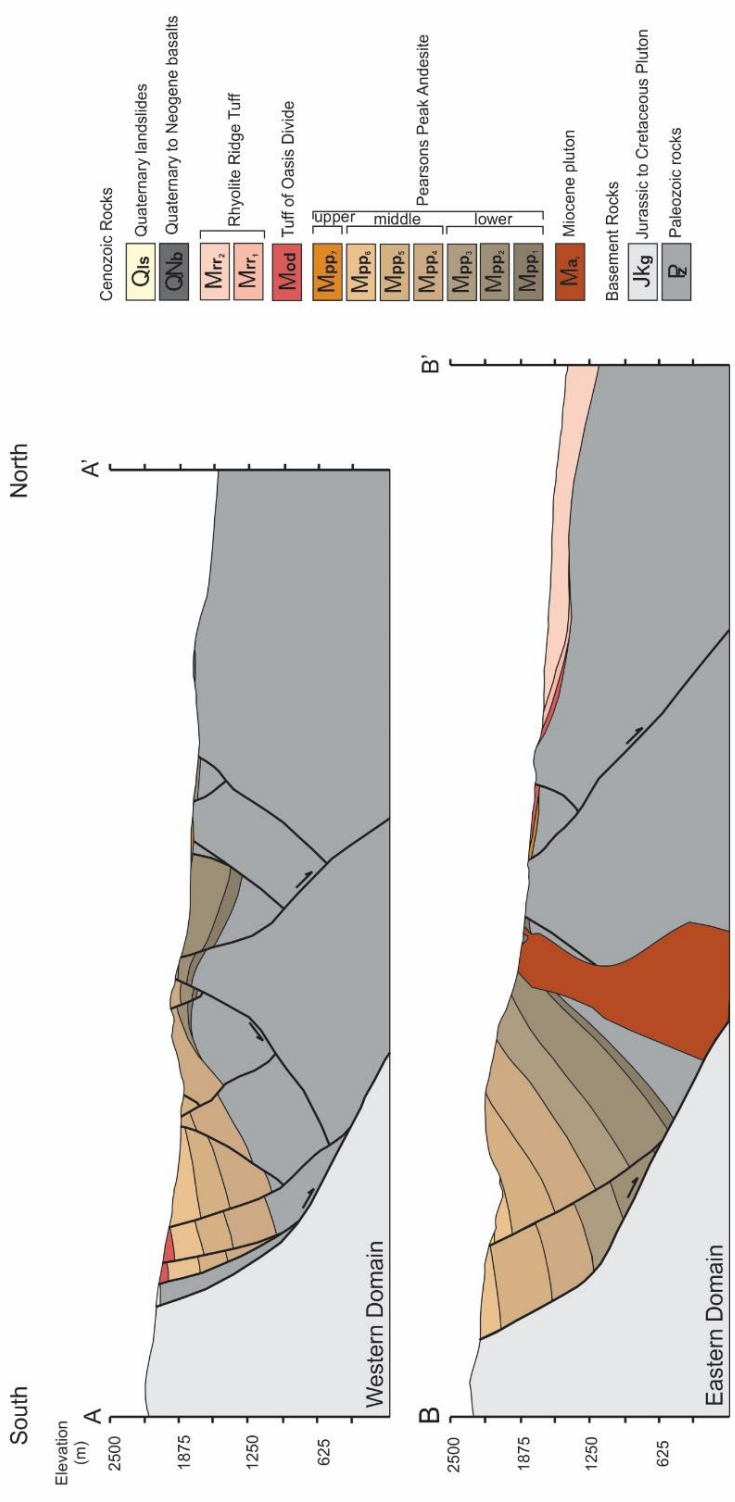

Figure 1.5. Cross Sections of the Palmetto Mountain area.

length of at least 10 km but is buried by late Miocene tuffs for the 5 km distance between Pearsons Peak and Clayton Ridge. The lower Pearsons Peak andesite is dropped down by a rectilinear network of west-northwest and north-northeast—striking faults that bound the unit on all sides juxtaposing the andesite with Paleozoic and Mesozoic rocks. Lower Pearsons Peak andesite within the basin predominately strikes east-west and dips 25 to 50 degrees south except where it dips shallowly north, whereas the upper andesite that overlaps the basin rest sub-horizontally on lower Pearsons Peak andesite and Paleozoic rocks. The eastward tilt of late Miocene tuffs exposes the base of the Pearsons Peak andesite near the Oasis Divide fault demonstrating that the early Miocene andesite sits directly on Paleozoic rocks and the absence of the late Oligocene tuff seen at the base of the section elsewhere in the western Great Basin. In contrast to the steep dips of Pearsons Peak andesite within the basin, andesite outside the basin in the Cow Camp and Lida Wash areas is flat-lying to shallowly north-dipping. Restoration of the 20 degree eastward dip of the angular unconformity at the base of the overlying rocks indicates that the south and north-dipping andesite originally dipped south-southwest and north-northeast directly perpendicular to west-northwest—striking faults that bound the basin and was only later changed to their current orientations. The andesite will be referred to with in-situ orientations for the rest of the paper for simplicity's sake.

The Palmetto area experienced two generations of faulting and folding that temporally correlate to the early Miocene Pearsons Peak andesite and the late Miocene to Quaternary section. Early Miocene faults formed a rectilinear system of coeval west-northwest and north-northeast—striking structures that formed the west-northwest—trending half-graben that controlled deposition of the Pearsons Peak andesite and the south and north tilts of the unit.

Contemporaneous deposition and fault movement is recorded by growth relationships in the early Miocene strata and burial of faults by late Miocene to Quaternary rocks, and will be discussed in detail later in the paper. The lower Pearsons Peak andesite and Paleozoic metasedimentary rocks in the west-northwest—trending basin were folded along an east-west—trending axis whereas the upper Pearsons Peak andesite and late Miocene tuffs that bury the basin did not experience the same folds. The onset of late Miocene to Quaternary faults and reactivation of west-northwest and north-northeast—striking faults that were originally part of the early Miocene basin is recorded by growth strata and unconformities preserved by late Miocene to Quaternary rocks. The late Cenozoic units are locally deformed into a north-northeast—trending fold that is spatially associated with north-northeast—striking faults and are also folded along west-northwest—trending axes. The buried early Miocene faults, and late Cenozoic folds and stratigraphy are all cross cut by a complex network of contemporary faults that are currently active.

The contemporary faults that disrupt the early to late Miocene geology intersect in the Palmetto area. The southern boundary of the intersection is defined by the west-northwest—striking and north-dipping Palmetto Mountain fault system that consists of a 0.5 to 1.0 km wide zone of anastomosing sinistral faults that stretch 20 km across the Palmetto area and separate extensive deposits of late Cenozoic rocks overlying pre-Cenozoic rocks to the north from sparse, thin deposits of Cenozoic rocks and pre-Cenozoic rocks to the south. The region north of the Palmetto Mountain fault zone is crossed by north-northeast—striking and curvilinear faults that segment and juxtapose various stratigraphic units as the faults merge with the south-bounding fault system. The north-northeast—striking faults predominately dip west and northwest

although individual strands may dip east or southeast. Curved faults that connect the west-northwest and north-northeast—striking faults show a north-to-south change in strike by at least 90 degrees from northeast, to east-northeast, to east-west over a north-to-south distance of 1 to 2 km as the faults merge with the Palmetto Mountain fault system. The curved faults anastomose and form horses exposing late Miocene tuff that are dropped down and surrounded by Pearsons Peak andesite on all sides. These younger faults are still active and offset Quaternary alluvium and landslide deposits.

Late Miocene to Quaternary Stratigraphy

The Late Miocene to Quaternary Stratigraphy is composed of five unconformity-bounded units that exhibit similar patterns to to age-equivalent synextensional strata in the Silver Peak Range (Oldow et al., 2009). The late Miocene to Quaternary stratigraphy predominately consists of late Miocene Tuff of Oasis Divide and Rhyolite Ridge Tuff but also contains the late Miocene sedimentary rocks, tuff, and lava flows attributed to the Cave Springs and Argentite Canyon Formations, Pliocene basalt lava flows, and Quaternary landslide deposits. The Tuff of Oasis Divide and Rhyolite Ridge Tuff form the base of the late Miocene to Quaternary stratigraphy in many areas and rest directly on Paleozoic metasediments, Mesozoic pluton, and Pearsons Peak andesite although the two late Miocene tuffs are themselves separated by an unconformity so that each unit rests on the substrate. The Tuff of Oasis Divide and Rhyolite Ridge Tuff form sheets that cover extensive areas whereas the overlying Cave Springs Formation, Argentite Canyon Formation, Pliocene basalts and Quaternary landslides are more spatially restricted and each rest on the late Miocene tuff units, Pearsons Peak andesite or Paleozoic metasedimentary rocks.

The late Miocene tuff units, Tuff of Oasis Divide and Rhyolite Ridge Tuff, each vary thickness across the Palmetto area (Fig. 1.4) and in some areas omit the older tuff unit as it pinches out from east to west. The Tuff of Oasis Divide has a stratigraphic thickness of 90 m but in some outcrops can be as thin as 10 m due to erosion of the upper part of the unit. The Tuff of Oasis Divide is deposited across an exposure belt covering approximately 50 km^2 and is locally omitted across high-angle faults and by thinning and pinching out of the unit that allows the overlying Rhyolite Ridge Tuff to sit directly on Paleozoic metasedimentary rocks and Pearsons Peak andesite. The Rhyolite Ridge Tuff is also widely distributed across the Palmetto area and unconformably overlies the Tuff of Oasis Divide, Pearsons Peak andesite and Paleozoic rocks. In contrast to the uniform stratigraphic thickness of the Tuff of Oasis Divide, the Rhyolite Ridge Tuff forms a prismatic wedge that shows an eastward increase in thickness from 45 to 400 m with abrupt thickness changes occurring across high-angle, north-northeast—striking faults.

The Cave Springs and Argentite Canyon Formations form the top of the late Miocene section and rest on Rhyolite Ridge Tuff and Pearsons Peak andesite with angular unconformity. Sedimentary rocks of the Cave Springs Formation have a maximum thickness of 12 to 14 m and fill a 270 to 350 m wide channel carved into the underlying Pearsons Peak andesite at Lida Wash but is absent elsewhere in the Palmetto area. Restriction of the Cave Springs Formation to the channel allows the Argentite Canyon Formation to lie in direct contact with the Pearsons Peak andesite and Rhyolite Ridge Tuff.

Pliocene to Quaternary rocks consist of basalts, landslides and alluvium, and depositionally overlie Miocene volcanic and sedimentary units and Paleozoic metasedimentary rocks. The basalt flows are 15 to 20 m thick and directly rest on Paleozoic rocks where the

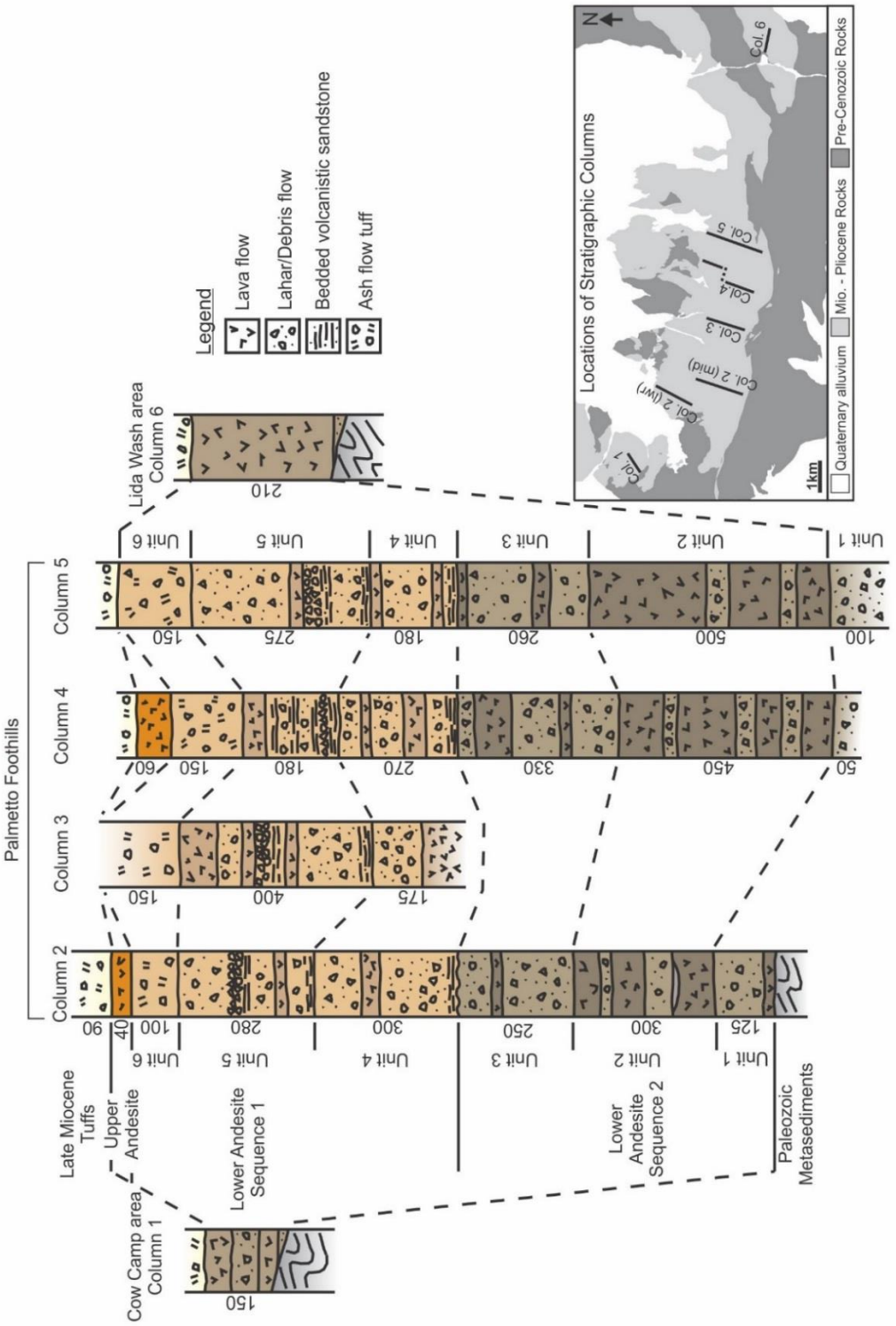

Figure 1.6. Stratigraphic columns in the Palmetto area illustrating lateral variations in thickness and lithology of the early Miocene andesite succession.

Pearsons Peak andesite and overlying Miocene rocks are stratigraphically omitted north of the early Miocene andesite basin. The flows may be related to basalts dated at 4.8 to 3.0 Ma (Oldow et al., 2009) in the Silver Peak Range. Quaternary landslides rest on the Tuff of Oasis Divide, Pearsons Peak andesite, Mesozoic pluton and Paleozoic metasediments among the intertwined strands of the Palmetto Mountain fault zone. The landslides are 20 to 60 m thick and bury older units that are occasionally exposed at the bases of rounded hills capped by the landslide deposits. The landslides consist dominantly of granitic clasts and boulders derived from the Palmetto pluton and minor amounts of Paleozoic and Miocene lithic fragments.

Tuff of Oasis Divide

The Tuff of Oasis Divide (Fig. 1.4) forms the base of the late Miocene stratigraphy in many areas of the Palmetto foothills but is absent in the Cow Camp and Lida Wash areas. From south to north, the Tuff of Oasis Divide in the Palmetto foothills rests on Mesozoic pluton, Pearsons Peak andesite, and Paleozoic metasedimentary rocks.

The Tuff of Oasis Divide crops out at the southern margin of the early Miocene basin along a west-northwest—trending axis that parallels to the Palmetto Mountain fault system along the southern Margin of the andesite basin. Outcrops of the tuff form 15 to 20 m high cliffs at thet type section where the unit is 90 m thick and can be laterally traced for 2 km. Elsewhere along this trend, the tuff forms isolated outcrops that are 15 to 20 m thick and tens to hundreds of meters wide.

The Tuff of Oasis Divide overlaps the northern margin of the andesite basin directly north of Pearsons Peak and rests unconformably on both early Miocene andesite and Paleozoic rocks but is not preserved 2 km to the west on the west flank of Jims Peak nor 1 km to the east

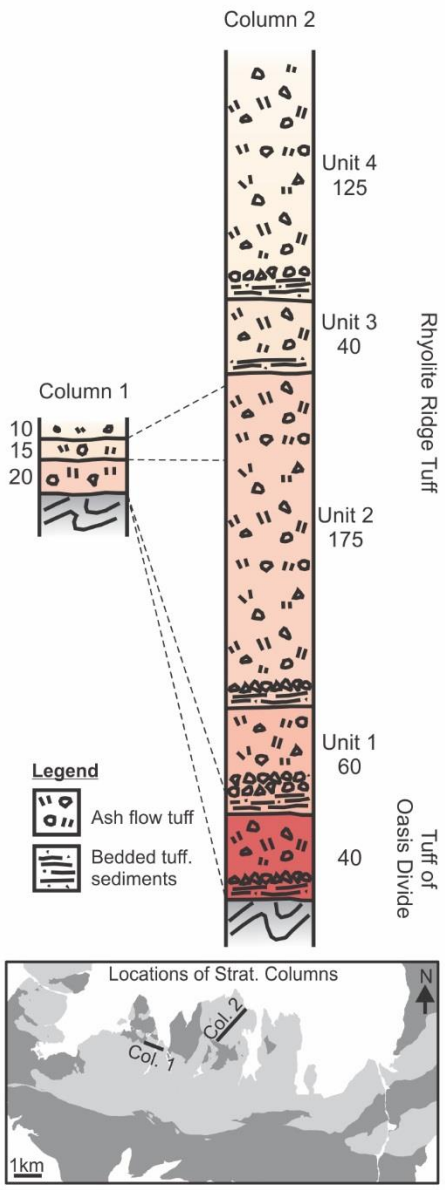

Figure 1.7. Stratigraphic columns of the Rhyolite Ridge Tuff illustrating lateral changes in thickness and lithology.

where the unit is stratigraphically omitted across a north-south striking fault. Absence of the Tuff of Oasis Divide puts the overlying Rhyolite Ridge Tuff in direct contact with Pearsons Peak andesite and Paleozoic rocks. Where the Tuff of Oasis Divide is preserved north of Pearsons

Peak, the unit has a maximum thickness of 40 m and thins westward to zero meters causing a gradual top-to-base removal of stratigraphic section from the unit over a distance of 1.5 to 2.0 km. The base of the Tuff of Oasis Divide is truncated by the Rhyolite Ridge Tuff near the east flank of Jims Peak allowing the younger tuff to overstep the Tuff of Oasis Divide and lie directly on Pearsons Peak andesite and Paleozoic rocks.

The volcanic unit is a lithic, feldspar, amphibole, biotite tuff that exhibits variable degrees of welding. The base of the unit ranges from 2 to 4 m thick and is equally divided between a lower volcaniclastic sediment that passes upward into a weakly-welded tuff. The basal unit is overlain by a 5 to 7 m thick zone of dense welding that progressively decreases upward over a transition of 10 m into moderately-welded tuff that constitutes the upper 70 to 75 m. The lower sections of the Tuff of Oasis Divide are consistently is composed of the basal breccia and the lower zones of the tuff, each of which maintain constant thickness, suggesting topography was subdued during deposition. Omitted section from the unit occurs at the top of the Tuff of Oasis Divide and likely resulted from erosion during subsequent faulting before Rhyolite Ridge Tuff deposited instead of synextensional depostion. The welded zone near the base of the Tuff of Oasis Divide is dated at 7.670 ± 0.016 Ma.

The distribution of lithic fragments and phenocrysts show different patterns of abundance within the tuff. The percentage of lithic fragments is uniform throughout the tuff but the phenocryst population and the abundance of fiamme vary through the section. The lithic fragments, which are angular and range in size from 1 to 5 mm, constitute about 10 percent of the rock and consist of about equal parts of andesite porphyry and Paleozoic metasediment. The phenocryst population consists of sanidine (50%), plagioclase (25%), hornblende (15%), and

biotite (10%). The relative abundance phenocryst minerals remain constant but the total concentration of phenocrysts increases upward from 5 percent in the basal unit and overlying densely-welded zone to 20 percent in the moderately-welded tuff. The phenocryst size and crystal habit varies by mineral species; euhedral sanidine ranges from 1 to 4 mm, subhedral to euhedral plagioclase is 1 to 2 mm, subhedral hornblende ranges from 2 to 4 mm, and subhedral biotite is 1 mm. The percentage of fiamme, which range from 1.0 to 3.0 cm long, decreases upward from 20 percent at the base of the tuff to 10 percent in the densely-welded zone, and to trace amounts in the moderately-welded tuff.

The basal sedimentary succession of the Tuff of Oasis Divide is composed of thinly-bedded breccia. The matrix-supported breccia exhibits lenticular bedding that extends along strike for several meters. The bedding ranges from 4 to 10 cm thick and has sharp upper and lower contacts. The breccia is composed 50 to 80 percent grains and clasts, ranging from 2 mm to 5 cm that consist of approximately equal amounts of angular to subangular andesite porphyry and Paleozoic metasedimentary rock in a volcanogenic wacke matrix. The matrix is composed of 70 to 80 percent lithic grains ranging in size from 0.1 to 1 mm supported in brown ash.

Rhyolite Ridge Tuff

The Rhyolite Ridge Tuff (Fig. 1.7) shows the same variation in thickness observed elsewhere in the region (Oldow et al., 2009) and is composed of interleaved ashflow tuff and tuffaceous sediment with an aggregate thickness that reaches up to 400 m. The lithologic unit rests unconformably on Paleozoic strata, Pearsons Peak andesite, and Tuff of Oasis Divide (Fig. 1.4) and is locally overlain unconformably by the Argentite Canyon Formation. The unit has the form of an easterly-thickening prism with stepwise increases in thickness occurring across faults.

In the northern part of the study area, the Rhyolite Ridge Tuff shows a systematic increase of thickness from 45 to 400 m across several faults over a distance of 1.5 to 3.0 km. In the southeastern part of the map area, the western limit of the unit coincides with a southeast-facing normal fault that juxtaposes 175 to 200 m of tuff against Pearsons Peak andesite. The overlying Argentite Canyon Formation rests directly on both the Rhyolite Ridge Tuff and Pearsons Peak andesite and is itself only offset by 60 m indicating that the fault was active during tuff deposition. The Rhyolite Ridge Tuff is dated in the Palmetto Mountains at 6.148 ± 0.019 Ma and on Clayton Ridge at 6.172 ± 0.014 Ma. The dates and lithologic descriptions of the Rhyolite Ridge Tuff are consistent with those of Elias (2005) and Oldow et al (2009).

The Rhyolite Ridge Tuff is divided into four depositional successions, each of which have a prismatic geometry that progressively thicken to the east. The units consist of a basal section of tuffaceous sediments from 2 to 2.5 m thick that passes upward into non-welded to weakly-welded ashflow tuffs that have maximum thicknesses ranging from 40 to 200 m. The ashflow sections commonly contain minor sedimentary interbeds that are laterally discontinuous over 3 to 10 m and reach thicknesses of up to 1.5 m. The lower-most depositional unit has a maximum thickness of 60 m and thins to the west over a distance 1.5 km to where it is overlapped by the overlying unit. Each of the three younger units progressively decreases from an aggregate thickness of 340 m to 45 m over a distance of 6.5 km and overstep the basal member toward the west by 3.5 km. The sedimentary rocks at the base of each succession maintain uniform thicknesses over distances of several kilometers even as the overlying tuff decreases in thickness from east to west. Where the lower-most unit pinches out, basal sediments are directly overlain by the sedimentary unit of the younger succession and show an

angular discordance in bedding of about 5 degrees. Elsewhere, similar discordance in bedding is suspected by not directly observed.

The four tuff successions are lithologically similar but differ in color and aspect ratio of the prismatic tuff bodies. The basal sections consistently are composed of tuffaceous diamictite that passes upward into thin-bedded volcanogenic wacke. The sedimentary rocks are overlain by tuff breccia, thought to be a basal surge deposit that varies in thickness from 0.5 to 1.0 m, which is overlain by lithic tuff. The tuff successions are generally white to pink and nonwelded with one unit weathering brown and showing weak welding (Unit 3). Locally within the tuff units, contacts between individual ashflows reaching thicknesses of 8 to 100 m can be distinguished by the presence of 0.5 to 1.0 m thick lenticular sedimentary interbeds. The sedimentary rocks are diamictites localized in channels ranging 1 to 2 m deep and 3 to 10 m wide.

The basal tuffaceous sediments for each unit consistently are composed of a 1.5 to 2.0 m thick horizon of amalgamated diamictites that pass upward into a 0.5 m thick upper unit of thin-bedded volcanogenic wacke and tuff breccia. The diamictites preserve scour and fill structures and occasionally exhibit internal organization with crude fining-upward features near the transition into the overlying bedded sandstone and breccia. The diamictite is composed of 60 to 80 percent subangular to subrounded clasts composed of andesite porphyry (50%), Paleozoic metasedimentary rock (40%), and tuff (10%) within a volcanogenic wacke matrix. The clasts range in size from 0.5 to 30 cm, but typically are 0.5 to 10 cm in diameter. The wacke matrix is composed of 60 percent lithic grains supported in a brown ash matrix. The lithic grains are subangular to subrounded and range in size from 0.1 to 1 mm. The overlying layered rocks consist of interbedded wacke and breccia from 5 to 15 cm thick that laterally pinch out over

several meters. The wacke is composed of 60 to 70 percent lithic grains supported in salmon-colored ash. The lithic grains are subangular to subrounded and range from 0.1 to 0.5 mm in diameter. The tuff breccia has the same composition as that of the overlying ashflow tuff section but contain smaller clasts that range from 0.5 to 1.0 cm.

The ashflow tuff units have a uniform composition consisting of lithic grains and sanidine, biotite, quartz phenocrysts but differ in the size of pumice clasts. Ashflow tuff typically contains 40 to 60 percent lithic and pumice clasts, in a matrix composed of 25 to 50 percent phenocrysts of sanidine (50%), biotite (40%), and quartz (10%) supported in an ash matrix. Phenocryst size and crystal habit differs with sanidine and biotite ranging from subhedral to euhedral and 1 to 3 mm, and anhedral quartz 1 mm in diameter. Clasts compose between 40 to 60 percent of the tuff and are equally divided between lithic fragments and pumice. Lithic clasts are subangular, ranging from 0.5 to 3.0 cm, and composed of equal parts andesite porphyry and Paleozoic metasedimentary rocks. Pumice fragments are subangular to subrounded and vary in size between the non-welded and weakly welded members of tuff. Pumice clasts in non-welded units are 0.5 to 3.0 cm in diameter but range from 0.5 to 7.0 cm in the weakly welded tuff. The breccia at the base of the tuff successions is massive and consists of 90 percent clasts of pumice (80%), Paleozoic metasediment (10%), and andesite porphyry (10%) in an ash matrix. The clasts are subangular to subrounded and range in size from 0.5 to 3.0 cm.

Cave Springs Formation

The Cave Springs Formation is a succession of tuff and tuffaceous sediment that passes upward into non-tuffaceous sediments. The succession consists of lithic tuff 5 to 6 m thick that is overlain by another 5 to 6 m of tuffaceous breccia that passes upward into a 2 m thick zone of

intercalated volcanic sandstone and breccia. In contrast to the lower two lithologies, the upper zone of volcanic sandstone does not have tuffaceous content. The contact between the tuffaceous and non-tuffaceous sediments in buried by float but the transition occurred over a distance no greater than 2 m.

The tuff has a uniform composition throughout exposures, shows no internal stratification, and is moderately sorted. The tuff consists of 10 percent lithic grains of volcanic and Paleozoic rocks in an ash matrix. The grains are subangular and are 1 to 5 mm in diameter. The tuff matrix is composed of 20 to 25 percent phenocrysts supported in yellow friable ash. The phenocrysts consist of sanidine (50%), hornblende (30%), and biotite (20%) that vary in size and crystal habit. Subhedral to euhedral sanidine is 2 to 3 mm, subhedral hornblende is 2 mm, and euhedral biotite is 0.5 to 1 mm in diameter.

The tuffaceous breccia is massive and shows an even distribution of grains and clasts. The breccia is composed of 80% lithic clasts and grains in a tuffaceous matrix. The lithic grains and clasts, consisting of andesite porphyry and Paleozoic metasedimentary rocks, range in size from 0.5 to 30 cm and are angular to subangular. The tuffaceous matrix is composed of 25 percent lithic grains and 50 percent mineral grains in friable ash that is white to yellow in color. The lithic grains and mineral fragments, consisting of biotite (50%), feldspar (30%), and amphibole (20%), are about 0.5 to 1 mm in diameter and are angular to subangular.

The sandstone is generally massive except for thin-bedded horizons of matrix-supported breccia that range 5 to 30 cm thick. The sandstone consists of 70 to 80 percent lithic grains in red argillite. The grains are 0.5 to 2 mm in diameter and are angular. Locally, the breccia horizons contain about 50 percent outsized clasts supported in a matrix of volcanic sandstone.

The clasts consist of andesite porphyry and Paleozoic metasediment that are angular to subangular and range in size from 1 to 3 cm.

Argentite Canyon Formation

The Argentite Canyon Formation variously consists of ignimbrites and lava flows. In the Palmetto Mountains, the unit forms 20 to 25 m high cliffs of welded tuff overlying Rhyolite Ridge Tuff and dips shallowly east. In Lida Wash, the unit is composed of lava flows and rests directly on Pearsons Peak andesite and Cave Springs Formation with angular unconformity. The upper contact of the unit is not preserved and the minimum thickness of the preserved section is about 120 m. The unit is lithologically correlated to exposures of the Argentite Canyon Formation in the Silver Peak Range dated at 5.9 Ma (Oldow et al., 2009).

Lava flows in the Lida Wash section are poorly exposed and largely covered by float. Where exposed, the lava often shows planar flow foliations and on occasion exhibits jointing oriented approximately normal to the foliations. No well-preserved contacts between individual flows are recognized.

Both volcanic lithofacies have the same phenocryst population although the tuff additionally contains lithic grains. The flows contain 35 to 40 percent phenocrysts supported in an aphanitic groundmass that weathers dark gray to blue-ray. The tuff contains 10 to 20 percent phenocrysts and 10 to 15 percent lithic grains suspended an igneous matrix of red to gray fine-grained ash. The lithic grains are angular and 1 to 5 mm in diameter. The phenocryst populations in of the flows and tuff consist of sanidine (40-60%), hornblende (30-35%), and biotite (10-25%).

Folds

There are two generations of Cenozoic folds (Fig. 1.8) recorded in the Palmetto Mountains that formed in the late Miocene to Quaternary and in the early Miocene. The folds typically have wavelengths of 250 to 2000 m and gently-dipping limbs. Many folds are spatially associated with normal faults suggesting a causative relationship between fault movement and folding.

Late Miocene to Quaternary Folds (F2)

North-northeast and west-northwest folds formed during or after the late Miocene and are most easily recognized in the late Miocene strata. The relative age folds is not recognized in the Palmetto Mountains but timing constraints for folds with the same geometry in the Silver Peak Range indicate that the west-northwest—trending folds are younger than the north-northeast folds (Oldow et al., 2009). These folds are associated with movement of high-angle, north-northeast—striking faults during mid to late Miocene motion of the detachment and post-detachment folding and formation of west-northwest—trending turtleback structures (Oldow et al., 2008).

North-northeast fold

A north-northeast—trending fold is exposed in one location on the northwest flank of Pearsons Peak and the east flank of Jims Peak, and is spatially associated with a north-northeast—striking normal fault and reverse fault similar to north-northeast—trending folds in the Silver Peak Range (Oldow et al., 2009). This structure is a syncline with an east-dipping axial surface. The fold lies in the hanging-wall of a north-northeast—striking fault and runs

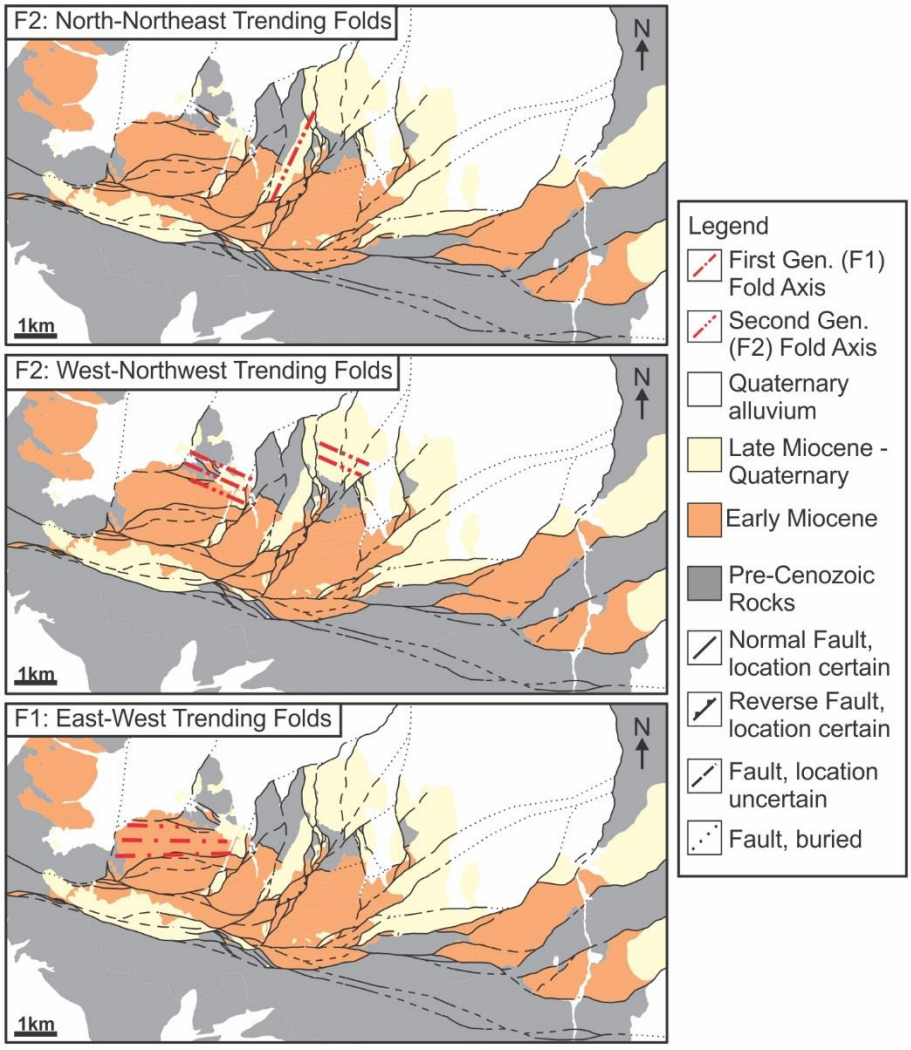

Figure 1.8. Map illustrating the orientation and spatial distribution of late Cenozoic folds.

parallel to the fault's strike. From south to north, the syncline exhibits a continuous increase in the half wavelength and interlimb angle of the fold. The half wavelength of the syncline increases to the north-northeast from 750 to 1000 m over a distance of 3 km. Similarly the interlimb angle increases from 115° to 150° over the same distance. At its southern extent, the north-northeast—striking fault that bounds the fold merges with an east-west striking fault that truncates the north-northeast—trending fold and juxtaposes the folded rocks against rocks that

are not folded by north-northeast folds. In addition to the syncline, a north-northeast—striking reverse fault is preserved in the footwall of the north-northeast normal fault and provides more evidence of localized shortening associated with the north-northeast—striking fault. The syncline, the east-west and north-northeast—striking normal faults and the reverse fault are all disrupted by post-Miocene faulting.

The syncline folds rocks of the Rhyolite Ridge Tuff, Pearsons Peak andesite, and Paleozoic strata. In the western limb, the base of the Rhyolite Ridge Tuff dips 15° to 20° east, and rests on the Pearsons Peak andesite to the south and Paleozoic rocks to the north. The eastern limb is dissected by post-Miocene normal faulting but shows a 30° decrease in dip along the strike of the limb. At the southern extent of the syncline, the Rhyolite Ridge Tuff dips 56° north. To the northeast across a northeast-striking fault, rocks of the Pearsons Peak andesite dips 44° northwest. Farther north the Rhyolite Ridge Tuff rests on Pearsons Peak andesite and the Tuff of Oasis Divide and dips 25° northwest.

West-northwest folds

These structures are west-northwest trending folds with upright to southwest-dipping axial surfaces. The folds have half wavelengths of 250 to 500 m and interlimb angles of 145° to 150°. The folds form anticline-syncline pairs and are exposed in a couple locations in the Palmetto foothills.

West of Jims Peak by 1 km, a syncline-anticline pair folded Rhyolite Ridge Tuff, Pearsons Peak andesite, and Paleozoic rocks. These west-northwest striking folds have a half wavelength of 300 m and axes that plunge shallowly east. The axial surface of the syncline is upright whereas that of the anticline dips steeply southwest. The southern limb of the syncline

dips 12° north and exposes Rhyolite Ridge Tuff and the underlying Pearsons Peak andesite. In the northern limb of the syncline, the Rhyolite Ridge Tuff dips 8° south and overlies Paleozoic rocks that are also exposed in the core of the connected anticline. The northern limb of the anticline, the base of the Rhyolite Ridge Tuff rests on Paleozoic rocks and dips 21° north.

Outcrops of Rhyolite Ridge Tuff north of Pearsons Peak are folded into a northwest to west-northwest trending anticline-syncline pair. The syncline has an axial surface that dips steeply southwest whereas the axial plane of the anticline is upright. The southwest limb of the syncline dips 19° north and the shallower northeast limb dips 14° south. The northern limb of the anticline dips 14° north.

Early Miocene Folds (F1)

The oldest Cenozoic folds are gentle, east-west trending folds with shallowly plunging axes that lie sub-parallel to the axis of the west-northwest—trending half-graben. These folds formed in the early Miocene as indicated by their prevalence in the lower Pearsons Peak andesite and absence in the upper Pearsons Peak and Late Miocene tuffs. Early Miocene folds have half wavelengths of 800 to 1000 m and interlimb angles of 140° to 150°. The folds are prevalent in the western part of the Palmetto foothills where they deform the lower sequence of the Pearsons Peak andesite and Paleozoic rocks into a set of anticlines and synclines.

Faults

The complex network of faults in the Palmetto area (Figs. 1.4 and 1.5) features new and reactivated structures although contemporary faulting disrupts early Miocene geometries. Even though most of these faults are Quaternary-aged, growth strata and buried faults often preserve

evidence of early Miocene activity. In this case, there is an early Miocene network of faults that was active during deposition of the lower Pearsons Peak andesite and buried by the upper Pearsons Peak andesite and late Miocene tuffs. Kinematic analysis of fault movement demonstrates that early Miocene faults operated under north-south extension instead of the late Miocene to Quaternary west-northwest to northwest extension.

Contemporary Geometry

The north-northeast and west-northwest—striking faults separate the Palmetto area into several structural panels that are bound and crossed by contemporary fault systems across which the Cenozoic stratigraphy varies in thickness and lithology. The Palmetto Mountain fault system forms the southern boundary of this fault network and separates 10 to 210 m thick deposits of Cenozoic rocks and pre-Cenozoic rocks to the south from Paleozoic metasediments overlain by Cenozoic rocks to the north that show abrupt changes in thickness and lithology across contemporary north-northeast—striking faults. The Oasis Divide and Clayton Ridge fault systems subdivide the hanging wall of the Palmetto Mountain fault zone into three main structural panels, the central of which is crossed by the Clayton Valley fault system. In the hanging wall of the Palmetto Mountain fault zone, the central 15 km of the fault zone forms the southern boundary of a 2 km thick section of Cenozoic rocks whereas the equivalent section just west of Oasis Divide fault system is 150 m thick and is 300 m thick east of the Clayton Ridge fault system although the early Miocene andesite unit is absent.

Palmetto Mountain Fault System. The Palmetto Mountain fault system (Fig. 4) is a 0.5 to 1.5 km wide system of three to four anastomosing west-northwest and east-west—striking

faults that stretches 20 km across the Palmetto area. The Palmetto Mountain fault zone in the Palmetto area has a slightly curved trace such that the western half of the fault zone strikes west-northwest and the eastern half strikes east-west. The fault zone as a whole dips 55° to 65° north although individual strands may dip south.

The width of the Palmetto Mountain fault zone is about 1 km in its western half, abruptly decreases to 0.5 km at the intersection with the Clayton Valley fault system, and then gradually increases width to 1.5 km to the east over a distance of 5 to 6 km. The southern edge of the fault zone consists of two west-northwest—striking parallel strands that dip north and juxtapose south-dipping Pearsons Peak andesite and the Tuff of Oasis Divide in the hanging wall with Paleozoic and Mesozoic rocks to the south. The northern edge of the Palmetto Mountain fault zone juxtaposes different parts of the Pearsons Peak andesite and consists of a single, south-dipping fault that strikes parallel to the west-northwest southern boundary on the western half and strikes east-west in the eastern half of the fault zone creating the eastward widening zone. Occasional fault splays create elongate horses that are 1 to 2 km long and 200 to 400 m wide and are variously composed of Cenozoic andesite and tuff, Mesozoic plutonic rocks, and Paleozoic metasedimentary rocks. The horses typically trend east-west and northwest, and are bounded on all sides by sub-vertical strike-slip faults

The western part of Palmetto Mountain fault system consists of several fault strands (Figs. 1.4 and 1.5). An east-west—striking strand juxtaposes the south-dipping Pearsons Peak andesite and the Tuff of Oasis Divide in the hanging wall with Paleozoic rocks to the south. Lower Pearsons Peak andesite forms a southward thickening wedge that reaches a maximum thickness of 725 m and is overlain by south-dipping Tuff of Oasis Divide. In this area, landslide

deposits temporarily buried several strands of the Palmetto Mountain fault system and were later offset by younger displacement.

The eastern part of the Palmetto Mountain fault system (Figs. 1.4 and .5), due south of Pearsons Peak, separates Paleozoic rocks overlain by thin (10 to 15 m) sections of Pearsons Peak andesite and the Tuff of Oasis Divide from a thick accumulation of Miocene volcanic rocks to the north. The Lida Wash section of the Pearsons Peak andesite (180 to 210 m thick) lies to the east on the same fault block, south of the southern extent of thick accumulations of Miocene strata. The base of the Tuff of Oasis Divide rests unconformably on Jurassic to Cretaceous pluton in a few locations at the southern margin of the fault zone. Anastomosing strands form horses of tuff that are juxtaposed on all sides with Mesozoic rocks. In the hanging wall to the north, both sequences of the lower Pearsons Peak andesite form a single southward thickening wedge overlain by east-dipping rocks of the Rhyolite Ridge Tuff and flat-lying Tuff of Oasis Divide and Argentite Canyon Formation. The southward thickening andesite decreases dip upsection from 55 to 25 degrees and truncates into the southern strands of the Palmetto Mountain fault zone.

Oasis Divide Fault System. The Oasis Divide fault system (Fig. 1.4) is composed of two north-northeast—trending strands that dip towards each other and run 3.5 km southward to merge with the Palmetto Mountain fault system. The two main fault strands are connected by an east-west—striking segment accompanied by an abrupt north-to-south decrease in the width of the fault system from 2.5 km to a single fault strand. The western fault strand is largely buried beneath alluvium but where it is exposed it juxtaposes the base of the Pearsons Peak andesite to the east with Paleozoic rocks to the west. The fault has an inferred linear trace because its

outcrop exposure aligns with the eastern range front near the Cow Camp area. The eastern fault strand forms the north-northeast—trending range front of a ridge of Paleozoic rock capped by Pliocene basalt and drops the basalt down-to-the west. The eastern strand then curves clockwise into an east-west—striking segment that juxtaposes various parts of the lower Pearsons Peak andesite. To the south, the Oasis Divide fault bifurcates as it merges with the Palmetto Mountain fault system.

Clayton Ridge Fault System. The Clayton Ridge fault system (Fig. 1.4) consists of one north-south—striking and west-dipping fault that trifurcates into northeast-striking fault strands that merge with the Palmetto Mountain fault system. The trifurcated fault strands run 6.5 km southwest from Clayton Ridge toward the Palmetto Mountain fault system and consist of two southeast-dipping faults that cross the southeast flank of Pearson Peak and a single northwest-dipping fault that forms the southeast range front bounding Clayton Valley. These fault strands diverge to the southwest reaching a maximum separated distance of 2 km and then converge again as the faults approach the Palmetto Mountain fault system. Occasional fault splays strike east-northeast and north-northeast.

The northeast-striking fault strands dip towards each other forming a horse with a 6.5 km long northeast—trending axis. The northeast—trending horse is composed of Pearsons Peak andesite and late Miocene tuffs covered by a thin layer of alluvium and is bounded on all sides by high-angle oblique-slip faults that juxtapose the tuffs with Pearsons Peak andesite and Paleozoic metasedimentary rocks. Internally, the northeast—trending horse is cross cut by north-east, east-west, and north-northeast—striking fault splays that form smaller east-northeast and north-northeast—trending horses that are 2 to 3 km long and 500 to 750 m wide.

Clayton Valley Fault System. The Clayton Valley fault system (Fig. 1.4) is a 3 to 4 km wide system of north-northeast, northeast and east-west—striking faults and has a north—south dimension of 4.5 to 5.0 km within the Palmetto area. The Clayton Valley fault system consists of four main north-northeast—striking fault strands that coalesce along the northern flank of bedrock exposures in the Palmetto area. The fault system as a whole exhibits a down-to-the west displacement although individual fault strands variably dip west and east. Faults of the Clayton Valley fault system curve into northeast—striking segments that merge with the Palmetto Mountain fault system.

The Clayton Valley fault system dissects and juxtaposes Pearsons Peak andesite, late Miocene tuffs and Paleozoic metasedimentary rocks. Strands of the Clayton Valley fault system that follow the western flank of Jims Peak cut across rocks of the Paleozoic and Pearsons Peak andesite. On the hanging wall to the west, Rhyolite Ridge Tuff overlies the Paleozoic rocks and andesite, all of which are folded into gentle west-northwest-trending folds and crossed by the north-northeast—striking fault. Along strike to the south, anastomosing fault strands segment and juxtapose various sections of the Pearsons Peak andesite and include a dropped down horse composed of the Rhyolite Ridge Tuff. Along the eastern flank of Jims Peak, strands of the Clayton Valley fault system separate the lower parts of the Rhyolite Ridge Tuff on the east from Paleozoic strata and Pearsons Peak andesite to the west. North of Pearsons Peak, multiple northeast-striking strands of the Clayton Valley fault system cross cut stratigraphic successions consisting of Paleozoic rocks, the Tuff of Oasis Divide, and the Rhyolite Ridge Tuff, and exhibit throws on the order of tens of meters. These faults merge southwestward forming an 800 m wide zone of anastomosing faults that flank the west face of Pearsons Peak and segment a lone reverse

fault. The reverse fault dips steeply northwest and places the basal part of lower Pearsons Peak andesite structurally above the central part of the same unit. The eastern most edge of the Clayton Valley fault system is connected to the Clayton Ridge fault system by three north-south striking normal faults that separate late Miocene tuffs from Paleozoic rocks, Pearsons Peak andesite and a hypabyssal pluton to the west and Paleozoic rocks and early Miocene andesite to the east.

Early Miocene Faults

Aside from the contemporary faults, there are also early Miocene faults that were buried by early to late Miocene strata and were subsequently cross cut by contemporary faults (Figs. 1.4 and 1.5). These faults have west-northwest and east-west strikes and variously dip north or south. The faults juxtapose early Miocene andesite and Paleozoic metasedimentary rocks.

Half way between the western halves of the Palmetto Mountain fault system and Jims Peak fault, east-west—striking faults juxtapose various parts of the lower Pearsons Peak andesite are buried by the upper Pearsons Peak andesite. The fault system as a whole dips 50 to 60 degrees south although individual splays may dip north. The east-west faults juxtapose north-dipping andesite from the lower part of the basin-fill with south-dipping andesite from the upper part of the basin-fill. The east-west—striking faults are buried by the upper Pearsons Peak andesite that overlies the lower andesite in both fault blocks and remains at the same elevation.

The most prominent early Miocene fault is the Jims Peak fault that forms the northern margin of the andesite basin and trends west-northwest along the southern flank of Jims Peak, the fault's namesake. The Jims Peak fault consists of a single strand but also exhibits occasional splays. The fault dips 55° to 60° south and separates the lower sequence of the Pearsons Peak

andesite in the hanging wall from Paleozoic rocks on the footwall. The fault is clearly exposed for most of its 7 km long trace but is locally buried by younger Miocene strata, cross cut by younger north-northeast-striking faults, and locally intruded.

The western half of Jims Peak fault separates shallowly north-dipping Pearsons Peak andesite from Paleozoic strata overlain by 15 to 20 m of flat-lying andesite. The fault truncates the northward-thickening lower Pearsons Peak andesite that reaches a maximum thickness of 600 m at the fault. Northwest-striking faults 300 m north of the Jims Peak fault truncate the thin section of flat-lying andesite on both the northeast and southwest. The Jims Peak fault and the northwest-striking faults are buried by the upper Pearsons Peak andesite and Rhyolite Ridge Tuff.

The eastern half of Jims Peak fault separates south-dipping Pearsons Peak andesite from Paleozoic strata overlain by flat-lying outcrops of the upper Pearsons Peak andesite, Tuff of Oasis Divide and Rhyolite Ridge Tuff. The fault juxtaposes the lower sequence of the Pearsons Peak andesite on the south with Paleozoic rocks to the north and has a maximum throw of 125 m. Along strike to the west, the fault is offset by several north-northeast-striking faults. Along strike to the east, the Jims Peak fault is intruded by an andesite porphyry pluton that follows the contact between Paleozoic rocks and the Pearsons Peak andesite.

Kinematics

In the late Miocene to Quaternary, the Palmetto area experienced two distinct extensional events whereas early Miocene rocks record an additional extension direction that the younger strata did not experience. This sequence of superposed late Cenozoic extension directions (Fig. 1.9) is recognized by analysis of 383 fault-slip measurements (slickenlines) that were collected in

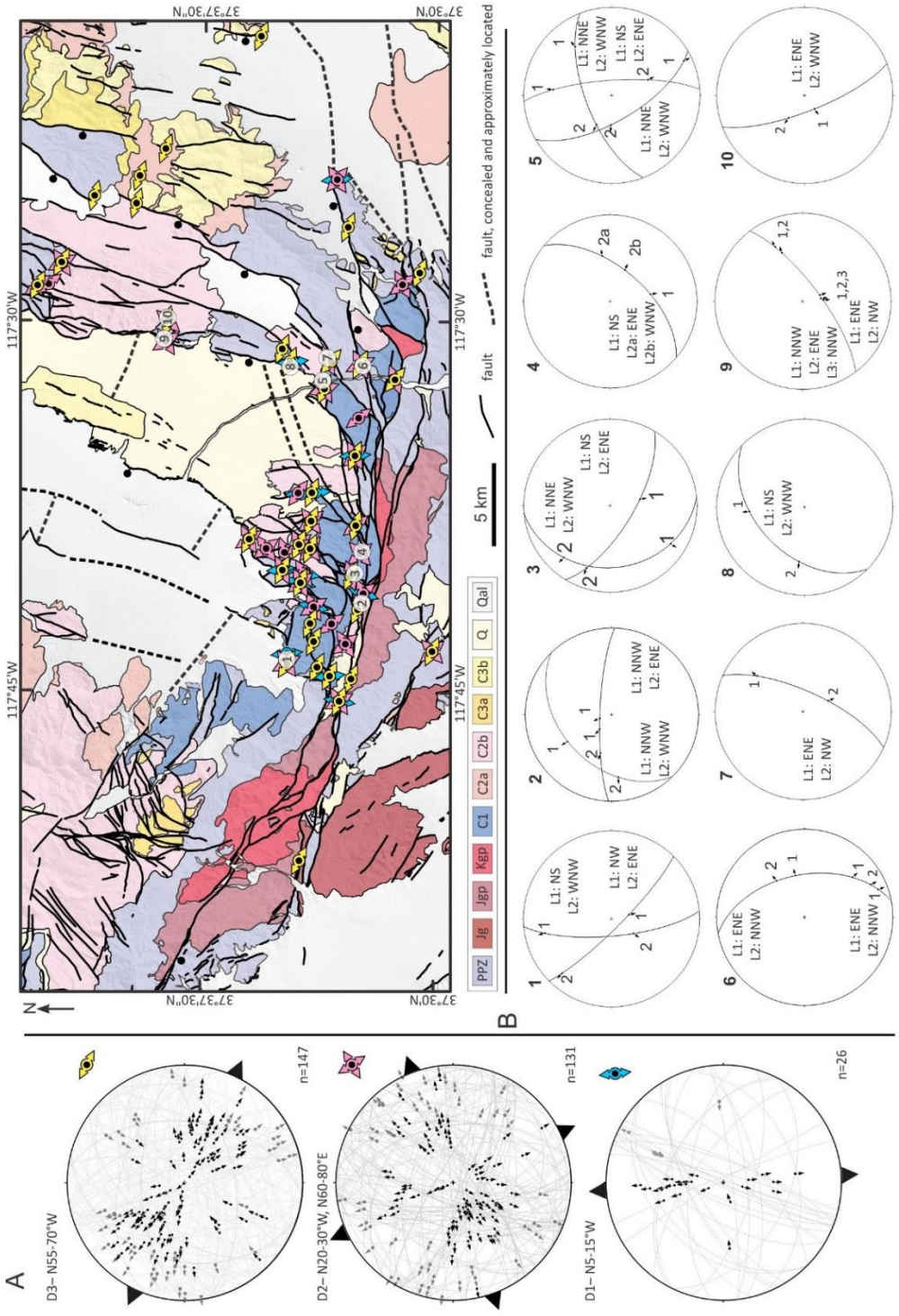

Figure 1.9. Geologic map showing the spatial distribution of fault-slip data, and steroenets illustrating superposition slickenlines and orientation of three extension directions.

rocks of all ages along the major faults and their damage zones (Katopody et al. in review). A subset of 26 measurements indicates early Miocene north-south extension and the remaining 357 measurements can be related to younger extensional events seen in the late Miocene to Quaternary stratigraphy. Directly following north-south extension, there was a period of non-plane strain expressed as simultaneous northwest and east-northeast extension (D2) followed by west-northwest stretching (D3).

The orientations and sequence of extensional events were determined using a graphical method (Gephart, 1990; Marret and Allmendinger, 1990) and were plotted first by hand and then by using FaultKin 7 (Allmendinger et al., 2012). Strain-rate axes were determined for each slip surface using three criteria measured in the field: 1) the attitude of slickensides, 2) rake of slickenlines on the slip surface, 3) the sense of fault motion along the slickenlines using shear sense indicators (Twiss and Unruh, 1999) established by Gamond (1987), Hancock et al. (1987), and Petit (1987). The relative ages of slip events was recorded where individual fault surfaces preserve multiple generations of cross-cutting slickenlines. Sets of similar cross-cutting relationships were used to create a sequence of three distinct events from which extensional axes for each event were derived. Non-superposed slip measurements were then parsed into groups of coordinated slip based on the orientation of superposed extensional axes beginning with the contemporary extension direction and proceeding into deeper time until the only remaining slip data formed a north-south extensional axis. The groups of fault-slip data were then inverted to strain-rate fields (Twiss and Unruh, 1999) and used to determine the orientation of extension.

The youngest and contemporary extension (D3) is oriented N55W to N70W and is recognized in rocks of all ages across the basin and certainly occurred post-7.6 Ma. This

extensional event has a secondary strain axis oriented north-northeast that geographically varies from extension to shortening in response to areal changes in fault geometry (Katopody et al., in press). Minor north-northeast extension occurs on the curved segments of faults as is documented in other parts of the central Walker Lane (Ferranti et al., 2009; Webber et al., 2017). In contrast, north-northeast shortening is spatially localized at fault intersections in the west-central part of the Palmetto foothills where the line of intersection between west-northwest—striking south-dipping faults and north-northeast—striking west-dipping faults are misaligned from the contemporary extension direction by 20° to 40° (Katopody et al., in review).

The second extensional event (D2) consists of two extensional axes oriented N20W to N30W and N60E to N80E that are recognized on faults across the Palmetto foothills. These two extension directions operated simultaneously as indicated by mutually cross-cutting slickenlines at stations 1, 6, 7, and 9. Given the simultaneous timing of the D2 extension directions, both groups of slip are younger than the north-south lineations cut by east-northeast lineations. Northwest and east-northeast (D2) lineations are themselves crossed by west-northwest (D3) lineations on two accounts at stations 2 and 10.

North-south extension (D1) consists of a single extension direction oriented N5W to N15W. Lineations associated with north-south extension are preserved in the damage zones of all west-northwest and north-northeast—striking faults that bound the early Miocene basin but are only developed in the Pearsons Peak andesite and older pre-Cenozoic rocks. Additionally, preservation of north-south slip on east-west—striking faults that are sealed by the upper-most unit of the Pearsons Peak andesite demonstrate that north-south extension was ongoing at least up until the end of Pearsons Peak andesite time. This is consistent with cross-cutting

relationships that show lineations associated with north-south extension (D1) are always cut by younger events as can be seen at stations 1, 3, 4, and 8. These stations show that north-south (D1) lineations are cut by D2 lineations (east-northeast) on three accounts and by west-northwest (D3) lineations on three accounts.

Reorientation of Fault Motion

The reorientation of crustal stretching indicates that early Miocene faults did not have the same shear senses as their late Miocene to Quaternary counterparts. West-northwest—striking faults originated as normal faults prior to reactivation as strike-slip faults whereas north-northeast—striking normal faults were originally sub-parallel to the extension direction.

Although contemporary faults disrupt much of the Palmetto area, early Miocene north-south extension is consistent with the generalized geometry of the west-northwest—trending andesite basin. The elongate basin is bordered by west-northwest—striking faults that dip basin-ward and are bordered by high-angle north-northeast—striking faults at the west and east edges of the basin. The north and south tilts of the lower Pearsons Peak andesite indicate that the west-northwest—striking faults had more dip-slip displacement than the north-northeast faults and controlled basin subsidence. The north-northeast—striking faults are aligned with the early Miocene extension direction and what little dip-slip motion the faults had merely accommodated basin subsidence and tilting along the west-northwest—trending master faults. Recognition of the relationship between north-south extension and the geometry of early Miocene faults precludes the possibility that the thick accumulation of Pearsons Peak andesite and stratal geoemtries seen in the Palmetto Mountain half-graben formed by the dip-slip component of

movement along a strike-slip fault as proposed by Speed and Cogbill (1979) for a similar basin in west-central Nevada.

EARLY MIOCENE BASIN GEOMETRY, STRATIGRAPHY AND STRUCTURES

The early Miocene west-northwest—trending half-graben controlled deposition of the Pearsons Peak andesite and emplacement of andesitic intrusive rocks. Andesite in and around the basin is divided into a lower synextensional unit and an upper post-extensional unit, the older of which is intruded by andesitic dikes and a hypabyssal pluton. The base of the andesite rests on Paleozoic metasedimentary rocks and within the basin dips north and south causing the depth to basement to increase across the axis of the half-graben into west-northwest—striking master faults. North-northeast—striking transfer faults segmented and bounded the basin and allowed along-strike changes in dip and thickness. Eastward tilting of the basin axis exposes the base of the andesite to the west and whereas the andesite is buried by northeast-dipping late Miocene tuff to the east.

Stratigraphy and Basin Geometry

Throughout the Palmetto area, the Pearsons Peak andesite is composed of lahar, lava flows, tuff and volcaniclastic sedimentary rocks that are grouped into several unconformity-bound, prismatic sequences that record early Miocene fault displacement or lack thereof. The lithology and thickness of the unit changes dramatically across the Palmetto area, with abrupt changes occurring across known and inferred high-angle faults. The uniform stratal geometries and thicknesses indicate that the Pearsons Peak andesite in the Cow Camp and Lida Wash areas lie outside the boundaries of the early Miocene half-graben whereas age-equivalent rocks in the

Palmetto Mountains can be split into a lower unit that lies within the basin and an upper unit that overlies the basin. Here, we outline the spatial variability in lithology and thickness of the Pearsons Peak andesite presented in stratigraphic sections (Fig. 1.6). The sections were measured from north to south across the width of the basin except for column 2 that was pieced together from several stratigraphic sections. Considering faults in the Palmetto foothills show normal displacement, some structural omission may exist despite our efforts to minimize it. Together with a geologic map (Fig. 1.4), the sections (Fig. 1.5) provide critical stratigraphic relations used to reconstruct the early Miocene basin geometry.

Cow Camp Area

In the Cow Camp area (Figs. 1.3, 1.4, and 1.6), the Pearsons Peak andesite depositionally overlies Paleozoic strata and is unconformably overlain by Rhyolite Ridge Tuff. The Pearsons Peak andesite varies from 120 to 150 m thick and is composed of four units of alternating lahar and lava flows. The basal unit consists of massive lahar that varies in thickness from zero to 30 m and fills depressions in the underlying Paleozoic strata. Where the basal unit is absent, overlying flows rest directly on Paleozoic rocks. These flows have a thickness of 40 m and pass upward into 30 m of lahar which in turn is overlain by another 50 m of flows. The lithologic transition between units is abrupt and, with the exception of the basal unit, the lithologic units have uniform thicknesses.

The compositions of the lahar and lava flows are uniform in the Cow Camp area. The lahar shows no internal stratification, is poorly sorted, and is composed of 50 to 80 percent grains and clasts supported in a porphyry matrix. The angular to subangular grains and clasts range in size from 2 mm to 40 cm and consist of about 85 percent andesite porphyry and 15 percent

Paleozoic metasedimentary rocks. The porphyritic matrix is composed of 40 to 50 percent phenocrysts consisting of plagioclase, hornblende, and biotite in a gray aphanitic groundmass. The andesite lava is massive and lacks any flow foliations or preserved contacts between individual flows. The lava composition is uniform and contains 20 to 30 percent phenocrysts of plagioclase, hornblende, and biotite supported in an aphanitic groundmass that weathers dark gray to dark red.

Lida Wash Area

Pearsons Peak andesite in the Lida Wash area (Fig. 1.6) rests unconformably on Paleozoic metasedimentary rocks and is overlain by the Argentite Canyon Formation with angular unconformity. The succession has a thickness of 180 to 210 m and consists of a lower section of volcaniclastic sediments and lahar overlain unconformably by an upper section of lava flows. The lower unit, which is absent at about 75 percent of exposures, ranges in thickness from zero to 35 m and is overlain by the upper unit which has a uniform thickness of 180 m.

The lower section is dominated by andesite lahar and subordinate volcaniclastic sediment that infills depressions in the Paleozoic substrate. The lahar ranges from zero to 20 m thick with lateral continuity of 400 to 800 m. The volcaniclastic sedimentary rocks are restricted to the base of the section and fill channels from 10 to 15 m thick and 50 to 70 m wide. The lahar has uniform composition throughout exposures, shows no internal stratification, and is poorly sorted. The lahar consists of 50 to 60 percent grains and clasts supported in a grey porphyritic groundmass. The angular to subangular grains and clasts range in size from 2 mm to 25 cm and consist of about 85 percent andesite porphyry and 15 percent Paleozoic metasedimentary rocks. The porphyritic matrix is composed of 20 to 30 percent phenocrysts of plagioclase (50%),

hornblende (30%), and biotite (20%) in a gray aphanitic groundmass. The sedimentary rocks consist of interbedded diamictite and volcanogenic wacke in sets that range in thickness from 2 to 4 m. The base of the sedimentary rocks consistently is a diamictite ranging in thickness from 1.5 to 2 m that passes upward into 0.5 to 1 m interbeds of volcaniclastic wacke and diamictite. The transition from diamictite into wacke occurs over 3 to 5 cm, in contrast to the upper contact of the wacke with overlying diamictite, which is sharp and erosional, showing occasional scour and fill structures. The diamictite contains 50 to 80 percent angular to subangular clasts ranging from 1 to 30 cm composed of andesite porphyry (80%) and Paleozoic metasediments (20%) in a brown wacke matrix. The wacke matrix is massive and composed of 70 to 80 percent angular to subangular lithic grains ranging from 0.5 to 1 mm in an argillite matrix. The interbeds of volcaniclastic wacke have wavy laminations ranging from 5 to 10 mm thick but exhibit the same composition and granulometry as the diamictite matrix.

The andesite lava of the upper unit is poorly exposed and largely covered by float. In cliff-forming outcrops, the lava generally is massive but does exhibit some ledges 30 to 40 m thick. No well-preserved contacts between individual flows are recognized. In some locations, however, 3 to 10 mm thick flow-foliations are preserved over distances of a few meters. The lava composition is uniform and contains 25 to 30 percent phenocrysts of plagioclase (50%), hornblende (30%), and biotite (20%) supported in an aphanitic groundmass that weathers dark red, purple, and gray.

Palmetto Foothills

In the Palmetto foothills, synextensional lower Pearsons Peak andesite within the basin records the asymmetric geometry of the half-graben (Fig. 1.5) and is overlain by post-extensional

upper Pearsons Peak andesite. The post-extensional upper Pearsons Peak andesite is 40 to 60 m thick and rests sub-horizontally on several tilted units of the lower Pearsons Peak andesite and Paleozoic rocks at isolated outcrops scattered across the Palmetto foothills. The lower Pearsons Peak andesite rests directly on Paleozoic rocks and reaches a maximum aggregate thickness of 1510 m.

The lower Pearsons Peak is composed of two synextensional stratal wedges that preserve the asymmetric geometry of the early Miocene half-graben (Figs. 1.4 and 1.5) through southward and northward dips at the base of the andesite section and divide the basin into eastern and western domains. In the eastern domain of the half-graben, southward dips of 50° near the base of the lower Pearsons Peak andesite indicate that the shallowest part of the basin occurs to the north along the Jims Peak fault and increases depth southward to the deepest part along the Palmetto Mountain fault system where the depth reaches 1.5 to 2.0 km depending on how the dip of the Pearsons Peak andesite is projected. In the western domain, the shallowest part of the half-graben lies in the basin's center, parallel to the basin axis and exposes the basal contact of the Pearsons Peak andesite with Paleozoic rocks. The basin depth increases to the north and south from this shallow area into the west-northwest—striking basin-bounding faults as indicated by the 10° to 15° north dip of sequence one and the 30° southward dip of sequence two.

The upper Pearsons Peak andesite and the stratal wedges of the lower andesite are composed of interleaved lava flows, lahar, tuff, and volcaniclastic sedimentary rocks. The upper Pearsons Peak consists of lava flows that are generally massive but locally exhibit folded flow bands. The flows locally comprise cliff-forming outcrops that exhibit ledges 3 to 10 m high that are traced along strike for 150 to 200 m but no well-preserved contacts between individual flows

are recognized. The two sequences that comprise the lower Pearsons Peak andesite exhibit an upward increase in the relative abundance of sedimentary rocks with respect to the volcanic rocks (Fig. 1.6). Sequence one is lithologically dominated by lava flows and lahars but contains minor sedimentary rocks and channel-filling tuff. Sequence two also contains flows and lahars but has large component of interleaved diamictites and lithic sandstones all capped by a tuff-tuffaceous sediment section.

Sequence One of the Lower Pearsons Peak Andesite. Sequence one of the lower Pearsons Peak andesite forms 600 to 905 m thick prismatic wedges that variously tilt south and north and are divided in to three depositional successions. The sequence increases thickness along strike from 600 m in the western domain to 905 m in the eastern domain across north-northeast—striking faults of the Clayton Valley fault system. The successions in the eastern domain take the form of a southward-thickening prism in contrast to the western domain where the units progressively thin to the south and onlap the underlying Paleozoic strata. In the western domain, the lower-most succession (Unit 1) has a minimum thickness of 40 m and pinches out to the south. The exact thickness and distance across which thinning occurs is veiled by the overlying units but we are confident in the estimated minimum thickness. The lower unit pinches out over a distance no greater than 1500 m and is overlapped by the middle unit (Unit 2) which rests directly on Paleozoic strata. The middle unit in turn thins to the south from a maximum thickness of 300 m over a lateral distance of 1700 to 2300 m. The overlying succession (Unit 3) oversteps Unit 2 by at least 625 m and has a thickness of about 260 m.

While the basal unit (Unit 1) predominately consists of lahar, the succession contains interleaved flows and sedimentary rocks. The lahar forms successions 30 to 40 m thick and are

mapped along strike for kilometers. The interleaved lava flows are about 5 m thick maintain a constant thickness along strike for hundreds of meters. In the eastern area (Figs. 1.4 and 1.6), the upper portion of the unit exhibits a 20 m thick succession of alternating sedimentary rocks and flows that fill a depression 800 to 1300 m wide in the lahar. The sedimentary rocks consist of interbedded diamictite 1 to 2 m thick and volcanic sandstone 20 to 50 cm thick. The sedimentary rocks amalgamate to form successions 3 to 5 m thick that are interleaved with lava flows 1 to 5 m thick.

The middle unit (Unit 2) is composed of lava flows and subordinate lahar that has a heterogeneous lateral distribution across the Palmetto foothills. In the eastern area, lahar comprises about 25 percent of the unit and decreases to about 10 percent over a distance of 3 km. Successions of flows, with individual thicknesses of 3 to 4 m, show cumulative thicknesses 40 to 70 m. The flow successions are separated by 10 to 20 m thick beds of lahar that were deposited in steeply-walled channels hundreds of meters wide that were cut down into the lava flow successions. In one instance, the unit exposes a 2 to 3 m thick bed of andesitic air fall tuff that is traced along strike for tens of meters and accumulated in a channel.

The upper unit (Unit 3) is composed of lahar interleaved with occasional beds of lava. The lahar is massive and well-preserved bedding was not recognized. Successions of lahar are traced along strike for a several kilometers and show an upward increase in thickness from 20 m in the lower portion of the unit to 90 m near at the top. The flows show a corresponding upward decrease in abundance but do not show a systematic change in thickness. The interleaved flows are 5 to 20 m thick and are localized in channels that are hundreds of meters wide.

Sequence Two of the Lower Pearsons Peak Andesite. Sequence two of the lower Pearsons Peak andesite consists of three successions that each take the form of southward-thickening prisms across both eastern and western domains, and tend to vary in thickness along strike. The units have an aggregate thickness that increases from 600 m in the eastern domain to 725 m in the western domain across north-northeast—striking strands of the Clayton Valley fault system. Lahar and lava flows decrease upward in abundance with respect to the sedimentary rocks that are overlain by a succession of tuff and tuffaceous sediments. The sequence consists of a basal succession (Unit 4) 180 to 270 m thick, overlain by a 175 to 325 m thick middle unit (Unit 5) that in turn passes upward in to an upper unit that is 100 to 120 m thick (Unit 6).

The basal unit (Unit 4) consists of alternating lahar and lava flows capped by a thin section of sedimentary rocks. Within the lower volcanic zone, lahar forms successions 30 to 50 m thick and are interleaved with lavas that progressively decrease in thickness and abundance upward from amalgamations 35 to 60 m thick to 3 to 5 m thick individual lavas. Flow and lahar successions generally form sheets and are laterally continuous over a few kilometers, but on occasion are localized in 3 to 30 m deep channels that are 400 to 500 m wide. At the base of the volcanic section, sedimentary beds of coarsening-upward volcaniclastic rocks fill channels, 0.5 to 1 m deep and 5 to 30 m wide that cut downward into the lower sequence. Sedimentary interbeds with similar dimensions and lithology are observed in lahar successions throughout the unit. The upper sedimentary section, about 20 m thick, is composed of interbedded diamictite and subordinate volcanic sandstone.

The middle unit (Unit 5) consists of a lower section of volcaniclastic sediments overlain by an upper section of volcanic rocks. The two sections show abrupt, east-to-west variations in

thickness across a 1 km wide zone of faulting. In the vicinity of Pearsons Peak, the sedimentary section is 105 m thick and is overlain by the volcanic section that is 75 m thick; whereas to the west, the sedimentary section thins to 65 m and the volcanic section thickens to 260 m. The sedimentary section consists of a 5 to 10 m thick basal succession of scoria breccia overlain by successions of diamictite that occasionally pass upward into clast-supported conglomerate and volcanic sandstone. Where outcrops preserve both contacts of an individual diamictite, beds range in thickness from 1 to 4 m. Elsewhere, successions of diamictite reach thicknesses of 20 m. The volcanic section is composed of lava flows and subordinate lahar. The flows range in thickness from 20 to 60 m and are laterally continuous along strike for a few kilometers. Lahar is 15 to 30 m thick and is localized in steep-walled channels 60 to 100 m wide.

The upper succession (Unit 6) is composed of three tuffs that are lithologically similar and are separated by interbeds of tuffaceous sediments. The tuffs generally consist of a basal vitrophyre that passes upward into a lithic ash flow overlain by air fall tuff. The basal vitrophyre, 1 to 10 m thick, is porphyritic and often shows folded flow banding. The ash flow typically is white in color and nonwelded with one unit weathering grey and showing weak welding. The upper air fall tuff is white and massive. Locally within the succession, contacts between individual tuffs reaching thicknesses of 30 to 40 m can be distinguished by the presence of lenticular sedimentary interbeds. The sedimentary rocks accumulated in channels 10 cm to 12 m deep and 15 to 200 m wide. The interbeds variously consist tuffaceous breccia, granitoid breccia, volcanogenic argillite, and fining-upward tuffaceous sediment.

Stratal and Fault Geometries

Although contemporary faults disrupt the geology of the Palmetto area, early Miocene faults formed a rectilinear network of west-northwest and north-northeast to north-south—striking faults as demonstrated by growth relationships that controlled the spatial distribution, thickness and dip of the lower Pearsons Peak andesite. The thickest accumulation of Pearsons Peak andesite lies within the west-northwest—trending basin outlined by the Jims Peak fault to the north, the Palmetto Mountain fault system to the south, the Oasis Divide fault to the west and the Clayton Ridge fault system to the east, whereas age-equivalent rocks outside this area are an order of magnitude thinner. The following sections outline the stratal geometry of the lower Pearsons Peak andesite and geometry of early Miocene faults to provide timing, areal extent, and displacement constraints on early Miocene faulting.

West-Northwest—Striking Master Faults

Andesite within the half-graben increases thickness across the basin axis (Fig. 1.5) forming prismatic wedges that mimic the asymmetric geometry of the basin and truncate into west-northwest—striking faults. The asymmetric wedges in the lower Pearsons Peak andesite were formed by upward decreases in the southward or northward dip by 10° to 25° degrees. The relationship between the asymmetric stratal patterns and west-northwest—striking faults indicate the basin-fill was incrementally tilted during deposition by movement on listric faults.

Differential south and north dips of coeval andesite units between the eastern and western domains show that influence of the each master fault on basin geometry varied through time. In the eastern domain, the entire lower Pearsons Peak andesite forms a single wedge that is tilted south consistent with the basin's southern polarity and decreases southerly dip upward from 50°

near the base of the section to 25° near the top along the Palmetto Mountain fault system. Pearsons Peak andesite in the western domain likewise reflects the area's bipolar geometry by comprising two stratal wedges with one deposited on the other. Sequence one of the lower Pearsons Peak andesite forms a wedge that increases thickness northward into the basin deep along the Jims Peak fault whereas the overlying sequence two decreases southerly dip upward from 35° to 25°, increasing thickness into the basin deep along the Palmetto Mountain fault system, consistent with age-equivalent strata in the eastern domain.

Fortunately, the early Miocene geometry of the Jims Peak fault preserves a type example of the master faults that bound the half-graben. Unlike the Palmetto Mountain fault system, the Jims Peak fault was not reactivated by late Miocene to Pliocene extension and therefore did not experience a change in shear sense. Slickenlines found along the fault and related east-west—striking faults to the south demonstrate dip-slip motion in the early Miocene consistent with northward thickening wedge of andesite that truncates into Jims Peak fault.

The early Miocene antecedent to the Palmetto Mountain fault system is disrupted by its contemporary incarnation. Although the present-day Palmetto Mountain fault system has a maximum length of 70 km, the trace-length of the antecedent structure occupied a 15 km long segment that lies between the modern Oasis Divide fault and Clayton Ridge fault system. The early Miocene segment of the fault system consists of the two southern fault strands that separate south-dipping lower Pearsons Peak andesite from Paleozoic and Mesozoic rocks underlying thin, flat-lying tuff to the south. Fault-slip data collected along these strands show dip-slip motion occurred prior to their reactivation as part of the Palmetto Mountain fault system.

North-Northeast—Striking Transfer Faults

The thickness and lithologic composition of the Pearsons Peak andesite changed along the axis of the west-northwest—trending basin in addition to across-strike changes. The thickness and lithologic changes abruptly occur across high-angle north-northeast—striking faults and are often accompanied by changes in dip direction and angle. The north-northeast—striking faults are orthogonal to the west-northwest—trending master faults and terminate the axis of the half-graben at its western and eastern edges. Although disrupted by modern normal displacement, the north-northeast—striking faults in the early Miocene were parallel to the extension direction and acted as transfer faults (Gibbs, 1984), accommodating basin subsidence along the half-graben's master faults.

The north-northeast—striking transfer faults are located along the western and eastern margins of Pearsons Peak andesite outcrops (Fig. 1.4) and in the center of the west-northwest—trending half-graben separating the eastern and western domains. The transfer faults are disrupted by contemporary faults that occupy the same location and exhibit normal displacement and late Miocene to Quaternary growth relationships. The transfer fault that segments the half-graben likely terminated to the north and south into the west-northwest—striking master faults because there's no significant early Miocene dog-leg in the center of the basin. The western and eastern bounding transfer faults align with the contemporary north-northeast—striking segments of the Oasis Divide fault and Clayton Ridge fault system that separate alluvium from bed rock and likely extended northward along the edges of the modern Clayton Valley. The transfer faults likely did not extend southward past the Palmetto Mountain fault system because offset segments of the structures are not present on the footwall of the contemporary fault system.

A transfer fault separated the eastern and western domains of the west-northwest—trending half-graben and is disrupted by late Miocene to Quaternary faulting. The transfer fault was oriented north-south parallel to strands of the Clayton Valley fault system that form the western flank of present-day Pearsons Peak and stretched from the Palmetto Mountain fault system to the Jims Peak fault. Late Miocene growth strata bury much of the region so the exact location of the transfer fault lies within the area that is 300 m wide to the east and west between Pearsons Peak and Jims Peak. The transfer fault juxtaposed shallowly north-dipping andesite of the western domain with steeply south-dipping andesite of the eastern domain. The transfer fault juxtaposed a 600 m thick section of lower Pearsons Peak andesite sequence one that dips shallowly north in the western domain with equivalent strata in the eastern domain that are 905 m thick and dip steeply south. Sequence two of the lower Pearsons Peak andesite increases thickness from 600 to 725 m across the transfer fault but dips south on both sides.

A north-northeast—striking transfer fault formed the western edge of the half-graben. The fault juxtaposes lower Pearsons Peak andesite resting on Paleozoic rocks in the Palmetto foothills to the east with Paleozoic metasedimentary rocks to the west. Early Miocene rocks are absent directly west across the fault but are present on the same fault block 2 to 4 km to the north in the Cow Camp area where Pearsons Peak andesite is thin and lies sub-horizontally and Paleozoic rocks. To the east, thick synextensional sequences of the lower Pearsons Peak andesite dip shallowly north and steeply south. The base of the Pearsons Peak andesite within the half-graben is exposed overlying Paleozoic rocks as a result of eastward tilting of the basin and erosion recorded by the late Miocene tuffs.

The transfer fault and eastern edge of the half-graben are buried by the eastward dip and extensive deposits of late Miocene tuff and thus no true structural juxtaposition is observed. Nevertheless, edge of the half-graben must lie along the 5 km east-west distance between andesite exposures near Pearsons Peak and Clayton Ridge where the andesite is absent and late Miocene tuff sits on Paleozoic rocks. The most likely location is along the range front of Clayton Ridge because the ridge provides the first indication that the Pearson Peak andesite is absent toward the east and the Lida Wash section of Pearsons Peak andesite lies nearby to the south although it is separated from Clayton Ridge and southeast Clayton Valley by northeast and east-northeast—striking faults of the Clayton Ridge and Palmetto Mountain fault systems.

Intrusive Rocks

In the Palmetto foothills (Fig. 1.4), Paleozoic rocks and Pearsons Peak andesite are intruded by a hypabyssal pluton and a series of dikes. The dikes, numbering 18 in total, have east-west trends that parallel the half-graben axis and steeply cross cut Pearsons Peak andesite. The hypabyssal pluton trends east-northeast and intrudes Paleozoic metasedimentary rocks and the base of the Pearsons Peak andesite. The pluton is surrounded by an elongate, west-northwest—trending alteration aureole (Figs. 1.4 and 1.10) that is 8 km long and 0.5 to 1.5 km wide, and tracks the Jims Peak fault. The alteration caused discoloring in Paleozoic rocks and argillization and silicification of the lower Pearsons Peak andesite and east-west—striking dikes. Altered rocks are intruded by the hypabyssal pluton and overlain by the upper Pearsons Peak andesite which both remain unaltered. The pluton, dikes and Pearsons Peak andesite have the same phenocryst composition suggesting that the extrusive and intrusive rocks are genetically related.

Hypabyssal Pluton

The hypabyssal pluton is exposed along the northern flank of Pearsons Peak (Fig. 1.4) and is mostly structureless but locally preserves columnar joints. The pluton intrudes lower Pearsons Peak andesite and the depositionally underlying Paleozoic rocks, and is elongate to the east-northeast and west-southwest for a distance of 2000 to 2125 m. The intrusive rock follows the contact westward for about 1250 m to where the pluton steps 125 to 150 m south and is entirely contained within the lower member of Pearsons Peak andesite. To the east and west, the pluton is cut by faults that strike north and northeast, respectively, and dip away from the intrusive rock. The hanging-walls of these faults do not expose the pluton so the full length of the intrusion is unknown. The width of the pluton greatly varies from 100 to 500 m but typically is in the range of 375 to 500 m. The hypabyssal pluton generally is massive but in a few locations where outcrops are well preserved at the margins of the pluton, it exhibits columnar joints that plunge 50° to 65° north.

The pluton is a plagioclase, hornblende, biotite porphyry. It is composed of 60 to 80 percent phenocrysts of plagioclase (40%), hornblende (30%), and biotite (30%) in an aphanitic groundmass that is dark purple to black. The phenocrysts are euhedral and exhibit a lateral increase in size from the margin of the pluton to the center. Generally, phenocrysts range in size from 1 to 5 mm but toward the center of the pluton crystals of hornblende reach widths of 8 mm and lengths of 5 cm.

East-West—Striking Dikes

The dikes generally crop out in the center of the Palmetto foothills (Fig. 1.4). Out of the 18 dikes recognized in the Palmetto foothills, 16 intrude Paleozoic rocks and the lower member

of Pearsons Peak andesite whereas the remaining two dikes extend upward into the middle member. The dikes typically crop out in groups of 4 to 8 that are 150 to 500 m wide and are traced along strike for 150 to 200 m but also occur individually. The orientations of the dikes vary in strike from east-northeast to west-northwest and in dip from 70° to 85° north and south indicating the dikes were emplaced during a period of north-south extension. Individual dikes typically range in width from 1 to 2 m but can be as thin as 30 cm. Where out crops are well preserved, dikes are traced along strike for 100 to 150 m. In a few locations, dikes are exposed perpendicular to the faces of sheer cliffs and can only be traced along strike for a few meters.

The dikes are plagioclase, hornblende and biotite porphyries that and vary from 10 to 45 percent phenocrysts. The phenocrysts consist of plagioclase (60 – 70%), hornblende (15 – 20%), and biotite (15 – 20%) all supported in an aphanitic, gray groundmass. The phenocrysts vary in size and crystal habit: subhedral plagioclase is 2 to 3 mm, subhedral to euhedral hornblende is 1 to 3 mm, and subhedral biotite is 2 mm in diameter.

Argillic Alteration

The Palmetto area underwent localized alteration (Fig. 1.10) ranging from argillic to advanced argillic. The higher end of alteration occurred exclusively in the Pearsons Peak andesite and andesitic dikes, whereas localized pods of alteration occurred in Paleozoic rocks. The alteration broke down the andesite into clay and also silicified localized areas. The effects of alteration on the andesite will be discussed in more detail below. Alteration of Paleozoic rocks is expressed as discoloration. Carbonate and siliciclastic rocks that were originally tan and green are discolored to pink or purple. The alteration is divided into two halos: an outer halo of argillic alteration and an inner halo of advanced argillic alteration. The outer halo is 300 to 1700

m wide and grades into the inner halo over 40 to 50 m. The inner halo is 4.5 km long and 700 to 1500 m wide.

Within the Pearsons Peak andesite section, the alteration changed the color, composition and degree of lithification of the altered rocks. The alteration bleached the andesitic rocks and discolored them to yellow or white. On occasion the altered rocks contain stockwork composed of silica veinlets that are red to purple in stark contrast to the bleached country rock. Within the outer halo, the alteration is gradational from the outer margin toward the center. Bedding, contacts, and foliations are in large preserved. Likewise, lithic clasts and phenocrysts are preserved although the color of the feldspar population is altered to white. In contrast, the advanced argillic alteration in the inner halo almost completely breaks down the andesitic rocks into clay and locally created silicified zones. Except where silicified, the lithification strength of the rocks is reduced to friable and often crumbles into powder upon touch. The alteration obliterated bedding, contacts and foliations, and lithic clasts and phenocrysts are rarely preserved. The most commonly preserved phenocrysts are feldspars that are bleached white. Biotite is rarely preserved and amphibole was not observed. Occasionally, the altered rocks contain crystals of gypsum measuring up to 14 cm in diameter. Locally, nodules of chert that are 0.5 to 2 m thick and 5 to 10 m wide are present. The andesitic dikes present within the inner halo are silicified and form “spines” that protrude from the less weather-resistant altered andesite.

The alteration forms a west-northwest trending exposure belt that follows the Jims Peak fault along strike in the Palmetto foothills, and elsewhere in the Lida Wash area, a pod of alteration occurs along major strands of the Palmetto Mountain fault system. The intensity of the

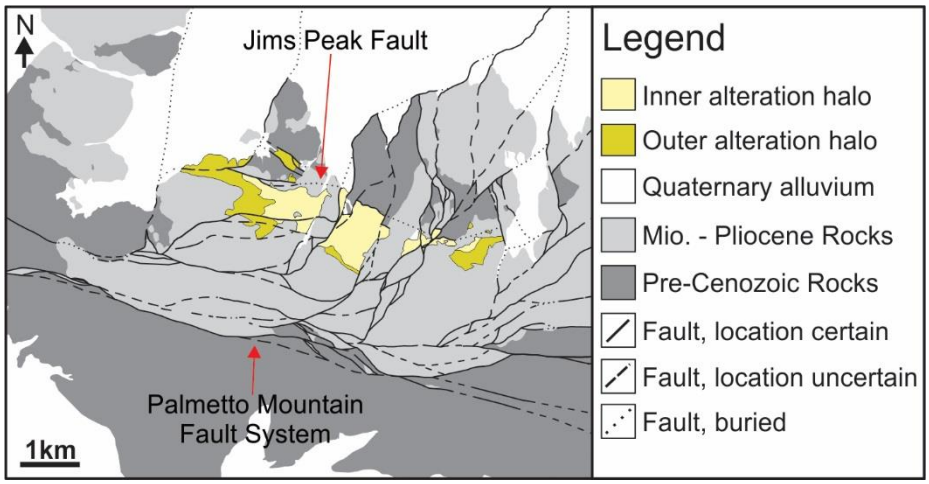

Figure 1.10. Geologic map illustrating the distribution of argillic alteration along the Jims Peak fault.

alteration sharply decreases across the Jims Peak fault which juxtaposes the Pearsons Peak andesite to the south with Paleozoic strata overlain by a thin section of andesite to the north. The alteration in the Pearsons Peak andesite along the southern side of the Jims Peak fault is argillic to advanced argillic. Along the northern side of the Jims Peak fault, the alteration developed as localized halos near the fault, following along strike for 100 to 230 m and extending up to 100 m into the country rock.

The alteration is most developed in the lower sequence of the Pearsons Peak andesite but locally alters the underlying Paleozoic rocks at the base of the andesite and extends upward into the base of the middle sequence of the Pearsons Peak andesite. The lower boundary of alteration coincides with the depositional base of the Pearsons Peak andesite. Here, the alteration either arrested at the depositional contact or extends 2 to 3 m into the underlying Paleozoic strata and grades into unaltered country rock over 15 to 30 cm. However, the lower parts of the andesite are not altered where the base of the section is exposed. The upper boundary of the alteration,

occurring within the Pearsons Peak andesite, has an irregular, sinusoidal geometry with a topology of 100 m. The upper boundary of alteration lies above the unconformity between the lower and middle sequences precluding the option that the alteration predates deposition of the middle sequence. In the eastern Palmetto foothills, the alteration exhibits the same sinusoidal shape but is less developed and does not extend into the middle sequence due to the thickness increase observed in the lower sequence across the Clayton Valley fault system.

The pluton was emplaced post-alteration and possibly formed as a late-stage upward migration of magma that plugged the Jims Peak fault and extruded lava flows of the upper Pearsons Peak. Altered rocks and the eastern half of Jims Peak fault are intruded by the andesitic pluton that shows no sign of alteration. In contrast to the irregular shape of the alteration, the pluton shows a more linear east-west to east-northeast trend, and as a result the pluton cross cuts the alteration boundary, intruding both altered and unaltered rocks. The plutonic contact is not well exposed and obscured by talus. Where in contact with Paleozoic rocks, the pluton is sharp and typically shows no sign of alteration. However, in a couple locations, a halo of alteration extends outward 65 to 70 m into Paleozoic strata from the contact with the pluton. The altered rocks and western half of Jims Peak fault are depositionally overlain by the upper Pearsons Peak andesite and the Rhyolite Ridge Tuff that contains clasts of argillic altered andesite at its base. The lower contact of the upper sequence is sharp and while the exact location of the contact is not exposed, it is resolved to within 1 to 3 m. These stratigraphic relationships indicate that the alteration, as well as activity on the Jims Peak fault is Miocene in age.

Andesite Correlation

Regional stratigraphic correlations of the early Miocene andesite section indicate that the Pearsons Peak andesite was deposited between 22 and 15 Ma. The Pearsons Peak andesite has similar lithologic composition and stratal patterns to andesite in the Monte Cristo Range and eastern Excelsior Mountains. The angular unconformity that divides the andesite stratigraphy into lower and upper units is recognized in all three areas. The lower Pearsons Peak andesite correlates to the Blair Junction sequence (22 to 15.7 Ma) because they share a generalized stratigraphic pattern with a basal lava flow and lahar-dominated section that passes upward into more clastic-rich rocks including, pyroclastic and sedimentary lithofacies. The correlation is consistent with the 22 to 19 Ma ages of the lower andesite unit in the eastern Excelsior Mountains that lie within the 22 to 15.7 Ma age range provided by the Blair Junction sequence. The lower unit in each of these areas is intruded by andesitic intrusive rocks that are associated with argillization and silification in the Palmetto Mountains and Excelsior Mountains. The upper Pearsons Peak andesite correlates to the Gilbert Andesite and upper andesite unit in the Excelsior Mountains because the section is dominated by volcanic lithofacies and the base of the section forms an angular unconformity recognized across the region. Deposition of the upper andesite unit occurred around 15 to 15.7 Ma after the lower andesite unit was tilted in each area.

DISCUSSION

There was a period of north-south extension in the early Miocene prior late Miocene to Quaternary extension and the formation of modern physiography. North-south extension is best exemplified by the west-northwest—trending Palmetto Mountains half-graben that controlled deposition of the Pearsons Peak andesite. The geometry of the early Miocene basin, faults, and

stratal patterns, the east-west orientation of early Miocene intrusive rocks, and fault-slip analysis all indicate north-south extension occurred in the early Miocene.

The Palmetto Mountains half-graben was disarticulated by younger extension related to the Silver Peak-Lone Mountain extensional complex and present-day Clayton Valley. After the Palmetto Mountains half-graben was sealed by the upper Pearsons Peak andesite around 15.7 to 15 Ma, the Palmetto area was tectonically quiescent until extension resumed between 7.6 and 6.1 Ma as indicated by the synextensional stratal geometry in the Rhyolite Ridge Tuff and the lack thereof in the Tuff of Oasis Divide. Contemporary faulting that started at 5 to 3 Ma exposes deeper parts of the half-graben which allows us to see nearly the entire geometry of the basin instead of the just the upper layers of the basin-fill like similar half-grabens elsewhere in the Great Basin (Speed and Cogbill, 1979; Hardyman and Oldow, 1991). Fortunately, motion and tilting on late Miocene to Quaternary faults is low enough that the internal geometry of the early Miocene basin is still preserved unlike in other examples of these east-west—trending basins where faulting and high-angle eastward and westward dips disrupt the internal geometry of the basins (John et al., 2008).

Kinematic History of the Palmetto Mountains Half-Graben

The master faults and transfer faults that formed the west-northwest—trending half-graben (Fig. 1.11) operated simultaneously as indicated by syndepositional relationships between each set of faults and the basin-fill. The recognition of coordinated fault motion acknowledges the equal influence that both the master faults and the transfer faults had on forming the geometry of the half-graben. Whereas master faults are commonly known to control the direction of hanging wall tilt (McClay and Ellis, 1987), the transfer fault that segmented the

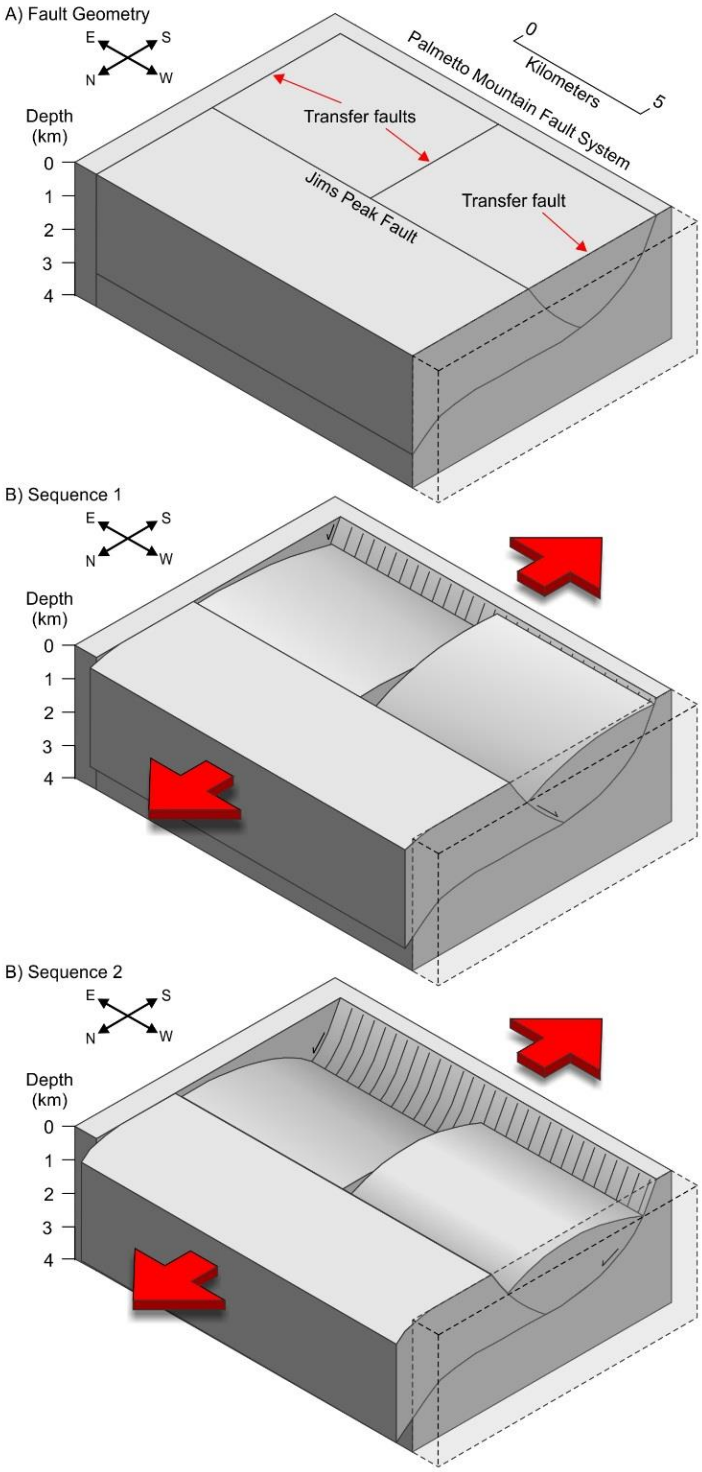

Figure 1.11. Block model of the Palmetto Mountains half-graben illustrating the history of basin subsidence, fault motion, and reversal of tilt direction during deposition of the Pearsons Peak andesite.

center of the Palmetto Mountain half-graben assisted tilting by transferring displacement from the Palmetto Mountain fault system northward to the Jims Peak fault which resulted in reversed polarity along the basin axis during deposition of the sequence one as indicated by the unit forming a southward thickening wedge east of the fault and a northward thickening wedge west of the fault (Fig. 1.5). Decoupling of the east and west sides of the half-graben enabled basin subsidence along opposing master faults to reverse the tilt direction similar to half-grabens of the Suez rift (Garfunkel and Bartov, 1977) and the East African rift (Rosendahl et al., 1986; Morley et al., 1990). During deposition of sequence two (Fig. 1.11), displacement was consolidated along the southern boundary of the half-graben decreasing the influence of the transfer fault. This is indicated by the southerly tilt of the sequence along the entire trace-length of the basin (Figs. 1.4 and 1.5) and caused the west domain of the half-graben to tilt south in contrast to the northerly tilt during deposition of sequence one. Reversal of basin polarity during andesite deposition in the west part of the basin caused strata of sequence two to overlie the sequence one with angular unconformity in contrast to the east domain where the same contact is paraconformable. The Jims Peak fault, along the northern margin of the half-graben, had either low displacement or was inactive during deposition of sequence two and was subsequently sealed by the upper Pearsons Peak andesite near the end of basin subsidence.

The asymmetric geometry of stratal wedges that recorded these tilt directions formed by syndepositional normal fault movement along listric master faults. The hanging walls within the half-graben formed rollover anticlines (Figs. 1.4 and 1.11) in response to the listricity of the master faults with a ramp-flat geometry which localized shortening (Dahlstrom, 1969; Gibbs, 1983; Buchanan and McClay, 1991; McClay and Scott, 1991) and deformed the basin-fill into

gentle, east-west—trending (F1) folds. The incremental rollover-related tilting of the hanging walls occurred simultaneously with deposition as indicated by the upward decrease in dips of the basin-fill (Hamblin, 1965; Gibbs, 1984; Leeder and Gawthorpe, 1987; Ellis and McClay, 1988; Janecke et al., 1997) meaning that the younger, upper parts of the basin-fill is less folded than the base of the section. The curvature of the master faults was modeled by using the downward increasing dips of sedimentary rocks within the stratal fans and a constant cutoff angle between synextensional strata and the master faults as the structures were projected to depth in order to preserve line length and fault-block volume despite the hanging wall changing shape (Dahlstrom, 1969; Gibbs, 1983; Morley, 1989). This method predicts that the master faults decrease in dip with increasing depth until forming a flat below the half-graben at a depth of 2 to 3 km (Fig. 1.11). Subsidence over the flat was negligible resulting in reduced accommodation space above the flat even though the depth of the basin continued to increase along the steeper parts of the master faults. The reduced accommodation space prevented younger units from overstepping the underlying units resulting in an offlap stratal pattern (Fig. 1.4) as opposed to the classic onlap geometry. The Palmetto Mountains half-graben is not alone in exhibiting this offlap geometry as it is seen in other basins (Janecke et al., 1997, Schlische, 1992) and is perhaps a more widespread phenomenon than originally thought.

Transfer faults that bound the half-graben (Fig. 1.11) accommodated basin subsidence by transferring excess displacement out of the fault system. The depth of the half-graben interpreted from synextensional basin-fill shows that displacement on the master faults was 1.5 to 2.0 km. This displacement must have transferred out of the fault system because 1.5 to 2.0 km of throw cannot be accommodated on isolated structures that were 10 to 15 km long as

demonstrated by displacement-length scaling relationships (Cowie and Scholz, 1992) without accumulating unresolved strain at the fault tips. Transfer faults bounded the half-graben and removed displacement from the fault system allowing the basin to maintain its depth at the western and eastern margins where the basin-fill is juxtaposed with pre-Cenozoic rocks. Displacement from the master faults of the half-graben was transferred northward to andesite basins in the neighboring Silver Peak Range or possibly to similar east-west—trending half-grabens (Fig. 1.1) recognized by Speed and Cogbill (1979) and Hardyman and Oldow (1991). The displacement was not transferred to the east or west because outcrops of Pearsons Peak andesite show no sign of synextensional deposition and are juxtaposed with asymmetric basin-fill across the basin-bounding transfer faults suggesting an abrupt termination of the half-graben axis. There are likewise no outcrops of age-equivalent andesite south of Lida Wash to suggest displacement was transferred to the south. Along this line of thought, we have yet to recognize southern continuations of the transfer faults that would have been offset eastwardly on the south side of the present-day Palmetto Mountain fault system which showed Pliocene to present sinistral motion after the early Miocene half-graben ceased activity (Katopody et al., in review). Displacement transferred northward through the north-south striking fault was taken up on another west-northwest striking fault that controlled deposition of the early Miocene andesite in the Silver Peak Range.

Estimation of Ancient Extension Directions

North-south extension determined from fault-slip inversion is consistent with the trend of the Palmetto Mountains half-graben, stratal wedges in the Pearsons Peak andesite, and east-west—trending intrusive rocks within the basin but it does not necessarily indicate that these

geometric features can be individually used to determine extension directions. The trend of the Palmetto Mountain half-graben was controlled by the late Cenozoic depositional boundary that also allowed the late Miocene to Quaternary reactivation of pre-existing structures as growth faults under different extension directions. Likewise, the east-west orientation of andesitic dikes and the hypabyssal pluton lies sub-parallel to the basin axis and therefore may also be influenced by crustal anisotropy as opposed to uniquely defining north-south extension. Pearsons Peak andesite stratal wedges within the half-graben indicate that the Jims Peak fault and the antecedent to the Palmetto Mountain fault system had early Miocene dip-slip motion but do not define a unique extension direction because the strike-slip component of displacement is not recorded. The in-situ dip direction of the Pearsons Peak andesite is the sum of multiple deformations unrelated to the extension direction including hanging wall rollover, localized shortening over a ramp-flat fault geometry, and eastward tilting recorded by the late Miocene Tuff of Oasis Divide and Rhyolite Ridge Tuff.

The strike of transfer faults are commonly thought to be aligned with the extension direction (Gibbs, 1984) and were identified in the Palmetto Mountains half-graben by the combined use of stratal patterns and fault geometry. Given the orthogonal geometry of the early Miocene faults, stratal wedges formed by lower Pearsons Peak andesite indicate that the west-northwest—striking faults were the master faults whereas the north-northeast—striking faults acted as transfer faults by accommodating changes in dip direction and thickness along the basin axis. The transfer faults are only misaligned by 5° to 20° from the extension direction so could be used to estimate the extension direction in cases where fault-slip inversion cannot be used or is impractical.

Spatial Extent of East-West—Trending Half-Grabens and North-South Extension

The prevalence of other west-northwest, east-west and east-northeast—trending half-grabens containing late Oligocene to early Miocene basin-fill (Figs. 1.1 and 1.2) suggests that north-south extension occurred in other areas outside the Palmetto Mountains. Half-grabens in the Mina deflection have similar geometries to basins in the Palmetto Mountains and Silver Peak Range although the basin axes trend east-northeast trends and east-west (Speed and Cogbill, 1979; Hardyman and Oldow, 1991; Kerstetter et al., 2016). The composition of basin-fill within the half-grabens varies in age from late Oligocene to early Miocene suggesting a complex spatial-temporal pattern of extension.

Deposits of andesite in and around a west-northwest—trending basin in the Silver Peak (Fig. 1.2) Range are of particular interest due to their proximity to the Palmetto Mountains. Aside from the Pearsons Peak andesite in the Palmetto Mountains, synextensional stratal patterns exhibited by the early Miocene andesite in the Silver Peak Range indicate that the Palmetto Mountains half-graben is just one part of a larger system of half-grabens that were active prior to the mid-Miocene to Quaternary. The half-graben system (Fig. 1.12) has a rectilinear geometry composed of west-northwest—trending basins with a 35 to 40 km trace-length and features an 8 km dog-leg in the basin axis between the Palmetto Mountains half-graben and the Silver Peak half-graben. The Silver Peak half-graben spans 25 km across the Silver Peak Range and is at least 5 km wide although the northern edge of the basin is buried by various units of the mid-Miocene to Pliocene rocks. The Icehouse Canyon fault bounded the basin to the south and exhibits across-fault thickness changes characteristic of synextensional deposition in both the early Miocene andesite and the overlying mid-Miocene to Pliocene sequence (Oldow et al.,

2009) similar to early and late Miocene sequences adjacent to the Palmetto Mountain fault system.

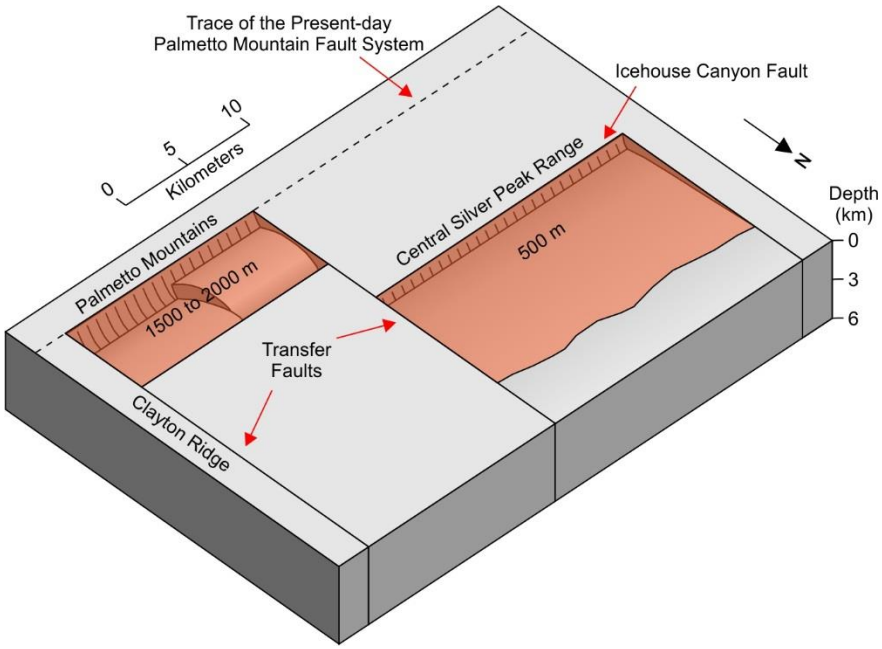

Figure 1.12. Schematic block model of the Palmetto Mountains half-graben, the Silver Peak half-graben and north-south—striking transfer faults.

The early Miocene half-grabens were connected by a north-south to north-northeast—striking transfer fault. The transfer fault accommodated the dog-leg in the basin axis between the Palmetto Mountains and Silver Peak Range parts of the half-graben system. The Palmetto Mountains half-graben has a depth of 1,500 to 2,000 m and is deeper than the Silver Peak half-graben that is 500 m deep (Oldow et al., 2009). Displacement was transferred from the Palmetto Mountain fault system with a depth of 1,500 to 2,000 m to the Silver Peak Range half-graben with a depth of 500 m. Due to the difference in depth between the Palmetto Mountains and Silver Peak half-grabens, the transfer fault likely reached northward past the Silver Peak Range to east-west or east-northeast—trending basins in the Mina deflection. The remaining

displacement not present on the Icehouse Canyon fault was likely transferred north to other late Oligocene to early Miocene basins.

The discrepancy in the trends of late Oligocene to early Miocene basins can be explained by post-late Miocene vertical-axis rotation. This includes the Palmetto Mountain half-graben within the region that experienced 20° to 30° of clockwise vertical axis rotation during the waning stages and folding of the detachment fault (Oldow et al., 2008). Restoration of the vertical axis rotations would change the original orientation of the west-northwest—trending half-grabens to an east-west or east-northeast trend (Fig. 1.12) and the azimuth of north-south extension to a more north-northwesterly orientation.

CONCLUSIONS

The late Cenozoic extension direction changed from north-south extension in the early Miocene to west-northwest extension. North-south extension was expressed by the formation of west-northwest—trending half-grabens in the early Miocene. Motion on west-northwest and north-northeast—striking faults acted together to accommodate deposition of the early Miocene andesite in the Palmetto Mountains. The internal geometry of the half-graben varied along strike from east to west as a result of differential displacement on basin-bounding faults. Half-graben activity began around 22 Ma and ceased motion by 15.7 to 15.1 Ma when the basin was sealed by the upper andesite sequence and was further buried by late Miocene tuff at 7.6 to 6.1 Ma. The west-northwest—trending half-graben provides insight into the tectonic setting prior to the onset of detachment faulting and formation of associated north-northeast—trending basins. North-south extension ended by 15.7 to 15.1 Ma after which the kinematics of the west-northwest and north-south—striking faults changed. During the late Miocene, rocks of the Coyote Hole Group

locally sealed the west-northwest—trending half-graben. Reactivated faults of the half-graben syndepositionally controlled the spatial distribution and internal geometry of the late Miocene tuffs.

CHAPTER 2

ARCHITECTURE, KINEMATICS, AND DEVELOPMENT OF WIDESPREAD LATE OLIGOCENE TO EARLY MIOCENE EAST-NORTHEAST AND WEST-NORTHWEST TRENDING EXTENSIONAL BASINS DURING NORTH-SOUTH EXTENSION IN THE WESTERN GREAT BASIN

INTRODUCTION

Prior to the onset of Basin and Range extensional faulting and topography, a late Eocene to early Miocene volcanic and sedimentary succession was deposited throughout the Great Basin (Fig. 2.1) although whether or not an older period of extensional faulting accompanied the magmatism remains controversial. The late Eocene to early Miocene succession consists of basalt lavas, andesitic flows and lahars that pass upward into silicic ignimbrites overlain by another succession of andesite flows, lahars, and sedimentary rocks (Proffett and Proffett; 1976; Burke and McKee, 1979; Whitebread and Hardyman, 1988; John et al., 2008). Late Eocene to early Miocene volcanism migrated 200 km south-southwest across the Great Basin from northern Nevada at about 40 Ma to south-central Nevada at about 20 Ma (Dickinson, 2006) at rates that decreased from 20 to 4 km/my (Henry and John, 2013). As volcanic fronts migrated south-southwest, late Eocene to early Miocene strata formed 100 to 200 m thick sheets that maintained uniform thickness over tens to hundreds of kilometers indicating paleotopography had minimal influence on deposition throughout most of the Great Basin (Best and Christiansen, 1991) except where the volcanic and sedimentary succession abruptly increased thickness up to 500 to 2500 m within deep basins (Burke and McKee, 1979; Henry et al., 2012). The basins trend east-northeast, east-west, and west-northwest, are 4 to 10 km wide and 0.5 to 2.5 km deep (Proffett,

1977; Speed and Cogbill, 1979; Henry and Faulds, 2010). Remnants of the easterly trending basins exhibit discontinuous trace-lengths of 10 to 25 km forming a dog-leg basin geometry exposed in the present-day mountain ranges (Hardyman and Oldow, 1991; Faulds et al., 2006). The origins of the basins are alternatively explained by extensional faulting or non-structural undulations in paleotopography (Burke and McKee, 1979; Henry et al., 2012; Henry and John, 2013) leading to debate about the tectonic state of the Great Basin during late Eocene to early Miocene magmatism. Understanding the mechanisms for forming these basins is key to understanding the tectonic setting of the Great Basin during Late Eocene to early Miocene magmatism.

Deposition of late Eocene to early Miocene volcanic and sedimentary rocks within east-northeast, east-west, and west-northwest—trending fault-bounded, extensional basins (Fig. 2.1) indicates that fault activity accompanied magmatism (Burke and McKee, 1979; Speed and Cogbill, 1979) but some of these basins are alternatively interpreted as erosion-controlled valleys that lack basin-bounding faults suggesting that faulting instead postdated magmatism (Henry and John 2013). Many of the east-west—trending basins are bounded by east-west—striking normal faults (Proffett, 1977; Ekren and Byers, 1985; Gonsior and Dilles, 2008) and have therefore been interpreted as asymmetric "volcano-tectonic toughs" or half-grabens in several cases (Burke and McKee, 1979; Speed and Cogbill, 1979; Hardyman and Oldow, 1991). The basin-fill within several basins forms south-dipping asymmetric stratal wedges with upward decreasing dips, and shows across-fault changes in thickness indicative of growth faulting similar to other extensional basins in the East African Rift, the Gulf of Mexico, and the present-day Basin and Range (Garfunkel and Bartov, 1977; Vreeland and Berrong, 1979; Bally, 1982; Gibbs, 1984; Ratcliffe,

et al., 1986; Rosendahl et al., 1986; Morley et al., 1990; Schlische, 1992; Hudec and Jackson, 2007). The easterly trends of the basins, southward tilts of strata within the basins, and east-west strikes of dikes that intrude the basin-fill have been used as evidence for an earlier period of north-south extension prior to the onset of modern west-northwest extension (Oldow and Steuer, 1985; Best, 1988; Hardyman and Oldow, 1991). In other cases, formation of the east-west—trending basins have been attributed to a network of westward-flowing rivers indicated by sparse fluvial sediments within the basins and are seemingly devoid of any structural control (Henry and Faulds, 2010; Henry et al., 2012).

Simultaneous magmatism and extensional faulting is demonstrated in the Mina-Dyer region of west-central Nevada (Fig. 2.2) by a network of six east-northeast and west-northwest—trending half-grabens that formed during late Oligocene to early Miocene volcanism and indicate a prior history of north-south extension before the onset of modern faulting and topography. Synextensional deposition is demonstrated by late Oligocene and early Miocene rocks within the half-grabens that form 0.5 to 1.5 km thick asymmetric wedges, exhibit upward decreases in dip, and thicken into east-northeast to west-northeast—striking faults that bound the basins. Age equivalent strata deposited outside the half-grabens are 100 to 200 m thick and flat-lying indicating that areas outside the late Oligocene and early Miocene basins did not experience synextensional deposition. The trends of basin axes, stratal geometry within the half-grabens, and east-west—trending dike swarms and hypabyssal plutons, all indicate that the basins formed under north-south extension. Superposed fault-slip data collected in all six half-grabens demonstrate that north-south extension is the earliest recognized extension direction and is restricted to development in the late Oligocene to early Miocene basin-fill and pre-Cenozoic

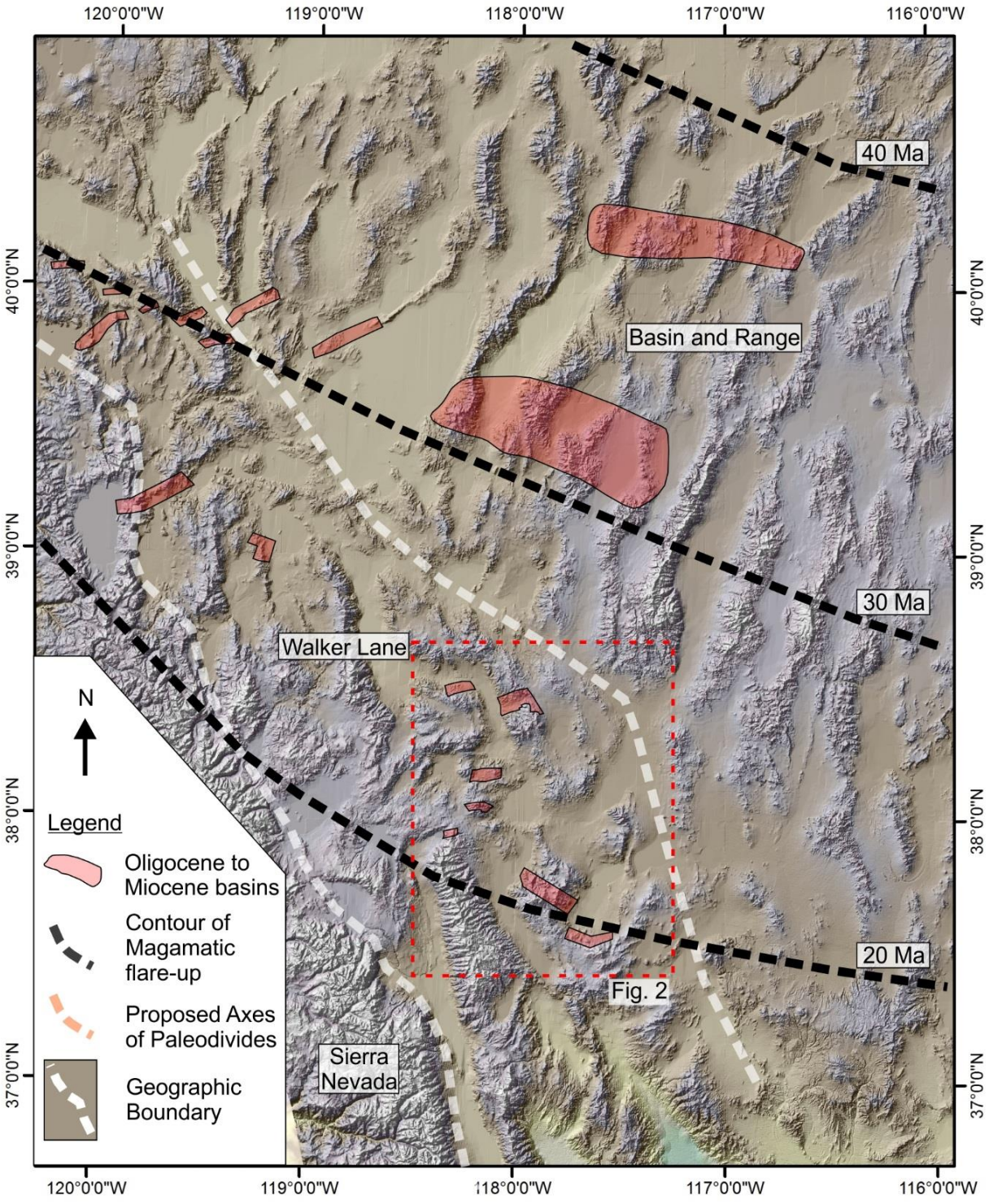

Figure 2.1. Annotated physiographic map of the western Great Basin.

rocks. Mid-Miocene to Quaternary rocks that postdate development of the half-grabens do not record slickenlines associated north-south extension. Uneven spatial distribution of late Oligocene and early Miocene synextensional strata indicates that the east-northeast and west-northwest—trending half-grabens formed asynchronously such that some basins are only late Oligocene, only early Miocene, or late Oligocene to early Miocene in age. Despite forming deep half-grabens, north-south extension was low-magnitude and formed low-relief long wavelength topography as indicated by the spatial distribution of Late Cenozoic and early Miocene strata.

REGIONAL SETTING

The Mina-Dyer region (Fig. 2.2) is a 15,000 km^2 area that consists of alternating mountain ranges and basins. The ranges and basins comprise approximately equal parts of the region and have east-west dimensions of 5 to 25 km and north-south dimensions that range from 10 to 70 km. The ranges and basins trend north-northwest, north-northeast, east-west. Basins in a couple locations exhibit triangular prismatic geometries adjacent to the intersections of north-northwest and east-northeast—trending ranges. Basin elevations range from 1300 to 1500 m whereas the ranges vary from hills at 1800 to 2100 m to mountains at 2400 to 2600 m elevation. The highest topography is found in the White Mountains that increase elevation from 2600 m in the south to a maximum of 4007 m in the north.

Fault Geometry

The Mina-Dyer region (Fig. 2.2) hosts an array of north-northwest, north-northeast, west-northwest, and east-northeast—striking faults that separate the present-day basins from the mountain ranges and also cross the ranges. The north-northwest faults form two 40 to 50 km

wide zones, the Fish Lake Valley-Owens Valley fault zone (FLV-OV) and the Walker Lane (WL), that are misaligned by 60 to 70 km and are connected to each other by a complex system of east-northeast, west-northwest and north-northwest—striking faults (Lock, 1940; Oldow, 1992; Oldow et al., 1994). The misaligned north-northwest fault zones are connected by east-northeast—striking faults of the Mina deflection (MD) that curve through over 90° at their terminal ends and merge with the north-northwest faults (Oldow, 1992). A 70 km long system of west-northwest—striking faults, the Palmetto Mountain fault system, emanate from the FLV-OV fault zone and curve to into an east-west trend (Katopody et al., in review). A horsetail array of north-northeast—striking faults splay 50 to 60 km northward from the PMFS and connect to north-northwest structures of the WL (Katopody et al., in review; Kerstetter et al., in prep). A set of low-angle extensional faults are locally exposed and crossed by contemporary north-northwest, north-northeast, west-northwest, and east-northeast faults (Oldow et al., 1994; Cland and Oldow, 2017) however gravity surveys suggest that some inactive north-northeast—striking faults may sole into the detachment faults at depth (Ng and Oldow, 2017).

Walker Lane faults (Fig. 2.2) predominately strike north-northwest and stretch for 50 to 70 km along strike but the areas between individual faults are often crossed by 2 to 5 km long east-west or east-northeast faults that terminate into the north-northwest structures (Hardyman and Oldow, 1991). Active north-northwest faults exhibit right-lateral motion indicated by offset markers and geodetic surveys (Lock, et al., 1940). Within the ranges, east-west and east-northeast faults show dog-leg steps of 3 to 20 km across the north-northwest faults (Oldow and Meinwald, 1992). The east-west and east-northeast faults step to the left and right across the north-northwest structures and do not consistently show a right step (Oldow and Dockery, 1993).

West-northwest to east-west faults of the PMFS and nearby unnamed structures (Fig. 2.2) form 25 to 70 km long fault zones that are connected via 10 to 15 km long north-northeast—striking faults (Oldow et al., 2009; Katopody et al., in review). Intersection of nearly perpendicular faults and termination into one another creates a dog-leg geometry such that faults variously step 1 to 10 km left and right across each other (Kerstetter et al., in prep). West-northwest and east-west—striking faults form the southern boundary of the fault array from which north-northeast faults diverge (Katopody et al., in review). Many north-northeast faults terminate at their northern and south ends into the through-going west-northwest and east-west faults whereas new and reactivated faults continue north toward the Walker Lane (Oldow et al., 2009).

Lithologic Units

In the Mina-Dyer region (Fig. 2.2), silicic tuffs, andesite flows and lahars, and sedimentary rocks associated with the ignimbrite flare-up and subsequent andesite magmatism are late Oligocene to early Miocene in age, are unconformably overlain by mid-Miocene to Quaternary strata and underlain by Proterozoic to Mesozoic metasedimentary, intrusive rocks, and metamorphic tectonites (Proffett and Proffett, 1977; Ekren and Mckee, 1985; Robinson et al., 1968; Crowder et al., 1972; Henry and John , 2013). The pre-Cenozoic rocks consist of Proterozoic to Mesozoic siliciclastic and carbonate metasedimentary rocks that are complexly folded and faulted by Paleozoic to Mesozoic shortening and are intruded by Jura-Cretaceous plutons (Snyder et al., 1976; Oldow, 1981, 1984; Oldow et al., 1989). Metamorphic tectonites were exhumed by low-angle normal faults and are not locally exposed in the mountain ranges (Oldow et al., 1994). Cenozoic rocks widely vary in lithology including lava flows, ash flows,

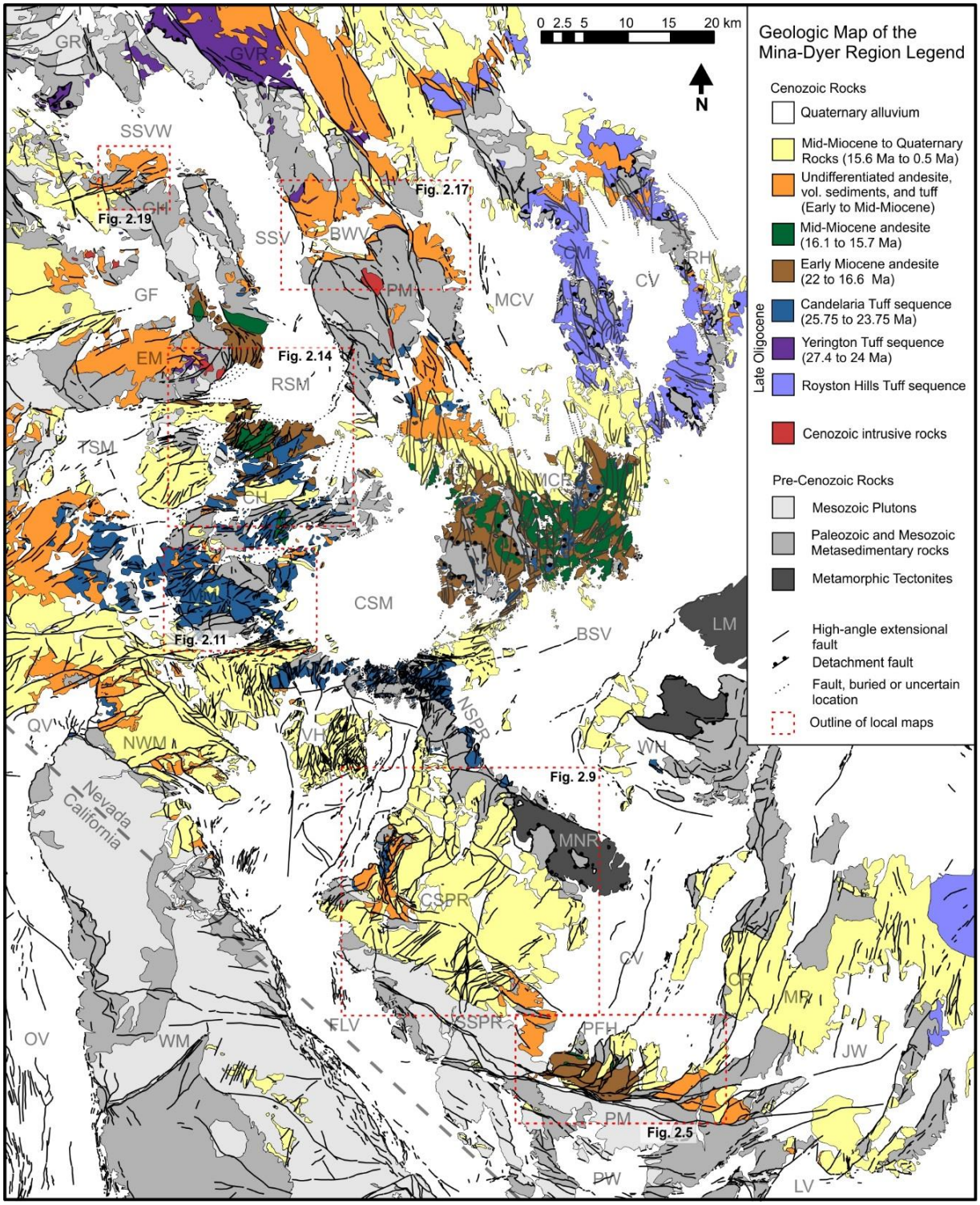

Figure 2.2. Geologic Map of the Mina-Dyer Region lahars, ignimbrites, sedimentary rocks, and intrusive rocks and composition including silicic, andesitic and basaltic igneous rocks (Albers and Stewart, 1972).

The Cenozoic stratigraphy in the Mina-Dyer region (Figs. 2.2 and 2.3) consists of three major successions: Late Oligocene to early Miocene, mid-Miocene, and late Miocene to Quaternary. The late Oligocene to early Miocene and late Miocene to Quaternary successions are lithologically diverse and show significant lateral variations in composition, age and thickness (Oldow et al., 2009; Henry and John, 2013). The late Oligocene to early Miocene succession varies in thickness from 100 to 2000 m and consists of several ignimbrite sequences that vary in composition and age and are overlain by andesite flows, lahars, tuff, and volcaniclastic sedimentary rocks (Robinson et al., 1968; Albers and Stewart, 1972; Stewart, 1974; Ekren and Byers, 1976; Garside, 1979; Speed and Cogbill, 1979; Ekren and McKee, 1985; Stewart et al., 1994; Petronis et al., 2009). The Late Miocene to Quaternary succession varies in thickness from 20 to 3600 m and consists of ash flows, air fall tuff, lava flows, and fluvial, alluvial, and lacustrine sedimentary rocks (Albers and Stewart, 1972; Bachman, 1978; Stockli et al., 2003; Elias, 2005; Oldow et al., 2009, 2016). In contrast, the mid-Miocene succession that lies between the two variable successions consists of only two lithologies, flows and lahars, and maintains a fairly constant thickness of 60 to 100 m where the unit is recognized throughout the region (Stewart et al., 1994; Cland and Oldow, 2017; Kerstetter et al., in prep). However, in many areas the andesite units are undifferentiated (Figs. 2.2 and 2.3) because the similar lithologic composition of mid-Miocene and early Miocene andesite units makes it difficult to differentiate the two successions.

Lateral variations in thickness and stratigraphic omission of entire Cenozoic successions form unconformities that separate the three Cenozoic successions such that each unit rests on the pre-Cenozoic substrate and each of the older Cenozoic successions (Albers and Stewart, 1972;

Garside, 1979; Stewart et al., 1994). In areas, where the late Oligocene to early Miocene succession is omitted, the mid-Miocene andesite succession rests directly on pre-Cenozoic rocks (Garside, 1979; Stewart et al., 1994). Likewise, the late Miocene to Quaternary succession rests on late Oligocene to early Miocene rocks and pre-Cenozoic rocks where the mid-Miocene andesite succession is absent (Robinson et al., 1968; Crowder et al., 1972; Stewart, 1979; Ekren and Byers, 1985). Many of these thickness changes and stratigraphic omissions occur across old and new faults as will be discussed in the following sections (Speed and Cogbill, 1979; Oldow et al., 2009; Tincher and Stockli, 2009).

Late Oligocene to early Miocene Succession

The late Oligocene and early Miocene succession consists of late Oligocene ignimbrites, tuffaceous sediments and andesite, and early Miocene andesitic flows, lahars, tuff, and volcaniclastic sedimentary rocks (Robinson et al., 1968; Albers and Stewart, 1972; Ross, 1961). Late Oligocene section that forms the base of the Cenozoic stratigraphy primarily consists of ignimbrites with minor interbeds of tuffaceous sediments, and locally contains a basal unit of andesite flows that are 15 to 50 m thick (Garside, 1979; Ekren and Byers, 1985). The late Oligocene rocks have an aggregate thickness that ranges from 20 to 1000 m as a result of deposition around faults that were active in the late Oligocene (Speed and Cogbill, 1979; Hardyman and Oldow, 1991). The early Miocene section is 100 to 1500 m thick and consists of andesite lava flows and lahars that pass upward into volcaniclastic sedimentary rocks and is sometimes capped by a sequence of ash flow tuffs and tuffaceous sediments (Dover, 1962; Robinson et al., 1968; Stewart et al., 1994; Kerstetter et al., in prep).

The late Oligocene succession consists of three age-equivalent sequences that are spatially segregated (Figs. 2.2 and 2.3) and are all unconformably overlain by early Miocene andesite (Proffett and Proffett, 1976; Ekren and Byers, 1985; Speed and Cogbill, 1979; Whitebread and Hardyman, 1988; Stewart et al., 1994; Henry and John, 2013). The three sequences are named after type sections in the Yerington district, the Candelaria Hills, and the Royston Hills and are all wells exposed in the Mina-Dyer region (Proffett and Proffett, 1976; Speed and Cogbill, 1979; Whitebread and Hardyman, 1988). The early Miocene andesite succession, dubbed the Blair Junction andesite by Stewart and other (1994), rests on all three late Oligocene tuff sequences in their respective geographic areas with angular discordances of 15° to 25°, and where the ignimbrites are absent, rests directly on pre-Cenozoic rocks (Garside, 1979; Speed and Cogbill, 1979; Oldow and Meinwald, 1992; Oldow and Dockery, 1993). The unconformity between the late Oligocene and early Miocene rocks is characterized by channels that are scoured into the silicic ignimbrites and filled with breccias at the base of the andesite section (Speed and Cogbill, 1979).

Late Oligocene Units. The late Oligocene tuff sequences are spatially separated (Figs. 2.2 and 2.3) by 10 to 25 km wide ranges and basins in the present day (Ekren and Byers, 1985; Speed and Cogbill, 1979; Whitebread and Hardyman, 1988). The Yerington sequence is separated from the Candelaria sequence by the Garfield Hills, Excelsior Mountains, and Pilot Mountains (Garside, 1979; Speed and Cogbill, 1979; Ekren and Byers, 1985; Oldow and Steuer, 1985). The Candelaria sequence is in turn omitted south of the northern White Mountains and central Silver Peak Range (Robinson et al., 1968; Crowder et al., 1972; Tincher and Stockli, 2009). The Yerington and Candelaria sequences are in separated from the Royston Hills

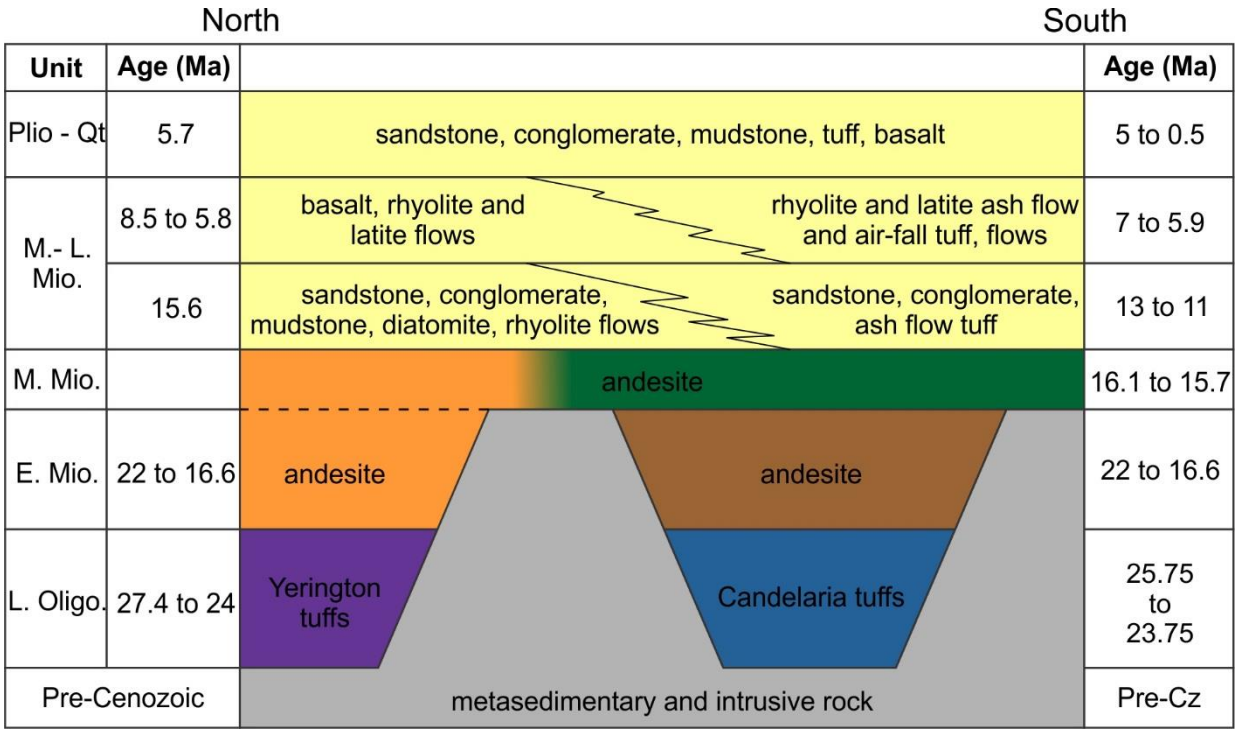

Figure 2.3. Stratigraphic correlation diagram for the Mina-Dyer region illustrating the timing relations, lithology, and north to south differences in the major rock units.

sequence by Monte Cristo Valley and Clayton Ridge (Oldow and Meinwald, 1992; Katopody et al., in review).

The boundaries of the tuff sequences often coincide with east-northeast and north-northeast—striking faults (Fig. 2.2) and more rarely, buttress unconformities, across which the units dramatically decrease thickness or are omitted from the stratigraphy (Speed and Cogbill, 1979; Hardyman and Oldow, 1991; Oldow et al., 2009). The spatial distribution of the Yerington sequence in the Gillis Range, Gabbs Valley Range and Bettles Well Valley shows a dog-leg geometry that aligns with faults along the northern Pilot Mountains and northern Garfield Hills (Ekren and Byers, 1985; Oldow and Dockery, 1993). The northern boundary of the Candelaria sequence coincides with faults along the southern flank of the Excelsior

Mountains (Garside, 1979; Speed and Cogbill, 1979) but depositionally laps onto the southern face of the Pilot Mountains (Oldow, personal communication). Likewise, faults form the southern boundary of the Candelaria sequence in the northern White Mountains and central Silver Peak Range (Tincher and Stockli, 2009; Oldow et al., 2009). The boundary that separates the Royston Hills sequence from the Yerington and Candelaria sequences coincides with the Clayton Ridge fault (Kerstetter et al., in prep) but it is uncertain whether the boundary at Monte Cristo Valley is structural or depositional given its proximity to the buttress unconformity in the southern Pilot Mountains.

Within these restricted areas, the tuff sequences individually form 100 to 200 m thick deposits that covered areas of 1,500 to 2,000 km^2 (Speed and Cogbill, 1979; Stewart, 1979). The tuff sequences locally increase thickness up to 1000 m across east-northeast and north-northwest—striking faults that were active during the late Oligocene (Speed and Cogbill, 1979; Hardyman and Oldow, 1991).

The Yerington sequence (Fig. 2.2) is composed of silicic ignimbrites, intermediate lavas and subordinate sedimentary rocks exposed in the Gillis Range, southern Gabbs Valley Range, northern Pilot Mountains and Excelsior Mountains (Proffett and Proffett, 1976; Proffett, 1977; Garside, 1979; Ekren and Byers, 1985). Yerington sequence tuffs are notably absent in the northern Garfield Hills, south of the Excelsior Mountains, and east of the Pilot Mountains (Speed and Cogbill, 1979; Oldow and Steuer, 1985). The sequence is predominately composed of the widespread Singatse Tuff (26.8 Ma) and Guild Mine member of the Mickey Pass Tuff (28 to 27.4 Ma) but locally contains less widely distributed tuffs that are dated as young as 23.6 Ma (Ekren and Byers, 1985; Oldow and Dockery, 1993; Oldow and Meinwald, 1992; Henry and

John, 2013). Ignimbrites form the base of the sequence in most areas but underlain by a thin section of intermediate lava flows that is 15 m thick in the Excelsior Mountains (Garside, 1979) and 50 m thick in the Gabbs Valley Range (Ekren and Byers, 1985). Similar lavas are exposed in the northern Pilot Mountains but their stratigraphic position with respect to the late Oligocene ignimbrites is ambiguous (Oldow and Meinwald, 1992).

The Candelaria sequence (Fig. 2.2) is composed of silicic ignimbrites and minor amounts of tuffaceous sediments and are exposed in the Candelaria Hills, the southern Pilot Mountains, the Monte Cristo Range, Miller Mountain, and the northern White Mountains (Ferguson, 1927; Ferguson and Muller, 1949; Robinson et al., 1968, 1976; Crowder et al., 1972; Speed and Cogbill, 1979, Stewart, 1984, Stewart et al., 1994; Tincher and Stockli, 2009). Candelaria sequence tuffs are contained within a geographic area surrounded by the Excelsior Mountains and Pilot Mountains to the north, the Royston Hills to the east, and the Silver Peak Range and White Mountains to the south, and are nearly absent outside of this region except for thin, sparse deposits in the Excelsior Mountains (Ross, 1962; Albers and Stewart, 1972; Garside, 1979). The Candelaria sequence predominately consists of the widespread Metallic City Tuff (25.76 Ma), the Candelaria Junction Tuff (24.09 Ma), and the Belleville Tuff (23.75 Ma) but in many areas contains localized, unnamed, and undated tuffs (Speed and Cogbill, 1979; Stewart, 1984; Petronis et al., 2009).

The Royston Hills sequence (Fig. 2.2) includes ignimbrites and sedimentary rocks exposed in the Royston Hills, and northern Jackson Wash and range in age from 29 to 26.7 Ma (John and McKee, 1987; Stewart et al., 1994). The Royston Hills tuff sequence is absent west of

Monte Cristo Valley, the Monte Cristo Range, and Jackson Wash (Albers and Stewart, 1972; Stewart et al., 1994).

Early Miocene Units. Deposits of early Miocene andesite cover much of the Mina-Dyer region (Fig. 2.2) and rest on each of the three late Oligocene sections and also shows substantial variation in thickness (Albers and Stewart, 1972; Speed and Cogbill, 1979). The andesite succession often has a thickness of 100 to 200 m over distances of 5 to 10 km and abruptly increase thickness to 600 to 1500 m across east-west, north-northeast, and north-northwest—trending faults (Garside, 1979; Speed and Cogbill, 1979; Oldow and Meinwald, 1992; Oldow and Dockery, 1993; Kerstetter et al., in prep). Many of the faults that caused thickness changes in the early Miocene andesite succession are also related to thickness changes in the late Oligocene tuff successions (Speed and Cogbill, 1979; Hardyman and Oldow, 1991).

The boundaries of the early Miocene succession (Fig. 2.2) often outline the rectilinear geometry of east-northeast, north-northeast, and north-northwest—striking faults (Speed and Cogbill, 1979; Hardyman and Oldow, 1991). The spatial distribution of the early Miocene strata in Bettles Well Valley and the northern Garfield Hills highlight the east-west trends of faults that juxtapose the andesite succession and late Oligocene tuffs with mountains composed of pre-Cenozoic strata (Oldow and Steuer, 1985; Oldow and Dockery, 1993). Likewise, the southern boundary of the early Miocene succession in the Mina-Dyer region is bounded by east-west and west-northwest—striking faults in the Palmetto Mountains, Central Silver Peak Range and northern White Mountains (Oldow et al., 2009; Tincher and Stockli, 2009; Katopody et al., in review).

Exposures of the andesite succession are have similar ages across the region but show some slight variations (Fig. 2.2). The base of the early Miocene section is intruded by east-west—trending hypabyssal plutons dated at 22 Ma giving age of the sequence's base in the Excelsior Mountains and Monte Cristo Range (Garside, 1979; Stewart et al., 1994). The upper part of the andesite succession is dated at 19 Ma in the Excelsior Mountains, 17.4 in the Candelaria Hills, and 16.6 Ma in the Monte Cristo Range (Marvin et al., 1977; Garside, 1979; Stewart et al., 1994). The early Miocene succession if often accompanied by andesitic east-west—trending andesitic dikes dated at 17.4 Ma (Garside, 1979; Oldow and Steuer, 1985; Kerstetter et al., in prep).

Mid-Miocene Succession. The middle Miocene andesite succession (Figs. 2.2 and 2.3), named the Gilbert Andesite, forms a thin (60 to 100 m) layer that overlies many older units with angular unconformity (Stewart et al., 1994; Kerstetter et al., in prep). The thickness of the Gilbert andesite does not noticeably change across faults and seems to maintain a fairly uniform thickness where the unit is recognized in the central and southern areas of the Mina-Dyer region (Garside, 1979; Stewart et al., 1994; Kerstetter et al., in prep). The mid-Miocene andesite succession forms blocky outcrops that cap present-day hills and ridges where the unit flatly overlies tilted beds of the early Miocene Blair Junction andesite, late Oligocene tuffs, and pre-Cenozoic rocks (Stewart et al., 1994). The unit primarily consists of massive lava flows dated at 16.1 to 15.7 Ma but also contains lahars in some areas (Garside, 1979; Stewart et al., 1994).

Mid-Miocene to Quaternary Succession. The mid-Miocene to Quaternary section (Figs. 2.2 and 2.3) varies in lithology and thickness between the north and south parts of the Mina-Dyer

region. The rocks comprise two major successions, mid to late Miocene and Pliocene to Quaternary, that as a whole ranges in thickness from 20 to 3600 m across late Miocene to Quaternary faults (Oldow et al., 2009, 2016).

The mid to late Miocene sequence (Fig. 2.3) consists of sedimentary and volcanic rocks of the Coyote Hole Group (Oldow et al., 2009) and other age-equivalent rocks and varies thickness from 20 to 1830 m (Garside, 1979; Stewart, 1979; Speed and Cogbill, 1979; Ekren and Byers, 1985). The mid to late Miocene succession varies thickness from 20 to 1830 m as a result of synextensional deposition in the south (Oldow et al., 2009) and is less than 200 m thick over most of the northern area but locally reaches 1000 m thick (Stewart, 1979; Ekren and Byers, 1985; Oldow, 1985). The rocks consist of a lower sedimentary section of sandstone, conglomerate, and mudstone interleaved with lava flows and ignimbrites, that passes upward into a succession of intercalated ash flows, air fall tuffs, lava flows and tuffaceous sediments (Robinson et al., 1968; Speed and Cogbill, 1979; Ekren and Byers, 1985; Oldow et al., 2003). Volcanic rocks interleaved in the sedimentary rocks of the lower section are rhyolitic ignimbrites in the south but consist of rhyolite lavas in the north (Robinson et al., 1968; Ekren and Byers, 1985). The upper volcanic section consists of rhyolite and latite tuffs and flows dated at 7 to 5.9 Ma in the south whereas the age-equivalent rocks in the north are slightly older and consist of rhyolite, latite, basalt, and basaltic andesite that range in age from at 8.5 to 5.8 Ma (Ekren and Byers, 1985; Oldow, 1985; Oldow et al., 2009).

The Pliocene to Quaternary sequence (Fig. 2.3) consists of sandstones, conglomerates and mudstones deposited in fluvial, lacustrine, and alluvial environments and are intercalated with basalt flows and tuff (Bachman, 1978; Oldow et al., 2009). The rocks range in thickness

from 50 to 550 where exposed in the ranges (Oldow et al., 2009) and may be up to 1800 m thick within the present-day basins (Oldow et al., 2016; Katopody et al., in review). The relative abundance of basalts to varies geographically such that some areas are dominated by sedimentary rocks whereas others are primarily basalt (Oldow, 1985; Petronis et al., 2009; Tincher and Stockli, 2009; Oldow et al., 2016). Basalt flows intercalated within the sedimentary successions are dated at 4.8 to 3.0 (Robinson et al., 1968; Lee et al., 2003; Oldow et al., 2009; Mueller et al., 2016).

Late Cenozoic Basins

Synextensional deposition is an ongoing process in the Mina-Dyer region and older histories of contemporaneous faulting and deposition are recognized in the rock record (Oldow et al., 2009; Speed and Cogbill, 1979). The mid to late Miocene and Pliocene to Quaternary rocks were deposited in predominately north-northeast and north-northwest—trending basins (Fig. 2.2) that formed under west-northwest extension (Bachman, 1878; Oldow, 2003; Ferranti et al., 2009; Oldow et al., 2009) whereas late Oligocene to early Miocene rocks were deposited within east-northeast—trending basins (Fig. 2.4) that lie perpendicular to present-day basins and nearly parallel to the modern extension direction (Hardyman and Oldow, 1991).

Synextensional deposition in the each generation of basins is indicated by across-fault changes in thickness, asymmetric wedges of basin-filling strata that thicken into basin-bounding normal faults, and dip decreasing upward in the stratigraphy (Oldow et al., 2009; Kerstetter et al., in prep). The asymmetric geometries of the basins and basin-fill are recognized through geologic mapping, gravity surveys and seismic surveys (Zampirro, 2005; Oldow et al., 2009; Katopody et al., in review). Examples of the fault and stratal geometries similar to those seen in

the Mina-Dyer region occur in other extensional settings such as the East African Rift, the Gulf of Mexico, the Suez Rift, the Newark Basin, the North Sea, and the Basin and Range (Garfunkel and Bartov, 1977; Vreeland and Berrong, 1979; Bally, 1982; Gibbs, 1984; Ratcliffe, et al., 1986; Rosendahl et al., 1986; Morley et al., 1990; Schlische, 1992; Hudec and Jackson, 2007).

Late Miocene to Quaternary Basins

The spatial distribution, variable thickness, and stratal geometries of late-Miocene to Quaternary rocks (Fig. 2.2) indicate that an array of north-northwest, north-northeast, west-northwest, and east-northeast—striking high-angle faults formed two generations of extensional basins during the late-Miocene to Pliocene and Pliocene to Quaternary (Oldow et al., 2016). Formation of the contemporary basins and physiography began with the onset of west-northwest extension at 3 to 5 Ma and accommodated deposition of up to 1800 m of the Pliocene to Quaternary sedimentary and volcanic succession (Bachman, 1978; Henry and Perkins, 2001; Stockli et al., 2003; Mueller et al., 2016; Oldow et al., 2016). Before 3 to 5 Ma and since at least 13 Ma, extension formed a network of north-northeast—trending half-grabens that controlled deposition of late Miocene strata resulting in an aggregate thickness ranging from 20 to 1830 m (Elias, 2005; Oldow et al., 2009).

Pliocene to Quaternary Basins

Pliocene to Quaternary north-northeast and west-northwest—striking faults (Fig. 2.2), together with north-northwest and east-northeast—striking faults formed the north-northwest, north-northeast and triangular basins and mountain ranges that form the present-day physiography (Bachman, 1978; Oldow, 1992; Henry and Perkins, 2001; Oldow et al., 2008;

Ferranti et al., 2009). North-northeast and north-northwest—trending basins formed along linear north-northeast and north-northwest—striking faults (Albers and Stewart, 1972; Speed, 1981; Ekren and Byers, 1985; Oldow and Dockery, 1993; Oldow et al., 2016; Katopody et al., in review) whereas triangular basins formed at the curved intersections of east-northeast Mina deflection faults and north-northwest Walker Lane faults (Oldow et al., 2008; Ferranti et al., 2009). Gravity surveys and well data reveal that the basins have complex, asymmetric subsurface geometries and the basin-fill varies in thickness across buried and active faults (Ferranti et al., 2009; Dunn et al., 2016; Oldow et al., 2016). Gravity surveys indicate that the depth of some basins increases across north-northeast--trending basin axes into north-northeast—striking normal faults that bound the basins (Katopody et al., in review). Tilted seismic reflectors on 2D profiles reveal that the dip of the basin-fill decreases upward through the stratigraphy the basin-fill increases thickness into north-northeast faults (Zampirro, 2005).

The contemporary extension direction in the Mina-Dyer region is N55W to N65W as indicated by earthquake focal mechanisms, geodetic surveys, strain meters, and fault-slip inversion (Oldow, 2003; Ferranti et al., 2009). Slickenlines that mutually cross cut each other and a strain meter that alternates between northwest and north-northeast strain axes indicate that north-northeast extension occurs simultaneously with west-northwest extension in proximity to faults that curve through 90° in strike although the west-northwest extension remains dominate (Ferranti et al., 2009).

Late Miocene Basins

A network of north-northeast—trending basins bounded by north-northeast—striking normal faults and west-northwest—striking transfer faults controlled deposition of eastward-

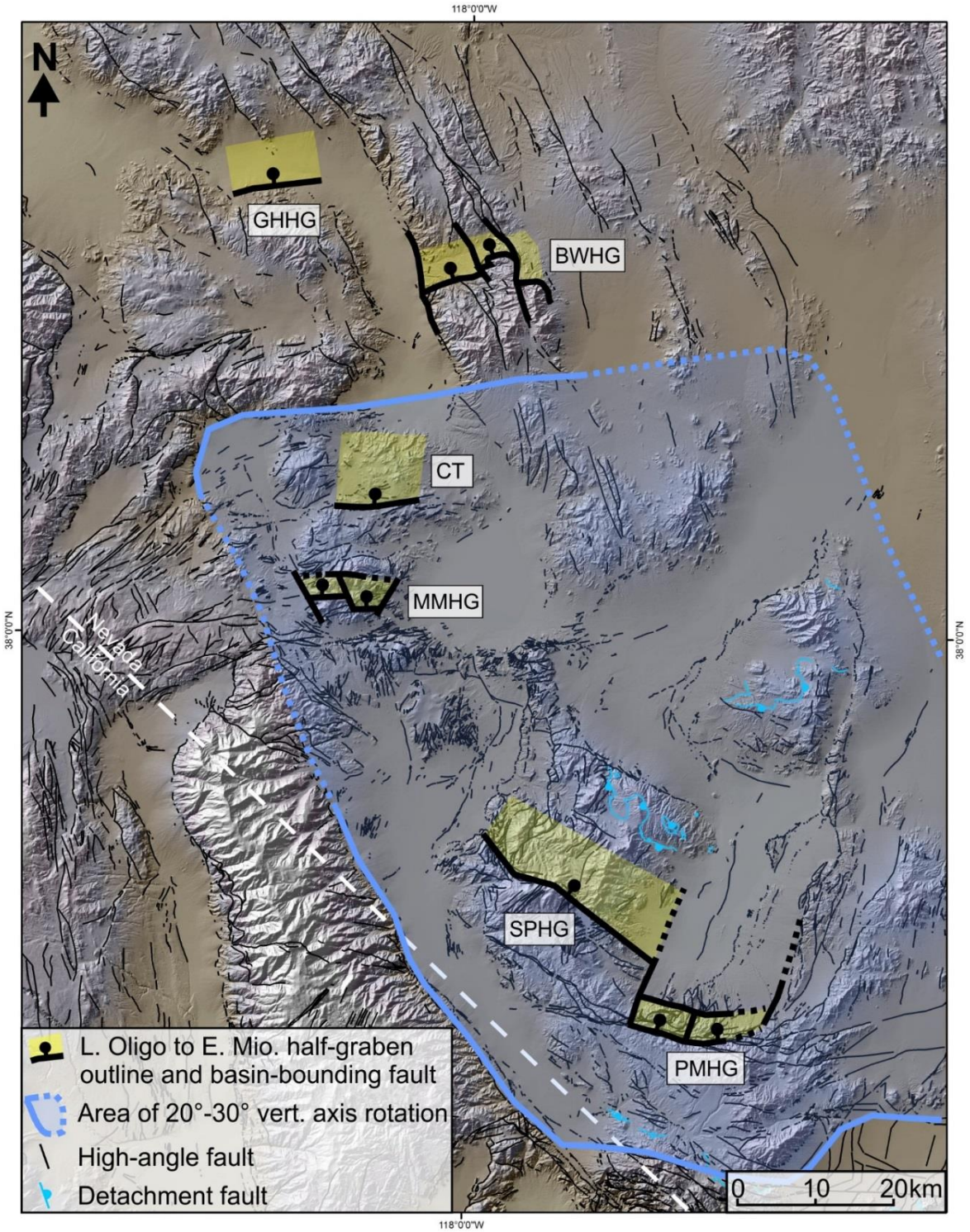

Figure 2.4. Physiographic map of the Mina-Dyer region showing the distribution of late Oligocene and early Miocene basins with respect to modern topography and faults, and post-late Miocene vertical-axis rotation.

thickening prismatic wedges of late Miocene volcanic and sedimentary rocks (Oldow et al., 2009). The axes of the north-northeast—trending basins terminate to the north and south into through-going transfer faults causing dog-leg steps in the axes of the half-grabens (Oldow et al., 2009). Within the basins, the bases of stratal wedges are tilted up to 30° east and decrease dip upward showing up to 20° angular differential tilt between the base and top of the synextensional stratigraphy (Oldow et al., 2009). Synextensional units change thickness by two to ten times across north-northeast and west-northwest faults and are occasionally omitted from the stratigraphy (Oldow et al., 2009).

The extension direction during the formation of the late Miocene basins is presumed to be northwest to west-northwest due to lack of well-preserved slickenlines (Oldow et al., 2009). The extension direction is presumed to be west-northwest to northwest because the synextensional strata thicken eastward indicating that north-northeast faults experienced more dip-slip motion than the transfer faults which were apparently dominated by strike-slip movement (Oldow et al., 2009).

The north-northeast—trending basins structurally overlie a low-angle detachment fault that, together with the synextensional basin-fill and some late Miocene faults, were deformed into broad doubly-plunging folds (Oldow et al., 2009). The end of late Miocene basin activity and formation of folds was accompanied by a paleomagnetically-determined vertical-axis rotation of the southern part of the Mina-Dyer region by 20° to 30° clockwise (Oldow et al., 2008; Petronis et al., 2009).

Late Oligocene to Early Miocene Basins

A series of east-northeast, east-west, and west-northwest—trending basins (Fig. 2.4) populate the Mina-Dyer region (Hardyman and Oldow, 1991; Kerstetter et al., in prep). The basins exhibit asymmetric geometries indicated by geologic mapping of south-tilted strata (Speed and Cogbill, 1979; Oldow and Meinwald, 1992; Oldow and Dockery, 1993). The asymmetric geometries are emphasized by gravity surveys that indicate the basins reach 1000 m deep at their southern margins and are filled with an equal amount of late Oligocene and early Miocene rocks (Speed and Cogbill, 1979; Meinwald, 1982; Hardyman and Oldow, 1991). The remnants of the basins are 10 to 15 km long and 4 to 6 km wide (Hardyman and Oldow, 1991). The basins are bounded to the south by east-northeast, east-west, and west-2.3northwest—striking extensional faults that dip north and are often bounded to the north by antithetic structures (Oldow and Dockery, 1993; Kerstetter et al., in prep). The array of basins has a dog-leg geometry such that basin axes are separated by 10 to 20 km left and right steps across north-northwest—striking late Oligocene and early Miocene transfer faults that were later reactivated by younger extension (Hardyman and Oldow, 1991).

Synextensional deposition within the late Oligocene and early Miocene basins is indicated by thickness changes and stratal geometry of the silicic ignimbrite sequences and Blair Junction andesite (Speed and Cogbill, 1979; Hardyman and Oldow, 1991). Late Oligocene and early Miocene rocks outside are 100 to 200 m thick whereas units within the basin form south-dipping asymmetric stratal wedges that reach thicknesses of 1000 to 1500 m (Speed and Cogbill, 1979; Oldow and Dockery, 1993; Kerstetter et al., in prep). The synextensional units within the basins increase thickness into east-west faults and exhibit abrupt across-fault changes in

thickness or are entirely omitted from the stratigraphy outside of the basin (Speed and Cogbill, 1979). Likewise, individual tuffs and flows that comprise the stratal wedges increase thickness to the south or north into basin-bounding faults (Speed and Cogbill, 1979; Dockery, 1982). The across-strike changes in thickness create fanning-stratal patterns and upward decreases in dip showing angular discordances of 10° to 30° between the base and top of the section (Speed and Cogbill, 1979; Kerstetter et al., in prep).

The trends of the half-grabens (Fig. 2.4) vary from east-northeast to west-northwest by geographic location (Kerstetter et al., in prep). West-northwest and east-west—trending basins are located in the south part of the Mina-Dyer region (Speed and Cogbill, 1979; Kerstetter et al., in prep) that underwent 20° to 30° of clockwise vertical-axis rotation (Fig. 2.4) since the late Miocene (Oldow et al., 2008; Petronis et al., 2009). In contrast, east-northeast—trending half-grabens (Fig. 2.4) are located in the northern part of the Mina-Dyer region (Hardyman and Oldow, 1991) where Cenozoic and pre-Cenozoic rocks did not rotate about a vertical axis (Ferranti et al., 2009).

The array of basins has a dog-leg geometry (Fig. 2.4) such that transfer faults formed the eastern and west margins of the basins and segmented the basins (Hardyman and Oldow, 1991). East-northeast, east-west and north-northeast faults are 5 to 15 km long and intersect the north-northwest and north-northeast faults at nearly perpendicular angles (Oldow and Meinwald, 1992; Kerstetter et al., in prep). The easterly trending faults that bound the basins exhibit dog-leg steps to the left or right where they intersect the north-northwest and north-northeast faults (Hardyman and Oldow, 1991). Steps in basin axes occur across north-northwest and north-northeast faults (Fig. 2.4) that were active in the late Oligocene and early Miocene as indicated by abrupt

changes in stratal thickness and basin depth across the structures (Dockery et al., 1993). The synextensional units abruptly change thickness from 1500 within basins to 100 to 200 outside the basins (Kerstetter et al., in prep).

The basins (Figs. 2.2 and 2.4) all share similar fault and stratal geometries but the age of rocks within the basins varies (Speed and Cogbill, 1979; Hardyman and Oldow, 1991). Most basins contain both late Oligocene and early Miocene rocks (Hardyman and Oldow, 1991) but one basin in the Palmetto Mountains only contains early Miocene strata (Kerstetter et al., in prep). Additionally, basins with late Oligocene strata either contain the Yerington sequence (Oldow and Meinwald, 1992; Oldow and Dockery, 1993) or the Candelaria sequence (Speed and Cogbill, 1979) but never both given the spatial segregation of the units.

The late Oligocene and early Miocene half-grabens are used as evidence of an earlier period of north-south extension due to their easterly trends, southward tilted basin-fill, and east-west trend of dikes that intrude the basin-fill (Hardyman and Oldow, 1991). These lines of evidence fall short of documenting a change in the extension direction because fault geometry, stratal tilt directions, and dike orientations are inherently unable to uniquely define strain axes. For example, fault geometry and dike orientation are subject to crustal anisotropy and therefore may be influenced by pre-existing structures (Delaney et al., 1968). The tilt direction of faulted strata does not reflect the direction of extension because the dip direction is dependent on the geometry of the footwall (Gibbs, 1983). As a result, fault-induced dips only record the dip-slip component of fault motion and do not record strike-slip motion which is needed to calculate the direction of extension.

Extension Directions and Fault-Slip Analysis

A change in the extension direction prior to the present-day west-northwest extension is implied by the easterly trends of the late Oligocee and early Miocene basins, the southward-thickening geometry of strata within the basins, and east-west strike of dikes that intrude the basin-fill, assuming that the east-west—trending basins were indeed structurally controlled (Burke and McKee, 1979; Best, 1988; Oldow and Steuer, 1985; Hardyman and Oldow, 1991). These lines of evidence fall short of documenting a change in the extension direction because fault geometry, stratal tilt directions, and dike orientation are inherently unable to uniquely define strain axes. For example, fault geometry and dike orientation are subject to crustal anisotropy and therefore may be influenced by pre-existing structures (Delaney et al., 1968). The tilt direction of faulted strata does not reflect the direction of extension because the dip direction is dependent on the geometry of the footwall (Gibbs, 1983). As a result, fault-induced dips only record the dip-slip component of fault motion and do not record strike-slip motion which is needed to calculate the direction of extension. Fault-slip inversion can accommodate the shortcomings of other techniques by using any orientation of a fault-planes, the rakes of slickenlines within those planes, and shear sense determined by kinematic indicators to calculate strain-rate axes for individual slip events on each fault (Twiss and Unruh, 1998, Petit, 1987). The technique works on fault planes of any orientation and with any shear sense and is therefore beyond the influence of crustal anisotropy and reactivated faults. Furthermore, the use of fault-slip inversion to determine extension directions has been validated in modern conducted in tandem with earthquake focal mechanisms, GPS velocities, and strain meters (Oldow, 2003; Ferranti et al., 2009).

Fault-slip data collected along major fault systems of east-trending half-grabens in the Silver Peak Range, Miller Mountain, the Candelaria Hills, Bettles Well Valley and the northern Garfield Hills record a period of north-south extension that occurred prior to two younger episodes of deformation in the mid-Miocene to Quaternary. The younger events include simultaneous northwest and northeast extension (D2) followed by simultaneous west-northwest and north-northeast extension (D3). North-south extension (D1) appears to have operated under plane strain conditions. The same extension directions are recognized in each of the east-trending basins and in each case north-south extension is the oldest event. A total of 952 fault-slip measurements were collected along the major east and north-trending fault systems that bound and cross the east-trending half-grabens in these ranges, and are combined with 383 measurements from the Palmetto Mountains (Katopody et al., in prep; Kerstetter et al., in prep.) for a total of 1335 fault-slip measurements. A subset of 218 measurements indicate a period of north-south extension whereas the remaining 1117 measurements can be attributed to mid-Miocene to Quaternary extension.

The orientations and sequence of the three extensional events were determined graphically (Gephart, 1990; Marret and Allmendinger, 1990) and were plotted first by hand in the field and later plotted in FaultKin 7 (Allmendinger et al., 2012). Strain-rate axes were determined for each slip surface using three criteria measured at any given faulted outcrop: 1) the attitude of slickensides, 2) rake of slickenlines on the slip surface, 3) the sense of fault motion along the slickenlines using shear sense indicators (Twiss and Unruh, 1999) established by Gamond (1987), Hancock et al. (1987), and Petit (1987). Cross cutting slickenlines from separate slip events on individual fault surfaces at 24 stations demonstrate the relative ages of

fault-slip events. The three generations of extension were recognized by grouping superposed slip lineations that shared similar strain-rate axes and cross cutting relationships after which non-superposed slip measurements were assigned to one of the three generations. Segregation of the non-superposed data started with the present extension direction and proceeded into deeper time to not overestimate the prevalence of the older extensional events. The three groups of fault-slip data, or strain-rate fields (Twiss and Unruh, 1999), were used to determine the orientation and uncertainty of the changing extension directions.

The end of north-south extension and transition to younger extension directions is recorded by the Palmetto Mountains half-graben and demonstrates that the half-graben formed under north-south extension (Kerstetter et al., in prep). Here, north-south slip lineations (D1) show restricted development to half-graben basin-fill and are excluded in the overlap sequence that buries the basin. Slip lineations associated with the younger extensional events (D2 and D3) are found in the overlap sequence, the basin-fill and pre-Cenozoic rocks. Under north-south extension (D1), west-northwest to east-northeast—striking master faults were dominated by dip-slip motion allowing the faults to control the asymmetric geometry of the east-trending half-grabens.

Extensional Strain Calculation Method

The horizontal component of extension across the six half-grabens was calculated by constructing rectilinear models of each half-graben and Oligo-Miocene syndepositional faults. The extension calculation for each fault uses the in-situ strike and dip of each syndepositional fault, and the extension direction determined by fault-slip analysis in each basin to account for 20° to 30° of vertical-axis rotation that occurred since the late Miocene (Petronis et al., 2009).

Magnitudes of Oligo-Miocene fault motion were determined by the thickness of syndepositional units. Vertical displacement provided by fault-controlled thickness changes, together with the strike and dip of the syndepositional faults, were used to trigonometrically calculate the horizontal component of displacement on each structure using the same method as Dunn et al. (2016) and Katopody et al., (in review). Uncertainty in horizontal extension calculations mainly comes from uncertainty in fault dips and but can also include fault strike in the case of buried structures.

Palmetto Mountains

In the Palmetto Mountains (Figs. 2.4 and 2.5), outcrops of Cenozoic rocks are concentrated in low-lying foothills located along the northern flank of highlands that expose Paleozoic Metasedimentary rocks and Mesozoic pluton (Dover, 1962). The pre-Cenozoic rocks consist of lower Paleozoic carbonate and siliciclastic metasedimentary rocks and Mesozoic pluton (Albers and Stewart, 1972). The Cenozoic rocks consist of early Miocene andesite lava flows, lahars, tuff, and volcaniclastic sedimentary rocks and their intrusive equivalent, all unconformably overlain by extensive sheets of late Miocene tuff units dated at 7.6 to 6.1 Ma (Kerstetter et al., in prep). The early Miocene andesite is further divided into lower and upper sequences that correspond to unconformities recognized within the andesite stratigraphy in many parts of the Mina-Dyer region (Garside, 1979; Stewart et al., 1994; Kerstetter et al., in prep). Correlation of the lower and upper sequences to the Blair Junction sequence and Gilbert andesite provides age ranges of 22 to 16.6 Ma and 16.1 to 15.1 Ma, respectively.

Contemporary faults in this area segment and juxtapose various Cenozoic and pre-Cenozoic units forming network of anastomosing, curved faults that change strike from west-

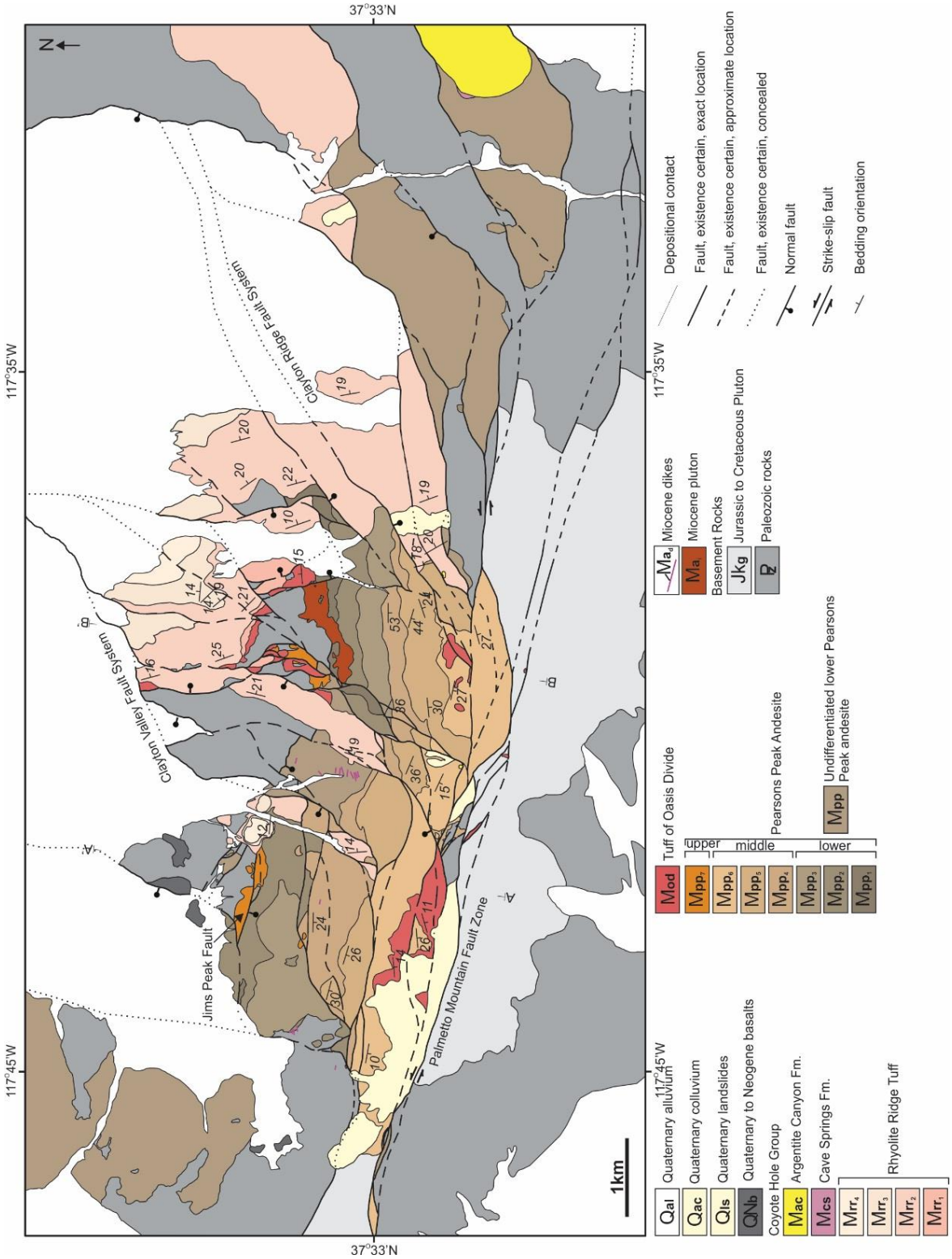

Figure 2.5. Geologic Map of the northern Palmetto Mountains. From Kerstetter et al., in prep.

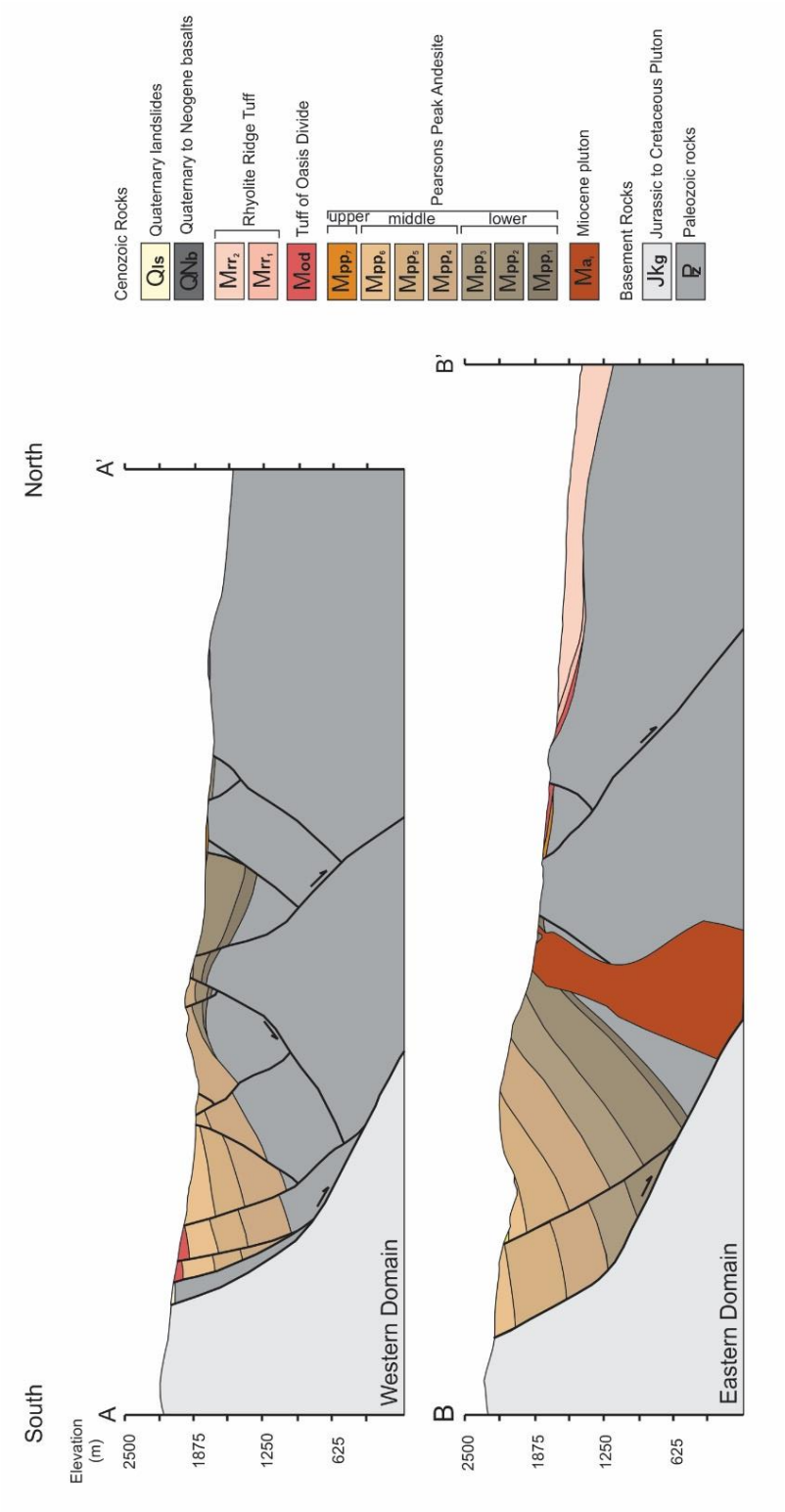

Figure 2.6. Cross sections of the northern Palmetto Mountains. From Kerstetter et al., in prep.

northwest to north-northeast as they are traced across the Palmetto Mountains. The southern edge of this fault system consists of the west-northwest to east-west—striking left-lateral, strike-slip Palmetto Mountain fault system that separates extensive outcrop of Cenozoic strata overlying Paleozoic metasediments to the north from Paleozoic and Mesozoic rocks overlain by thin, isolated exposures of Cenozoic strata to the south. Curved fault segments diverge toward the north from the Palmetto Mountain fault system, cross the Cenozoic outcrops and merge with north-northeast—striking normal faults. This complex network of faults has acted together to transfer displacement from the Palmetto Mountain fault system to the north-northeast—striking faults since the late Miocene (Katopody et al., in prep), but the thickness patterns, stratal geometry and spatial distribution of early Miocene andesite demonstrate an older history displacement on these faults. The early Miocene movement on these faults is most easily demonstrated by the Jims Peak fault that forms the northern boundary of the lower andesite sequence and is buried by the upper andesite sequence and late Miocene tuffs.

Early Miocene Half-Graben

The geometry of high-angle faults and early Miocene strata preserve a west-northwest—trending half-graben in the Palmetto Mountains that controlled deposition of the lower andesite sequence (Kerstetter et al., in prep). The basin has an asymmetric geometry (Figs. 2.5 and 2.6) as indicated by andesite within the basin that strikes east-west and predominately dips south but locally dips north. In the eastern half of the basin, southward dips of 50° near the base of the andesite along the northern margin indicate that the basin increases depth across the basin axis reaching depths of 1500 to 2000 m along the southern margin of the half-graben. In the western half of the basin, there are two deep parts of the basin along the northern and southern margins of

the basin separated by an intervening high that parallels the basin axis. This is indicated by the lower section of andesite basin-fill that dips north at 10° to 15° increasing depth to the north whereas the upper section of basin-fill dips southward at 30°.

The asymmetric geometry of the basin (Fig. 2.6) was controlled by the Jims Peak fault and antecedent to the Palmetto Mountain fault system bounded the half-graben to the north and south whereas transfer faults allowed changes in basin geometry along the basin axis. The depth of the basin increases into the west-northwest—striking faults indicating that they accommodated the most displacement and therefore served at the basin's master faults. A series of east-west—striking faults ran parallel to the intra-basin high in the western half of the basin. The along-axis change from a southward basin polarity in the east to a bipolar geometry in the west was accommodated by a north-striking transfer fault that allowed differential tilting during basin subsidence. The half-graben was also terminated at its western and eastern edges by north to north-northeast—striking transfer faults that preceded the modern normal faults that occupy the same locations along the eastern flank of the Silver Peak Range and the western face of Clayton Ridge. The basin-bounding transfer faults separated thin successions of andesite (160 to 210 m) outside the half-graben in the Cow Camp and Lida Wash areas from thick accumulations of andesite (1510 m) within the basin.

Simultaneous deposition, fault movement and half-graben subsidence is demonstrated by growth relationships in the lower andesite sequence (Fig. 2.6). Aside from the abrupt change in thickness between andesite outside and inside the half-graben, andesite basin-fill forms asymmetric wedges that thicken into basin deeps and truncate into the west-northwest—striking master faults. In the eastern half of the basin, the lower andesite forms a southward-thickening

prismatic wedge that increases thickness up to 1510 m where the wedge truncates into the Palmetto Mountain fault system. The southward increase in thickness is expressed as bedding that dips 50° south at the base of the wedge and progressively decreases dip to 25° up section creating a fanning-stratal pattern indicative of synextensional deposition. In the western half of the basin, the lower section of basin-fill andesite forms a stratal wedge that increases thickness northward up to 675 m where it truncates into the Jims Peak fault. The upper section of basin-fill increases thickness southward up to 680 m and decreases dip up section from 30° at the base of the section to 25° at the top.

The half-graben subsidence and fault movement ceased by the mid-Miocene when the basin was buried by the upper sequence of andesite (Fig. 2.5) that sits flatly within and outside the basin and maintains a uniform thickness of 60 m showing no sign of synextensional deposition. The upper andesite sequence buried the Jims Peak fault as well as the east-west—striking faults that run parallel to the intra-basin high in the western half of the basin. Late Miocene tuffs further buried the half-graben at 7.6 to 6.1 Ma as seen by the sealed Jims Peak fault that remains inactive to the present.

Fault Kinematics of the Palmetto Mountain Half-Graben

Fault-slip data (Fig. 2.7) collected along the damage zones of basin-controlling faults in the Palmetto Mountains reveal two distinct extensional events that occurred since the late Miocene whereas the early Miocene andesite records an older period of north-south extension that is not seen in the younger rocks that bury the early Miocene half-graben (Kerstetter et al., in prep). A total of 383 slip measurements were separated into the three extensional events based on cross-cutting relationships at ten stations (Katopody et al., in prep). Both younger extensional

events represent non-plane strain events as indicated by slip lineations from two strain-rate axes showing mutually cross cutting relationships. Contemporary extension (D3) consists of a primary extensional axis oriented N62W±7° and a minor north-northeast—trending axis that geographically varies from extension to shortening in response to areal changes in fault geometry (Katopody et al., in prep). Mutually cross cutting extensional axes of the second extensional event (D2) are oriented N25W±5° and N70E±10°. In contrast to D3 and D2 extension, the north-south extension (D1) consists of a single extension direction oriented N10W±5°. North-south slip lineations (D1) are preserved in the damage zones of the master faults and transfer faults that controlled development of the early Miocene half-graben and only developed in the lower andesite sequence and pre-Cenozoic rocks. Furthermore, the early Miocene age of north-south extension is further demonstrated by preservation of north-south slip lineations on east-west—striking faults that were overlapped by the mid-Miocene upper andesite sequence during the waning of half-graben subsidence.

Extension across the Palmetto Mountains Half-Graben

The Palmetto Mountains half-graben experienced about 1032±83 m 1073±111 m of horizontal extension (Fig. 2.8) across the western and eastern sides of the half-graben, respectively. Extension was accommodated by two west-northwest to east—striking master faults, the antecedent to the Palmetto Mountain fault system and the Jims Peak fault, that form the southern and northern margins of the basin. Variations in vertical displacement occurred along the strike of the master faults as indicated by changes in dip direction and thickness of the synextensional basin-fill and was accommodated by a north-striking transfer fault that decoupled

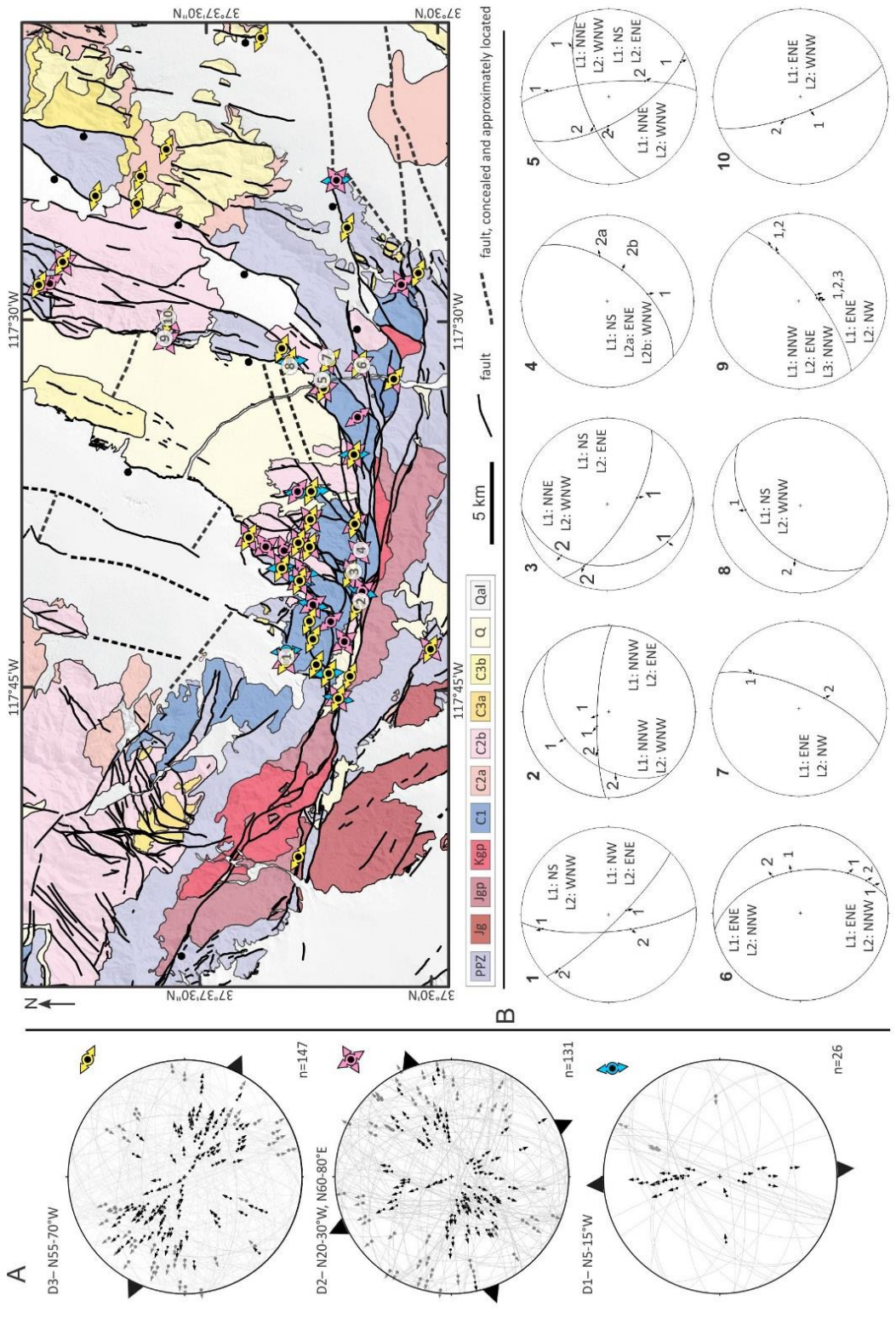

Figure 2.7. Palmetto Mountains fault-slip data. From Katopody et al., in prep.

the east and west sides of the basin. Horizontal extension was calculated using a transport direction of N10W±5° (Kerstetter et al., in prep).

On the east side of the basin (Fig. 2.8), synextensional andesite basin-fill forms a southward thickening wedge indicating that the antecedent of the Palmetto Mountain fault system accommodated most of the displacement across the basin and the Jims Peak fault played a less dominant role. The antecedent to the Palmetto Mountain fault system strikes N90W and dips 60°±5° north. Vertical displacement of 1510 m is indicated by the maximum thickness of the southward tilted synextensional stratal wedge as it truncates into the north-dipping fault. The antecedent to the Palmetto Mountain fault system indicates 984±110 m of horizontal motion on the fault. The Jims Peak fault is antithetic to the antecedent of the Palmetto Mountain fault system, dips 55° south where measured in outcrop and strikes N75W. The Jims Peak fault experienced 125 m of vertical displacement that indicates 89±11 m of horizontal extension. On the west side of the basin (Fig. 2.8), synextensional andesite forms two stratal wedges that dip in opposite directions into the antecedent to the Palmetto Mountain fault system and the Jims Peak fault indicating that extension was accommodated nearly equally by both faults although they did not necessarily operate simultaneously. The two stratal wedges are juxtaposed by an intervening system of east-striking faults that were in turn overlapped by post-extensional andesite. The antecedent of the Palmetto Mountain fault system strikes N75W and dips 60°±5° north. The fault controlled deposition of a 680 m thick section of andesite indicating an equal amount of vertical displacement resulting in 482±58 m of horizontal movement. The Jims Peak fault strikes N75W and dips 55° south. Vertical displacement is indicated by synextensional andesite that thickens to a maximum of 675 m where the unit truncates into the Jims Peak fault

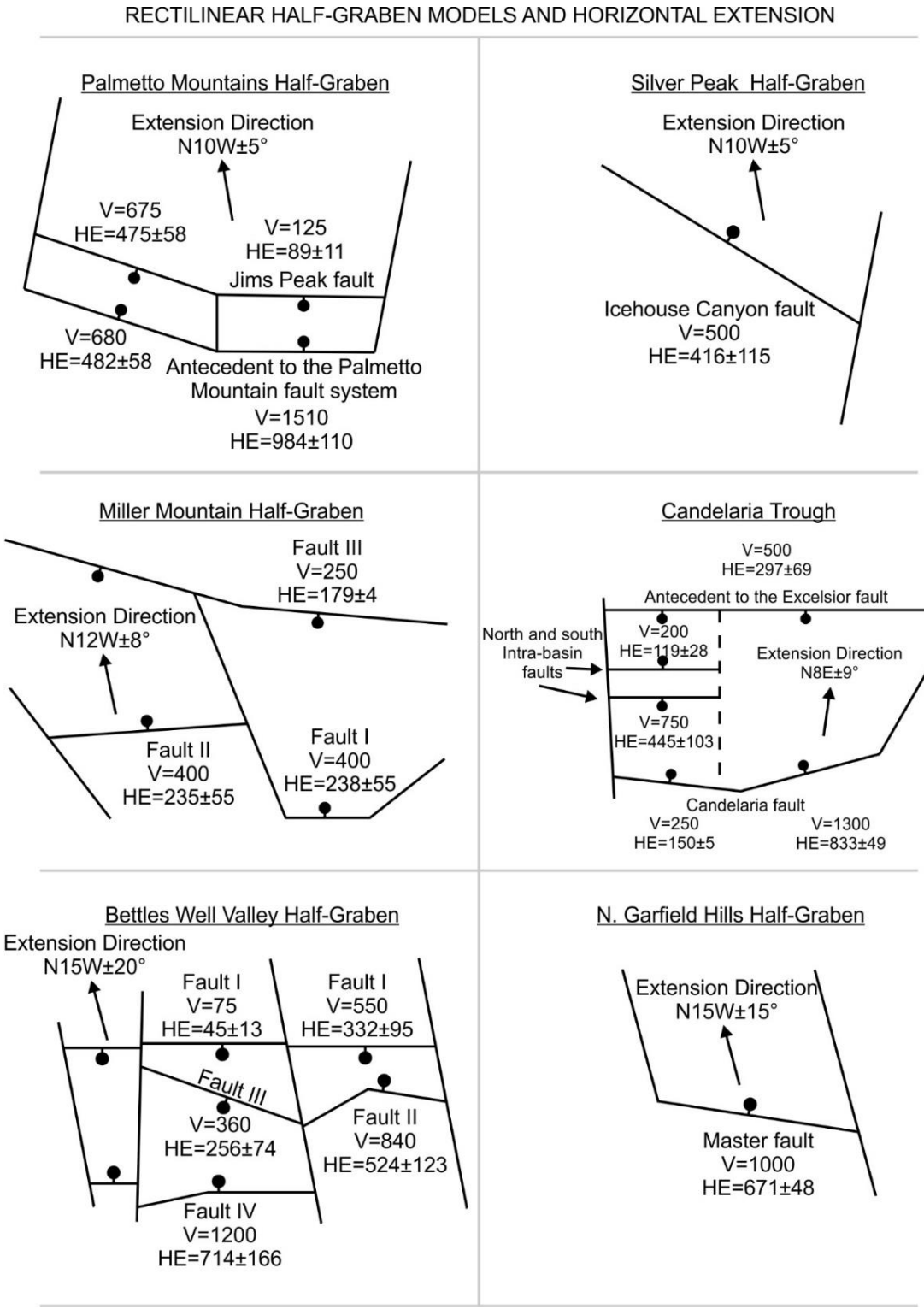

Figure 2.8. Rectilinear half-graben models and horizontal extension.

and indicates horizontal movement of 478±58 m. The east-striking faults that juxtapose the south and north-dipping andesite units dips 55°±5° south and experienced 100 m of throw prior to being sealed resulting in 72±16 m.

The Silver Peak Range

Cenozoic volcanic and sedimentary rocks occupy highlands in the central Silver Peak Range (Fig. 2.9) bordered to the north and south by outcrops of pre-Cenozoic rocks (Oldow et al., 2009). Cenozoic rocks form a 15 to 20 km wide and 25 to 30 km long exposure belt that lies west-northwest across the central Silver Peak Range. Cenozoic rocks consist of a 500 m thick section of a basal ignimbrite, early Miocene andesite flows, lahar, tuff and sedimentary rocks, overlain by a 20 to 2755 m thick section of mid-Miocene to Quaternary rhyolitic tuffs, flows and sedimentary rocks. The ignimbrite at base of the section is dated at 22.8 to 21.5 Ma (Robinson et al., 1968) and overlying andesite is likely 22 to 15.1 Ma base on correlation to andesite in the Monte Cristo Range (Stewart et al., 1994). Pre-Cenozoic units consist of Paleozoic siliciclastic and carbonate sedimentary rocks and Mesozoic pluton that depositionally underlie the Cenozoic stratigraphy, and metamorphic tectonites and Cenozoic intrusive rocks that structurally underlie the central Silver Peak Range and are exposed in the turtleback structure at Mineral Ridge (Kirsch, 1971; Oldow et al., 1994; Oldow et al., 2003).

A network of west-northwest and north-northeast—striking faults formed prismatic fault blocks composed of Cenozoic and pre-Cenozoic rocks (Oldow et al., 2009). West-northwest faults exhibit continuous traces as they span the width of the range and separate thick accumulations of Cenozoic strata in the central highlands from pre-Cenozoic rocks overlain by thin layers of Cenozoic rocks to the north and south. North-northeast—striking faults terminate

to the north and south into the west-northwest—striking faults. Many of these faults exhibit modern displacement but previously formed mid-Miocene to Pliocene north-northeast—trending half-grabens as indicated by 10° to 30° east-dipping prismatic wedges of synextensional strata. The Silver Peak detachment structurally underlies the central Silver Peak Range and served as a decoupling surface that the west-northwest and north-northeast—striking faults soled into from the mid-Miocene to Pliocene. Detailed gravity surveys in the Silver Peak Range indicate that Pliocene to recent displacement on reactivated north-northeast—striking faults offsets the detachment at depth (Ng and Oldow, 2017).

Early Miocene Basin

The Silver Peak Range (Fig. 2.9) provides evidence of an early Miocene history of synextensional deposition along a west-northwest—striking fault like that seen in the neighboring Palmetto Mountains despite the early Miocene section being largely buried by extensive deposits of mid-Miocene to Quaternary strata (Kerstetter et al., in prep). The west-northwest—striking Icehouse Canyon fault formed the southern-most boundary of early Miocene syndepositional faults in the central Silver Peak Range (Oldow et al., 2009). At Icehouse Canyon, the andesite section is exposed beneath mid-Miocene to Quaternary rocks and shows an abrupt increase in thickness from 100 m to 500 m across the west-northwest—striking Icehouse Canyon fault and is overlain mid to late Miocene tuff, flows and sedimentary rocks on both sides of fault. The early Miocene andesite lies flatly on Paleozoic metasedimentary rocks on the footwall to the south whereas age-equivalent rocks in the hanging wall to the north are tilted steeply east by mid-Miocene to Pliocene extension.

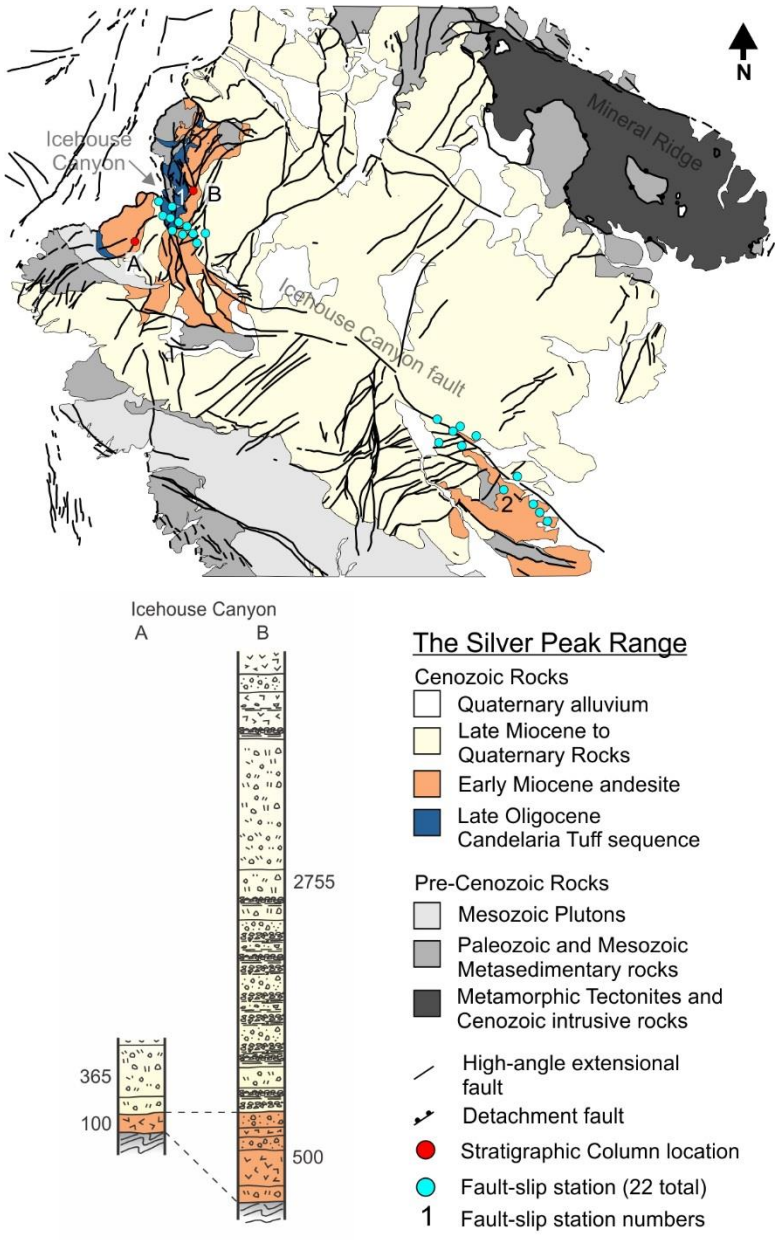

Figure 2.9. Geologic Map of the central Silver Peak Range. Modified from Oldow et al., 2009.

Fault Kinematics of the Silver Peak Half-Graben

Fault-slip data collected along the Icehouse Canyon fault (Fig. 2.10) and supplemented by cross cutting slickenlines from the neighboring Palmetto Mountains (Fig. 2.7) indicates that

the area underwent three extensional events. A total of 125 measurements were collected at 22 stations. Superposition at 2 stations, SPR-1and SPR-2, provides the general progression of extension directions indicating that north-south stretching preceded younger northeast and northwest extension. Cross cutting relationships from the neighboring Palmetto Mountains (Katopody et al., in review) provide a more complete picture of the sequence of extension directions. A subset of 14 north-south trending slickenlines are recorded in the early Miocene, late Oligocene and Paleozoic metasedimentary rocks and are absent in the mid Miocene to Pliocene tuffs and sedimentary rocks whereas slip lineations attributed to D2 and D3 extension are recorded in rocks of all ages. There are 50 fault-slip measurements related to D3 extension and 58 measurements related to D2 extension.

Extension across the Silver Peak Range Half-Graben

The Silver Peak half-graben experienced at least 416±115 m of horizontal extension (Fig. 2.8) and is bounded to the south by the Icehouse Canyon fault. The Icehouse Canyon fault strikes N55W to N60W and dips 60°±5° north and controlled deposition of a 500 m thick section of andesite (Kerstetter et al., in prep). The vertical component of displacement on the Icehouse Canyon fault accommodated thickness changes in the synextensional andesite unit and under an extension direction of N10W±5° results in at least 416±115 m of horizontal motion.

The estimate of horizontal extension across the Silver Peak half-graben is much lower than those of the neighboring Palmetto Mountains (Fig. 2.8). The magnitude of horizontal extension in the Silver Peak Range may be underestimated by not accounting for all the faults that formed the half-graben. The only early Miocene fault that can be confidently recognized is the Icehouse Canyon fault because most of the region is overlain by extensive deposits of late

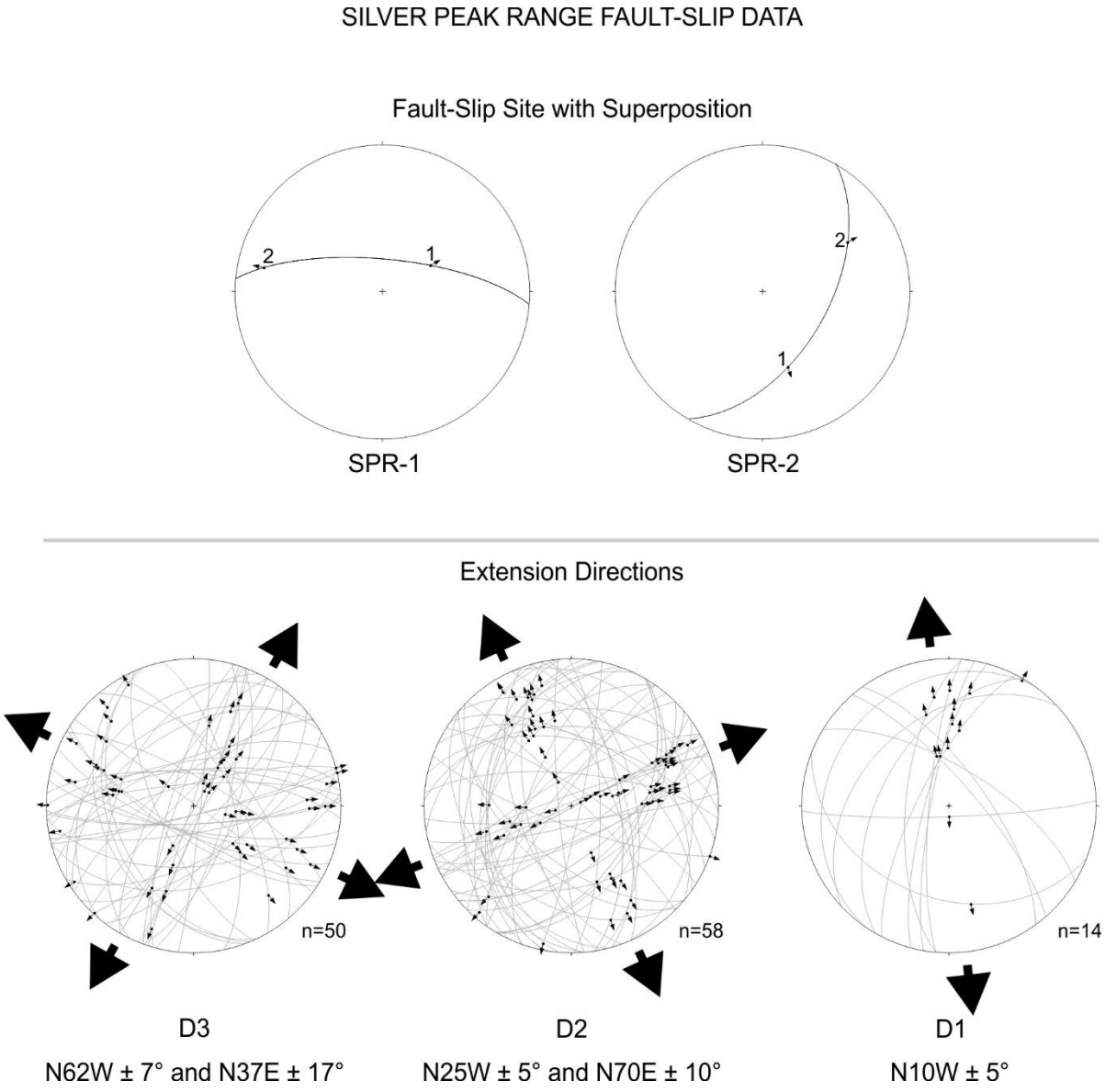

Figure 3.10. Central Silver Peak Range fault-slip data.

Miocene to Pliocene rocks. Ignored or overlooked faults could dramatically increase horizontal extension across the Silver Peak Range. Alternatively, the difference in displacement could indicate that excess displacement from the Palmetto Mountains half-graben was transferred northward to early Miocene half-grabens in the Mina deflection.

Miller Mountain

Miller Mountain (Figs. 2.11 and 2.12) exposes pre-Cenozoic rocks to the south and north of a highland occupied by Cenozoic strata (Stewart, 1979). The pre-Cenozoic rocks consist of Paleozoic metasedimentary rocks and Mesozoic plutons. The Cenozoic stratigraphy is composed of extensive sheets of Candelaria sequence tuffs that are 50 to 400 m thick and thin, isolated deposits of mid Miocene to Pliocene sedimentary rocks and Pliocene to Quaternary basalt (Stewart, 1979; Petronis et al., 2009). The late Oligocene ignimbrites consists of a basal section of undated tuff overlain by the Metallic City Tuff dated at 25.76 Ma, the Belleville Tuff dated at 24.09 Ma, and the Candelaria Junction Tuff dated at 23.75 Ma (Stewart, 1979; Petronis et al., 2009). The tuffs rest relatively flatly on the pre-Cenozoic rocks and fill in an east-west—trending depression in the pre-Cenozoic substrate. Rocks within the basin consist almost solely of Cenozoic strata except for couple locations where basement highs expose pre-Cenozoic rocks amidst the adjacent and overlying Cenozoic strata.

Miller Mountain is bounded at its margins by contemporary high-angle faults (Figs. 2.11 and 2.12) with 1 to 10 km of displacement and separate bedrock in the mountain range from alluvium in the surrounding basins. Miller Mountain is bounded to the east by a north-northeast—striking fault, to the west by a north-northwest—striking fault and to the south by an east-northeast—striking strike-slip fault. Contemporary northeast, east-west, and west-northwest—striking faults that cross Miller Mountain and the surrounding highlands have tens of meters of displacement so the original geometry of the late Oligocene tuffs is well preserved. East to east-northeast—striking faults form the walls of the east-west basin filled by the late Oligocene ignimbrites.

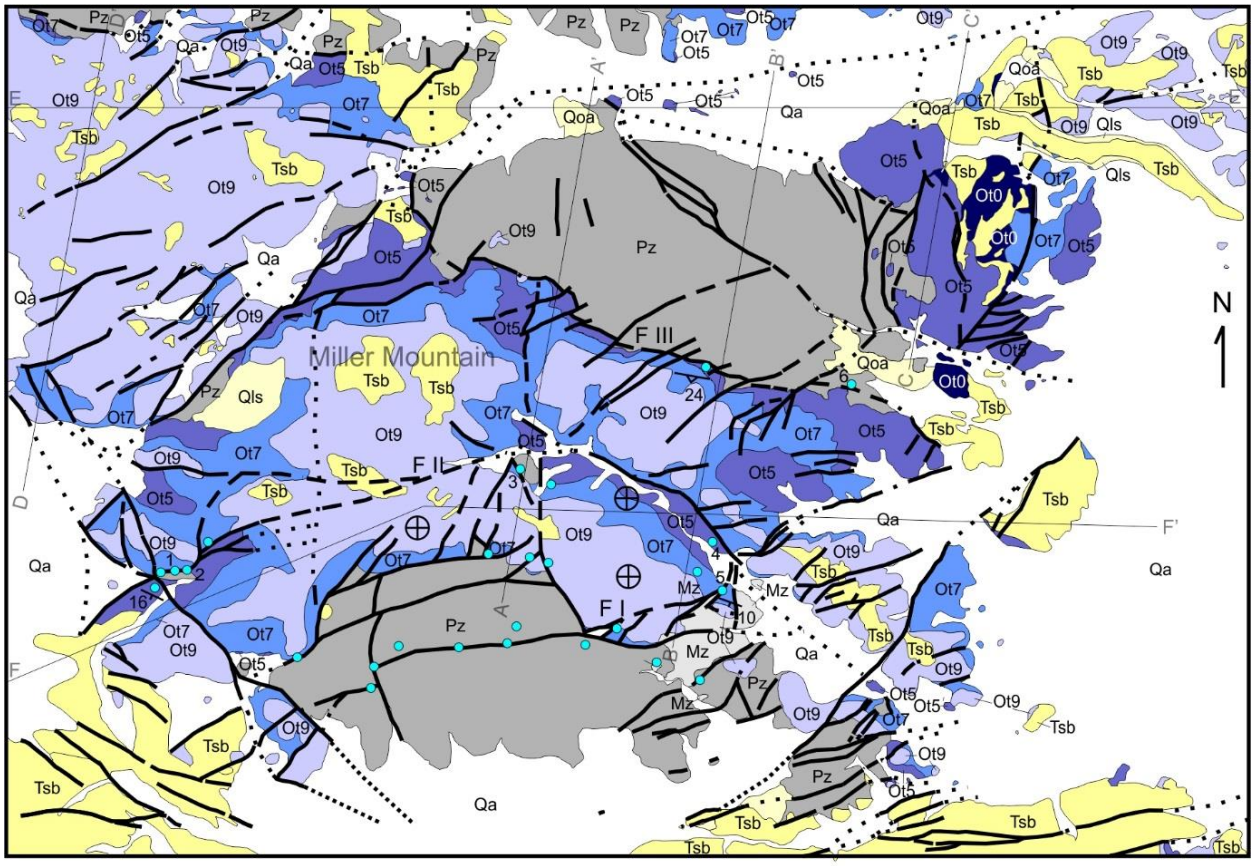

Late Miocene to Quaternary

- Qa — Quaternary alluvium
- Qls — Quaternary landslide and talus
- Qoa — Quaternary older alluvium
- Tsb — Tertiary sedimentary rocks and basalt flows

Oligocene

Candelaria tuff Seq.

- Ot_9 — Tuff 9 - Candelaria Junction Tuff (23.75 ± 0.09 Ma)
- Ot_7 — Tuff 7 - Belleville Tuff (24.09 ± 0.29 Ma)
- Ot_5 — Tuff 5 - Metallic City Tuff (25.76 ± 0.12 Ma)
- Ot_0 — Older tuff (~27 Ma)

Pre-Cenozoic

- Mz — Mesozoic pluton
- Pz — Paleozoic metasedimentary rocks

- Fault, location certain
- Fault, buried
- F II — Fault label
- Horizontal strata (less than 5°)
- Compaction foliation, strike and dip
- Bedding, strike and dip
- Fault-slip station (26 total)
- 4 — Fault-slip station number

Figure 2.11. Geologic Map of Miller Mountain.

Late Oligocene Half-Graben

Stratal patterns of the late Oligocene ignimbrites at Miller Mountain indicate that the east-northeast and west-northwest—striking faults that form the walls of the basin were active during deposition and formed an east-trending asymmetric half-graben (Fig. 2.12). The depth of the basin increases across the basin axis from north to south as indicated by late Oligoocene tuffs that form southward-thickening prismatic wedges. The Metallic City tuff and Belleville tuff were deposited within the half-graben and form a prismatic wedge that shows a north to south increase in thickness from 250 m to 400 m emphasizing the asymmetric geometry across the basin axis. The half-graben was overlapped at 23.7 Ma by the Candelaria Junction tuff that maintains a stratigraphic thickness of 90 m inside and outside the half-graben and shows no sign of synextensional deposition.

The half-graben was controlled by east-northeast—striking master faults, a west-northwest—striking antithetic fault and north-northwest transfer faults that segment the basin (Figs. 2.11 and 2.12). The Miller Mountain half-graben is bounded to the south by east-northeast—striking and north-dipping normal faults that juxtapose Metallic City tuff and Belleville tuff overlying Paleozoic metasedimentary rocks within the basin (400 m thick) to the north with Paleozoic metasedimentary rocks and Mesozoic pluton overlain by thin deposits of the equivalent ignimbrites (10 to 50 m thick) outside the basin to the south. Candelaria Junction Tuff unconformably rests on older late Oliocene and pre-Cenozoic rocks on both sides of the south-bounding fault system. The south-bounding faults have a dog-leg geometry accommodated by a north-northwest—striking transfer fault that crosses the center of the basin and exposes Paleozoic metasedimentary rocks on basement highs surrounded and overlain by

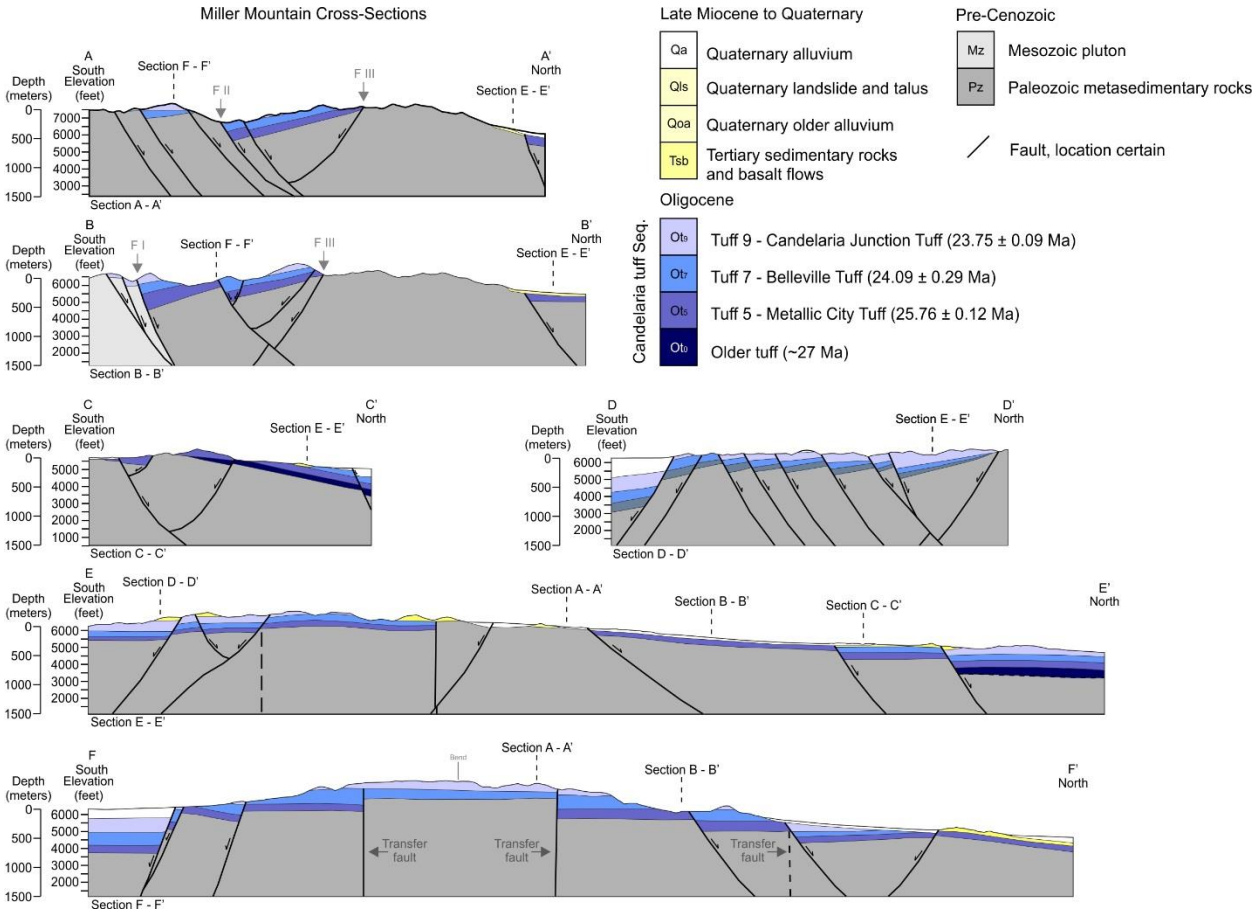

Figure 2.12. Cross sections of Miller Mountain.

late Oligocene tuffs. The northern boundary of the half-graben was formed by an antithetic normal fault that strikes west-northwest and dips 55° south. The north-bounding fault separates Metallic City tuff and Belleville tuff overlying Paleozoic metasedimentary rocks in the hanging wall with Paleozoic carbonates and siliciclastic rocks. Erosion of the half-graben and its basin-fill exposed the low-angle, depositional base of the ignimbrites within the basin making the northern contact depositional in some locations while in other locations it is demonstrably a high-angle structural contact as indicated by the presence of fault breccia, slickenlines and fault gouge with shear fabrics showing normal displacement. Ignimbrites within the basin contain

siliciclastic lithic clasts that were sourced from Paleozoic rocks in the adjacent footwall demonstrating that the footwall of the northern basin-bounding fault was exposed to erosion as the half-graben filled in.

Fault Kinematics of the Miller Mountain Half-Graben

A total of 142 fault-slip measurements (Fig. 2.13) were collected along the east, northeast and northwest striking faults that bound the half-graben. Superposed slickenlines at six stations divide the fault-slip data into the three generations of extension. A subset of 69 measurements are attributed to contemporary deformation, 58 to late Miocene to Pliocene extension, and the remaining 15 lineations are related to north-south extension. The slip lineations were collected in late Oligocene ignimbrites and sedimentary rocks of the Candelaria sequence, and Paleozoic metasedimentary rocks at 26 stations (Fig. 9).

Contemporary extension (D3) consists of two strain axes (Fig. 2.13) oriented N61W ± 21° and N45E ± 15°. Coeval motion of the two extension directions is demonstrated by slickenlines that mutually cross at station MM-6. A total of 40 measurements are attributed to west-northwest extension and another 29 measurements are related to north-northeast extension. The second extensional event (D2) is composed of simultaneous north-northwest and east-northeast extension (Fig. 2.13) oriented N22W ± 12° and N75E ± 15°, respectively. Fault-slip lineations associated with north-northwest and east-northeast extension cross each other at three stations demonstrating contemporaneous activity. North-northwest lineations cut east-northeast lineations on one slip surface at station MM-6 whereas the east-northeast lineations cross west-northwest lineations in three cases at stations. Slip lineations associated with north-northwest and east-northeast extension (D2) are crossed by D3 striations that trend west-northwest

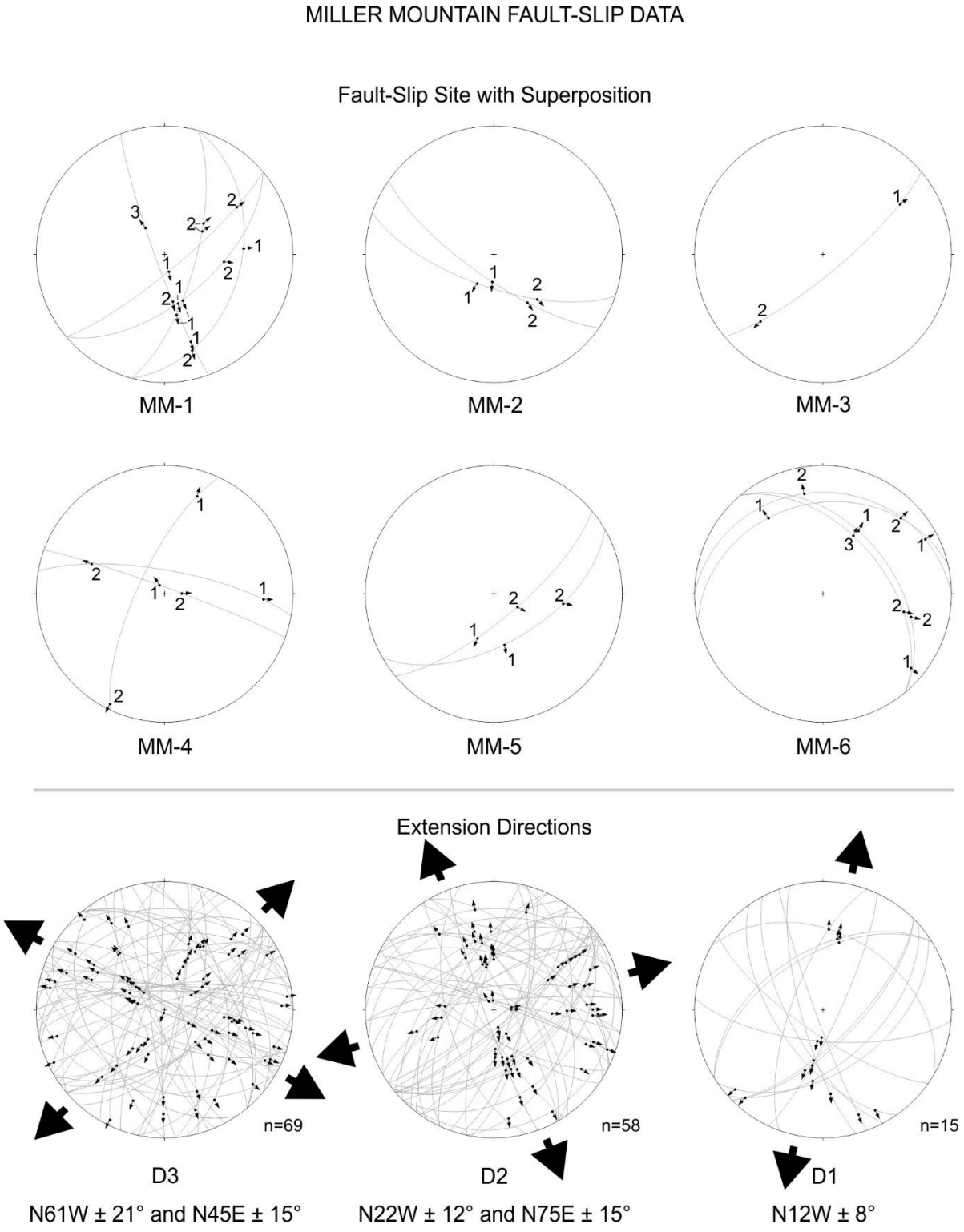

Figure 2.13. Miller Mountain fault-slip data.

and north-northeast on eleven accounts at all six stations. A group of 35 measurements comprise north-northwest extension and 23 lineations are related to east-northeast extension.

North-south extension (D1) is oriented N12E ± 8° and consists of 15 lineations (Fig. 2.13). Slip lineations related to north-south extension (D1) are crossed by both younger extensional events. West-northwest and north-northeast slip lineations (D3) cut north-south lineations twice at stations MM-4 and MM-5. North-northwest trending slip lineations (D2) are superposed on north-south lineations at station MM-2.

Extension across the Miller Mountain Half-Graben

Horizontal extension across the Miller Mountain half-graben is 414±55 m (Fig. 2.8). The geometry of the half-graben and stratal wedges within it were controlled by the Northern fault, the Canyon fault, and the Southern fault that were connected by northeast and north-northwest—striking transfer faults. The southern boundary of the half-graben has a dog-leg geometry such that that Southern fault controlled the eastern part of the basin and the Canyon fault controlled the western part. The northern boundary of the half-graben was controlled by the Northern fault.

Extension across the Miller Mountain half-graben was mainly accommodated on north-dipping faults I and II that form the southern margin of the half-graben (Fig. 2.8). Fault I dips north at 55° to 65° and strikes N90W. Vertical displacement on Fault I was about 400 m as indicated by thickness changes of Metallic City tuff and Belleville tuff indicate 238±55 m of horizontal movement occurred given an extension direction of N12E ± 8°. Fault II strikes N85E and experienced 400 m of throw resulting in 235±55 m of horizontal extension.

The west-northwest—striking fault (Fault III) on bordering the half-graben to the north (Fig. 2.8) acted as an antithetic structure to the master faults on the south side of the basin. Fault

III dips 55° where measured in outcrop and has a slightly curved trace that strikes N85W on the eastern half of the basin and N75W on the western half. Vertical displacement of 250 m provided by synextensional deposits of late Oligocene ignimbrites indicates that the fault experienced 179±4 m of horizontal movement.

Candelaria Hills and Excelsior Mountains

The Candelaria Hills and Excelsior Mountains (Figs. 2.4 and 2.14) host an east-west—trending half-graben recognized by Speed and Cogbill (1979) that formed in the late Oligocene and early Miocene and is now dissected by contemporary faults. Their work has been expanded upon by mapping and analysis of fault kinematics presented herein.

The Candelaria Hills and Excelsior Mountains (Fig. 2.14) expose the Yerington tuff sequence, the Candelaria tuff sequence, early Miocene andesite consisting of the Blair Junction sequence and Gilbert andesite, and Pliocene basalt flows that overlie Paleozoic metasedimentary rocks. The Candelaria Sequence is composed of seven undated tuffs, the Metallic City Tuff dated at 25.76 Ma, the Belleville Tuff dated at 24.09 Ma, and the Candelaria Junction Tuff dated at 23.75 Ma (Speed and Cogbill, 1979; Petronis et al., 2009). The early Miocene andesite consists of lower and upper sequences that correlate to the Blair Junction sequence and Gilbert andesite, respectively. The top of the Blair Junction andesite is dated at 19 to 17.4 Ma and the base of the Gilbert andesite is dated at 15.7 Ma (Marvin et al., 1977). The basalt overlies Oligo-Miocene units that each vary in thickness in and around the Candelaria trough, and rests directly on Paleozoic metasedimentary rocks where the older Cenozoic units are stratigraphically omitted. The late Oligocene Candelaria sequence is most prominent in the low-lying Candelaria

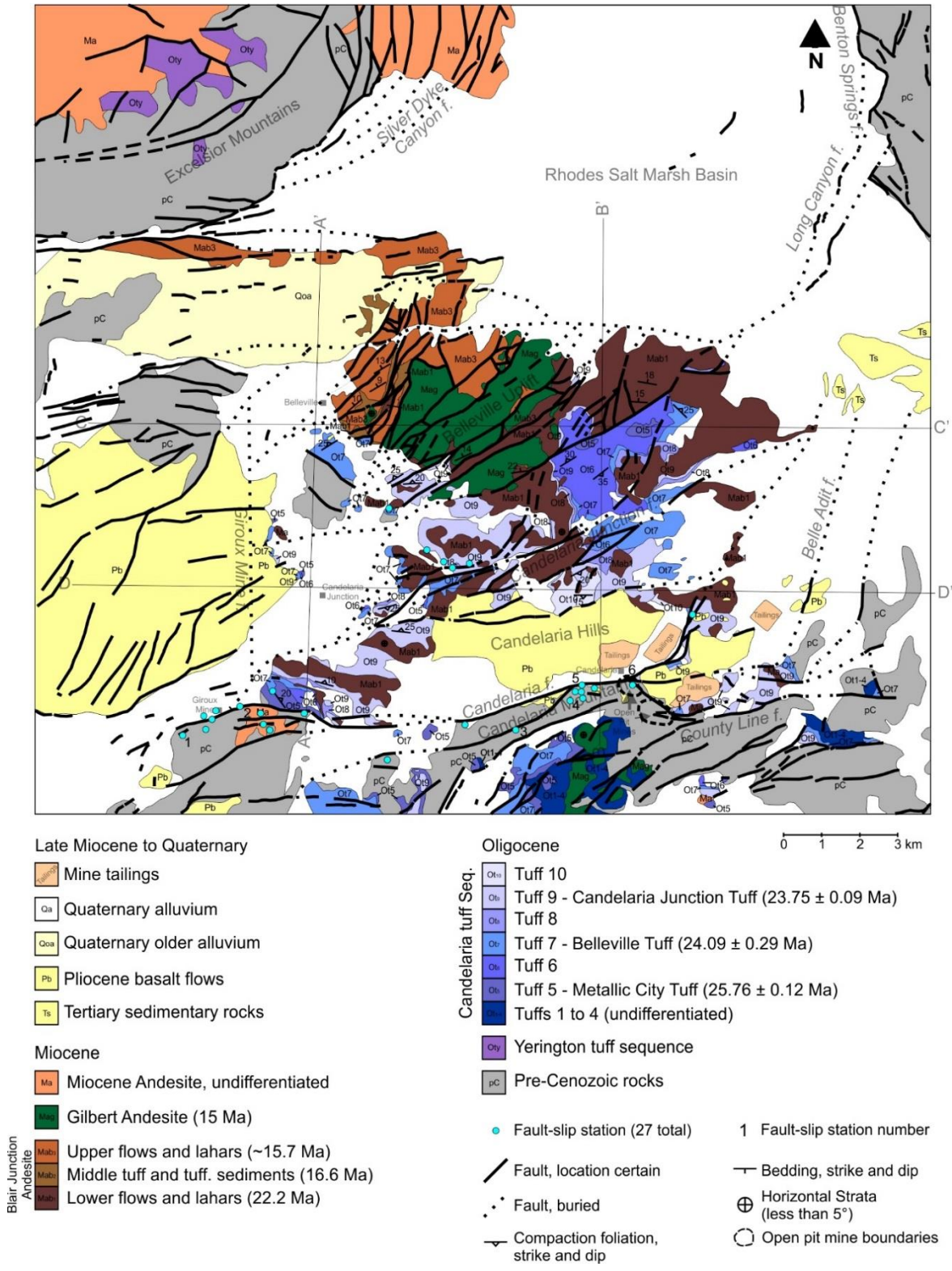

Figure 2.14. Geologic map of the Candelaria Hills and eastern Excelsior Mountains.

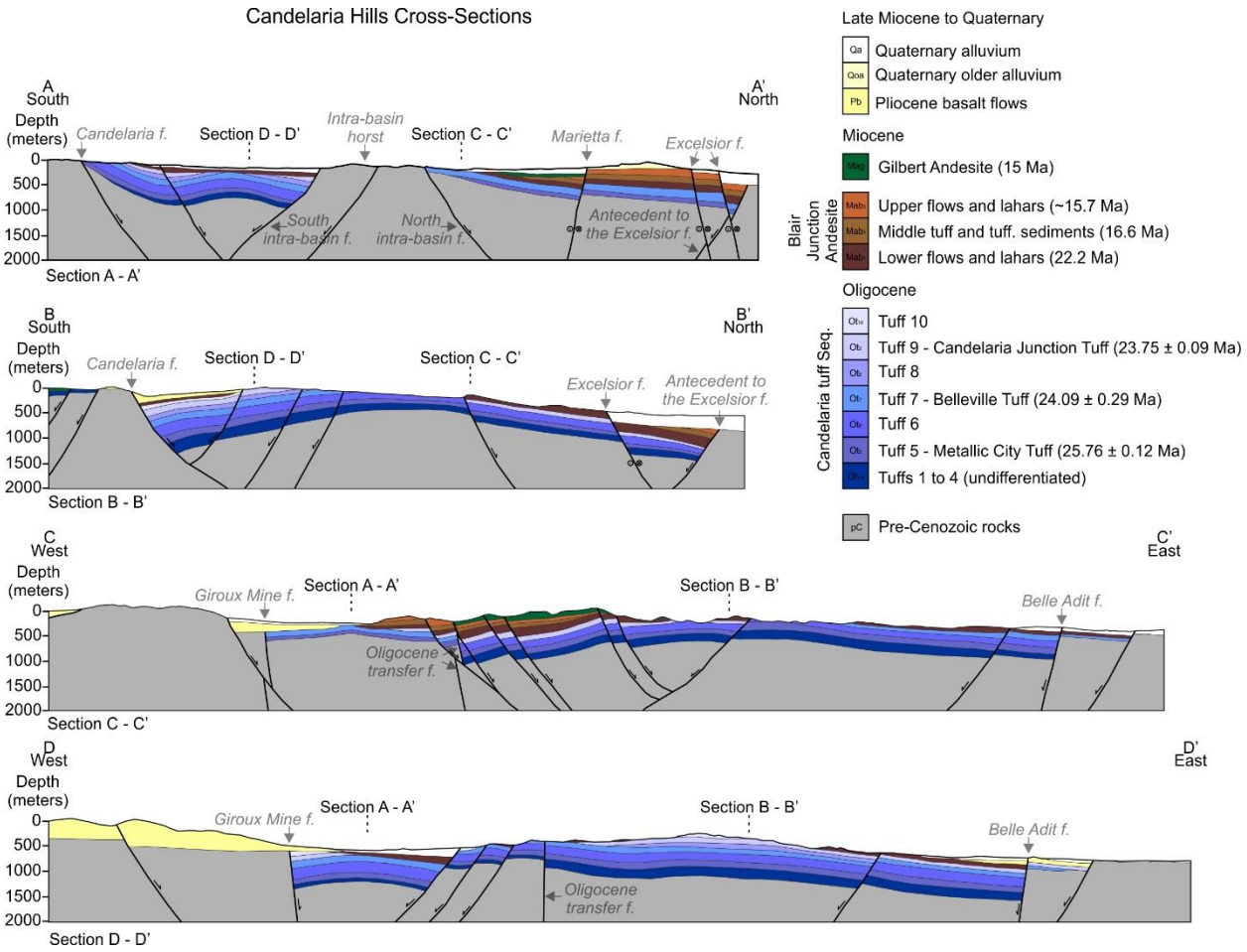

Figure 2.15. Cross section of the Candelaria Hills.

Hills between the physiographic highs of the Excelsior Mountains and Candelaria Mountain but also crops out on Candelaria Mountain.

Contemporary faults (Figs. 2.14 and 2.15) form a "Z" shaped geometry and some older, inactive faults are inferred but remain buried by Pliocene to recent strata and will be discussed later (Speed and Cogbill, 1979). The northern and southern edges of this fault system is controlled by the east-striking Candelaria fault and Excelsior fault that are connected by east-northeast and northeast—striking faults. The faults exhibit left-lateral strike-slip or oblique-slip

motion and vertical offsets of 10 to 150 m leaving the geometry of the Candelaria trough relatively intact.

Candelaria sequence tuffs within the basin are folded into gentle synclines and anticlines that trend east-west. The folds have interlimb angles that range from 130° to 145° and half-wavelengths of approximately 2 km. The overlying early Miocene andesite is not folded indicating that the Candelaria sequence was folded during a 1.5 to 2.0 million year period between the end of late Oligocene tuff deposition and the inception of early Miocene andesite deposition. The andesite sequence rests with profound angular unconformity on multiple units of the Candelaria tuff stratigraphy suggesting erosion of the late Oligocene strata accompanied or directly post-dated folding.

The Candelaria Trough

The Candelaria trough (Figs. 2.14 and 2.15) has a rectilinear geometry and controlled deposition of the Oligo-Miocene stratigraphy (Speed and Cogbill, 1979). The northern and southern margins of the basin trend east-west and are separated by 10 to 12 km. The basin is 10 to 15 km long and is bounded to the west by the north-striking Giroux Mine fault and to the east by the north-northeast—striking Belle Adit fault. The basin-fill is composed of the Candelaria sequence and Blair Junction sequence whereas the Gilbert Andesite forms a mid-Miocene overlap sequence.

Geometry. Thickness changes and spatial distribution of the late Oligocene Candelaria tuffs and early Miocene andesite indicate that the units were synextensionally deposited. The Candelaria sequence and Blair Junction sequence within the basin increase thickness up to 1500

m across the basin axis (Fig. 2.15) into the Candelaria and Excelsior faults whereas aqe-equivalent strata outside the basin are 10 to 200 m thick and often feature omitted stratigraphic units.

On and directly south of Candelaria Mountain (Fig. 2.14), the late Oligocene and early Miocene rocks rest flatly on Paleozoic rocks but exhibit stratigraphic omission of various tuff and andesite units. Candelaria sequence tuffs are present as thin, isolated outcrops and mainly consists of just the Metallic City tuff, the Belleville tuff, and the Candelaria Junction tuff whereas other undated and unnamed units are mostly absent. The Blair Junction andesite sequence is absent allowing the Gilbert andesite to rest directly on Candelaria sequence tuffs and Paleozoic metasedimentary rocks.

The eastern Excelsior Mountains (Figs. 2.4 and 2.14) expose Yerington Sequence tuffs, early Miocene andesite and very sparse outcrops of Candelaria sequence tuffs that depositionally overlie Paleozoic to Mesozoic metasediments, and Mesozoic to Cenozoic intrusive rocks (Garside, 1979). Although both the Yerington and Candelaria tuffs are present in the Excelsior Mountains, the two sequences are never seen in contact with one another. Yerington sequence consists of the Guild Mine and Weed Heights members of the Mickey Pass Tuff dated and is dated at 27.1 Ma (Marvin et al., 1977). The Yerington sequence is typically tens of meters thick but has a maximum thickness of 235 m. The Yerington tuff sequence shows gradual lateral thinning of individual units until the whole section pinches out. Individual tuff units are often omitted from the upper part of the sequence suggesting that thickness changes resulted from erosion instead of synextensional deposition. Yerington sequence tuffs do not appear to extent southward past the Excelsior fault despite their presence in the Excelsior Range. The Candelaria

tuff sequence is absent except for sparse deposits isolated to in the Camp Douglas area where the unit is less than 80 m thick. The Candelaria sequence consists of the Metallic City and Belleville tuffs that are separated by an angular unconformity such that each unit rests on the pre-Cenozoic substrate. The early Miocene andesite is 100 to 200 m thick and unconformably overlies Yerington sequence tuffs and Paleozoic metasedimentary rocks. Andesite in this is area is divided into lower and upper sequences that roughly align with the Blair Junction andesite and Gilbert andesite and is separated by an angular unconformity that shows up to 10° of angular discordance.

In the Candelaria Hills, the Candelaria tuff sequence and Blair Junction sequence within the basin record the asymmetric geometry of the half-graben (Figs. 2.14 and 2.15) and are overlain by post-extensional Gilbert andesite with angular unconformity showing 10° to 15° of angular discordance. The Gilbert andesite 30 to 60 m thick and often caps the tops of hills and ridges.

Candelaria sequence forms prismatic wedges that variously tilt south and north and consist of two to ten units throughout the basin. The Blair Junction sequence forms a northward-thickening wedge that overlies tuffs of the Candelaria sequence with angular unconformity. In the area surrounding Candelaria Junction, the Candelaria sequence is folded into an east-trending syncline-anticline pair and then overlain by flat-lying Blair Junction sequence showing angular discordance of 15° to 25° between the folded and unfolded units. Angular discordance of 15° to 25° between the folded and unfolded units allows the Blair Junction sequence to rest on multiple units of the underlying Candelaria sequence in the hinge of the anticline.

Differences in the tilt direction divide the Candelaria trough into two areas shown on Section A – A' and Section B – B'. The two north-trending sections are tied together by Section C – C' and Section D – D' to show changes in thickness along the basin axis.

Section A – A'. In the western part of the basin shown on Section A – A' (Fig. 2.15), the Candelaria sequence and Blair Junction sequence record the development of two smaller half-grabens with northward polarities that are separated by a horst exposing Paleozoic rocks at the surface 1.5 km south of Belleville and 2.0 km north of Candelaria Junction. The base of the Candelaria sequence rests on Paleozoic rocks along the western part of the Candelaria fault and 1.5 km south-southeast of Belleville, and dips steeply north consistent with northeast and northwest dipping compaction foliations measured in these areas. The basin-fill in the southern sub-basin beneath Candelaria Junction is folded and then overlain by unfolded, flat-lying Blair Junction sequence. The basin-fill of the northern sub-basin increases thickness northward and consists of both Candelaria sequence tuffs and Blair Junction andesite.

Section B – B'. In the eastern part of the basin shown on Section B – B' (Fig. 2.15), the Candelaria sequence forms a stratal wedge that is up to 1300 m thick and thins to 500 m to the north whereas the Blair Junction sequence forms a wedge that is thin in the south and increases thickness to the north like age-equivalent rocks to the west. Northward thinning of the Candelaria sequence is accommodated by tuff units that pinch out to the north. Tuff units 7, 8, and 10 of the Candelaria sequence all pinch out northward allowing the Belleville tuff (unit 9) to rest directly on unit 6 and be overlain by andesite units. The south to north pinch out of the Candelaria Junction tuff (unit 7) and unit 8 occurred over 2 km. Candelaria Junction tuff pinches

out allowing tuff unit 8 to overlie tuff unit 6 that in turn pinches out and is overlapped by the Belleville tuff (unit 9).

Faults. The rectilinear geometry of the Candelaria trough originates from east, north and north-northeast—striking faults that controlled basin development (Figs. 2.14 and 2.15). The basin is bounded to the south and north by east-striking faults, the Candelaria and Excelsior faults. The trough was terminated at its western and eastern margins by north to north-northeast—striking faults, the Giroux Mine and Belle Adit faults, that are late Oligocene to early Miocene in age and are currently inactive or reactivated. The Candelaria trough is also segmented by a north-striking transfer fault that separates the eastern and western areas within the half-graben. The southward and northward increases in the thicknesses of the basin-fill indicate that the east-striking faults acted as the master faults of within the half-graben fault system.

Master faults and antithetic faults: Candelaria fault, Excelsior fault, and intra-basin normal faults. Candelaria sequence and Blair Junction sequence increase thickness across the basin axis forming prismatic wedges that truncate into east-striking faults. The asymmetric wedges formed by the Candelaria and Blair Junction sequences, stratigraphic pinch outs, and stratigraphic omission indicate that the basin-fill was incrementally tilted along listric faults as the Candelaria trough was filled. The differential south and north tilts show that the east-striking faults influence on subsidence and tilt direction varies through time. In the western part of the basin, two south-dipping east-striking faults controlled the polarity of the sub-basins and the horst that separates the two half-grabens. These two master faults were active throughout deposition of the Candelaria sequence and Blair Junction sequence as indicated by the

northward-thickening wedges that both basin-fill units form. The master faults in this part of the basin are currently buried by Quaternary alluvium but their presence is indicated by the north-dipping strata that project into uplifted Paleozoic metasedimentary 1.5 km south of Belleville and in the Excelsior Mountains. During Candelaria sequence time, the Candelaria fault controlled subsidence in the eastern part of the basin as indicated by the southward-thickening Candelaria tuff. The influence of the Candelaria faults waned during deposition of the Blair Junction and subsidence was instead controlled by the antecedent to the Excelsior fault as indicated by the andesite unit increasing thickness to the north.

The western half of the basin is divided into smaller southern and northern basins (Figs. 2.14 and 2.15) by two east-striking faults that bound a horst that exposes Paleozoic metasedimentary rocks overlain by thin layers of tuff. The southern of these intra-basin faults dips south and acted as the master fault for the southern sub-basin. Candelaria sequence tuffs in the hanging wall of the southern intra-basin fault dip north and thicken into the south-dipping structure where they are juxtaposed with Paleozoic metasedimentary rocks of the intra-basin horst. The northern intra-basin fault dips north and acted as an antithetic structure to the south-dipping antecedent of the Excelsior fault. The late Oligocene tuffs and early Miocene andesite in the hanging wall of the northern intra-basin fault dip shallowly northward demonstrating the inferiority of the northern intra-basin fault with respect to the antecedent of the Excelsior fault.

Transfer faults: Giroux Mine fault, Belle Adit fault, intra-basin transfer fault. The thickness of the Candelaria sequence and Blair Junction sequence changed along the axis of the Candelaria trough (Fig. 2.15) in addition to across-strike changes. The thickness changes occurred across known and inferred high-angle faults that strike north to north-northeast. The

north to north-northeast striking faults are sub-orthogonal to the east-striking master faults and terminate the axis of the Candelaria trough at its western and eastern ends. Although disrupted by modern normal displacement or buried by Plio-Quaternary lava flows and alluvium, the north and north-northeast-striking faults in the late Oligocene to early Miocene acted as transfer faults (Gibbs, 1984), allowing basin subsidence to occur along master faults on either side of the basin.

A north-striking fault bounds the western margin of the Candelaria trough and is called the Giroux Mine fault. The fault is recognized by stratigraphic omission of the Candelaria and Blair Junction sequences. The fault is buried beneath Pliocene basalt flows and Quaternary alluvium but was active in the late Oligocene to early Miocene as indicated by the stratigraphic omission of the Candelaria sequence and Blair Junction sequence. The fault is now buried but juxtaposes Paleozoic metasedimentary rocks to the west with ignimbrites and andesites of the Candelaria and Blair Junction sequences that rest on Paleozoic rocks where the base of the Cenozoic section is preserved.

The north-northeast-striking Belle Adit fault forms the eastern boundary of the Candelaria trough. The fault dips steeply west and separates a 500 to 1300 m thick section of Candelaria sequence ignimbrites and Blair Junction andesite to the west from Paleozoic rocks overlain by a 100 m thick section of Oligo-Miocene rocks. Thinning of the Candelaria and Blair Junction sequences was accommodated by stratigraphic omission across the Belle Adit fault. Offset Pliocene basalts flows and Quaternary alluvium indicate that the Belle Adit fault remains active today.

A transfer fault segmented the basin allowing for the reversal of basin polarity and was later disrupted by Pliocene to Quaternary faulting. The transfer fault was oriented approximately

north-south parallel to the Giroux Mine and Belle Adit faults and flanked the eastern face of the intra-basin horst that exposes Paleozoic rocks. The fault juxtaposes south tilted Candelaria sequence and north-tilted Blair Junction sequence rocks on the east from north-dipping age-equivalent rocks and Paleozoic metasediments to the west.

Fault Kinematics of the Candelaria Trough

Fault-slip data (Fig. 2.16) was collected along the Candelaria fault that bounds the Candelaria trough to the south. A total of 248 fault-slip lineations were divided into the groups of coordinates slip based on 33 cross cutting relationships observed at six stations. A subset containing 91 lineations are related to present-day extension, 112 measurements formed by mid-Miocene to Pliocene extension, and the remaining 45 measurements are attributed to north-south extension. The fault-slip data was collected in outcrops of Paleozoic metasedimentary rocks, late Oligocene ignimbrites of the Candelaria sequence and the early Miocene andesite at 27 stations that lie adjacent to the Candelaria fault.

Contemporary deformation (D3) is characterized by a primary extensional axis oriented N62W ± 15° and second extensional axis that trends N40E ± 9° (Fig. 2.16). The contemporaneous motion of the two extensional axes is demonstrated by mutually cross cutting slickenlines. West-northwest trending lineations cross cut slip lineations associated with the secondary axis three times at stations CH-4 and CH-6, and are in turn cut by north-northeast trending lineations four times at stations CH-2, CH-4, CH-5, and CH-6. A subset of 51 fault-slip measurements indicate west-northwest extension and another 40 lineations are attributed to the secondary north-northeast extensional axis.

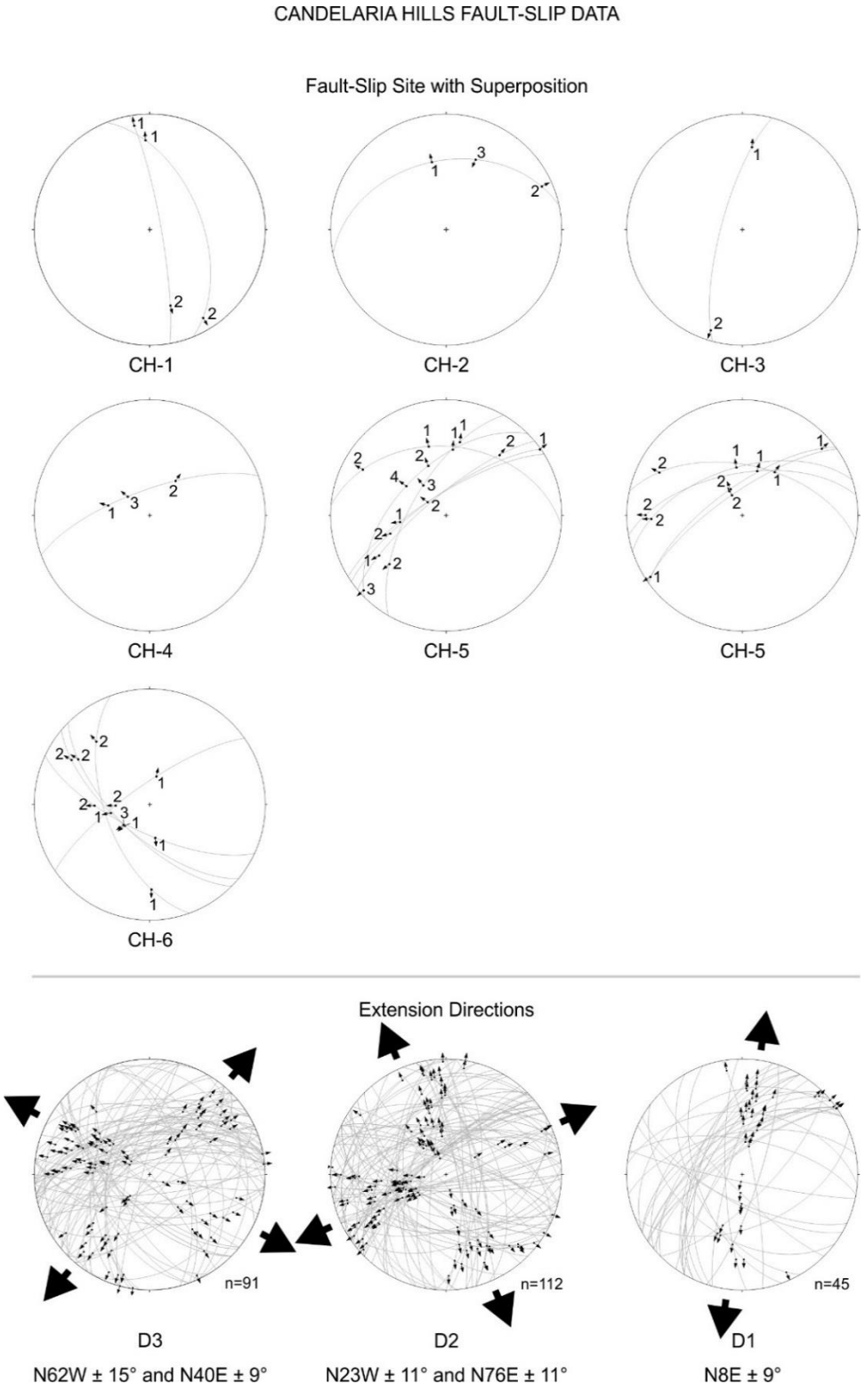

Figure 2.16. Candelaria Hills fault-slip data.

The second extensional event (D2) is characterized by two coeval strain axes (Fig. 2.16) oriented north-northwest at N23W ± 11° and east-northeast at N76E ± 11°. Mutually cross cutting slickenlines attributed to each extension direction are observed at stations CH-5 and CH-6. Fault-slip data associated with D2 extension is superposed on by both D3 extension directions. West-northwest trending slip lineations (D3) are superposed on north-northwest lineations (D2) on slip surfaces at station CH-5 and on east-northeast lineations (D2) in six instances at stations CH-5 and CH-6. Likewise, north-northeast slip lineations (D3) cut north-northwest slickenlines once at station CH-2 and cross east-northwest striations once at station CH-5. A total of 61 fault-slip measurements comprise north-northwest extension and a subset of 51 measurements make up east-northeast extension.

North-South extension consists of a single extension direction oriented N8E ± 9° (Fig. 2.16). A total of 45 north-south trending slickenlines indicate that the Candelaria fault was previously dominated by dip-slip motion. North-south extension is the oldest recognized extension direction as indicated by being cross cut by west-northwest and north-northeast lineations (D3) in six cases at stations CH-1, CH-3, CH-5, and CH-6, and by being cut by north-northwest and east-northeast slip lineations (D2) in six instances observed at stations CH-5 and CH-6.

Extension across the Candelaria Trough

The Candelaria Trough experienced 1011±85 m to 1130±127 m of horizontal motion across the western and eastern sides of the basin, respectively (Fig. 2.8). Extension was accommodated by a series of east-trending fault systems including the Candelaria fault and the antecedent to the Excelsior fault. Variations in vertical displacement occurred along the strike of

the master faults as indicated by changes in dip direction and synextensional basin-fill and was accommodated by a north-striking transfer fault that decoupled the east and west sides of the basin. The horizontal component of fault motion on each fault was calculated using the extension direction N8E ± 9° determined from fault-slip analysis.

On the east side of the basin (Fig. 2.8), extension first occurred on the Candelaria fault and later switched to the antecedent to the Excelsior fault master fault as indicated by the Candelaria sequence forming a southward thickening wedge and the lower andesite unit increasing thickness towards the north. The Candelaria fault dips 60° north where measured in the North Belle Mine and strikes N75E. Vertical displacement on the Candelaria fault is 1300 m as indicated by the maximum thickness of the Candelaria Sequence resulting in 833±49 m of horizontal motion. The antecedent to the Excelsior fault strike N90W and dips 60°±5° south. The fault experienced approximately 500 m of throw during the early Miocene resulting in 297±69 m of horizontal movement.

On the west side of the basin (Fig. 2.8), extension was accommodated on south-dipping normal faults that divided the basin into two smaller basins separated by a horst. The antecedent to the Excelsior fault formed the northern margin of the basin. The fault strikes N90W and dips 60°±5° south like in the east side of the basin and experienced 297±69 m of horizontal extension. The Candelaria fault acted as an antithetic structure to the antecedent of the Excelsior fault and formed the southern margin of the basin. The Candelaria fault dips 60° north and strikes N85E, and experienced 250 m of vertical displacement resulting in 150±5 m of horizontal extension. Between the Candelaria fault and antecedent of the Excelsior fault, extension was accommodated on two intra-basin faults that strike N90W and bound the intra-basin horst. The northern intra-

basin fault dips 60°±5° north and underwent 119±28 m of horizontal extension given the fault's 200 m of throw. The southern intra-basin fault dips 60°±5° south and has vertical displacement of approximately 750 m given projections of north-dipping Candelaria Sequence and therefore experienced 445±103 m.

Bettles Well Valley

Late Cenozoic rocks are concentrated in an east-west—trending upland valley called Bettles Well Valley (Fig. 2.17) that lies between the southern Gabbs Valley Range and the northern Pilot Mountains that expose pre-Cenozoic rocks (Meinwald, 1982). Pre-Cenozoic rocks consist of siliciclastic and carbonate metasedimentary rocks and Mesozoic intrusive rocks (Oldow, 1981). The Cenozoic stratigraphy consists of late Oligocene silicic ignimbrites of the Yerington tuff sequence, Oligocene lavas, early Miocene andesitic lavas and lahars and epiclastic sedimentary rocks overlain by Mid Miocene to Pliocene tuff, basalt and sedimentary rocks (Dockery, 1982). The Yerington tuffs consist of the of the Guild Mine member of the Mickey Pass Tuff dated at 28.0 to 27.4 Ma (Proffett, 1977; Ekren et al., 1980; Henry and John, 2013) and the Singatse Tuff dated at 27.2 to 26.9 Ma (Proffett, 1977; John and Henry, 2013). The stratigraphic position of the Oligocene lavas with respect to the Yerington tuffs is ambiguous (Meinwald, 1982). If the Oligocene lavas sit stratigraphically below the ignimbrite sequence, deposition within the basin may have started even earlier that 28 Ma. The early Miocene andesite in Bettles Well Valley correlates to andesite dated 17.4 to 15.1 Ma (Marvin et al., 1977; Stewart et al., 1994) in the Candelaria Hills and Monte Cristo Range based on the prevalence of volcanoclastic facies. The base of the andesite in Bettles Well Valley is not exposed so could be as old as 22 Ma. The late Oligocene and early Miocene sections are separated by a profound angular unconformity

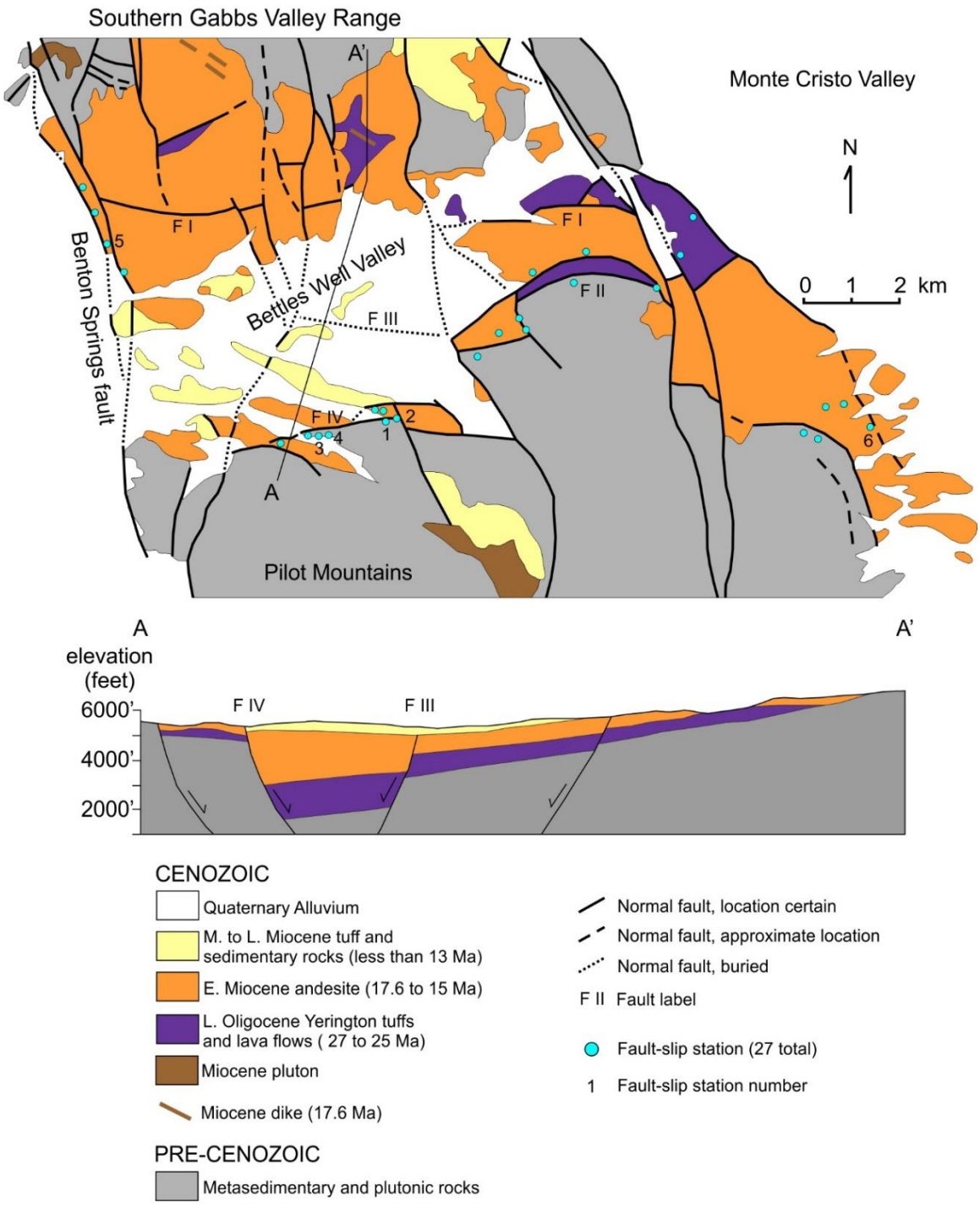

Figure 2.17. Geologic Map of Bettles Well Valley. Modified from Dockery (1982), Meinwald (1982), and Hardyman and Oldow (1991).

so that andesite sequence rests on each of the Oligocene units and represents at 4 to 5 million break in deposition.

Faults in this area predominately strike north-northwest and east forming a network of orthogonal structures (Oldow and Meinwald, 1992; Oldow and Dockery, 1993). The north-northwest—striking faults bound the western and eastern flanks of the southern Gabbs Range Bettles Well Valley, and northern Pilot Mountains separating alluvium in Soda Springs Valley and Monte Cristo Valley from bedrock exposures in the ranges and upland valley (Hardyman and Oldow, 1991). The east—striking faults cross the interface of the upland valley and bounding ranges and dip toward the valley separating thick accumulations of Cenozoic rocks within Bettles Well Valley from pre-Cenozoic rocks overlain by thin Cenozoic strata in the ranges (Dockery, 1982; Meinwald, 1982). The east—striking faults exhibit a dog-leg geometry across north-northwest—striking faults (Hardyman and Oldow, 1991).

Late Oligocene to Early Miocene Basin

The stratal patterns of the late Oligocene and early Miocene units (Fig. 2.17) indicate that the north-northwest and east-striking faults seen today were active as early as the late Oligocene and formed an east to east-northeast—trending half-graben (Dockery, 1982). A gravity survey conducted in Bettles Well Valley indicates that the late Oligocene tuffs and early Miocene andesite together form an asymmetric stratal wedge that thickens southward reaching at least of 1200 m and ultimately truncates into east—striking faults (Meinwald, 1982). The thickness of the section is inferred because the ignimbrites and andesites are best exposed in the southern Gabbs Valley Range and buried by late Miocene tuff and Pliocene to Quaternary basalt and alluvium within the upland valley. In outcrop, the Singatse tuff shows a southwestward

thickness increase into the upland valley. The maximum observed thickness is 60 m but the true stratigraphic thickness is unknown because the lower contact of the unit is not exposed. The presence of the angular unconformity within the basin-fill suggests that the half-graben experienced an initial period of late Oligocene subsidence that passed into a 4 to 5 million year break in subsidence and deposition, followed by renewed basin growth in the early Miocene.

The Bettles Well Valley half-graben (Fig. 2.17) was controlled by east—striking faults (Meinwald, 1982). The basin is bounded to the south by east-striking and north-dipping normal faults that separate the Guild Mine Member of the Mickey Pass Tuff, the Singatse tuff, and early Miocene andesite in the hanging wall to the north from pre-Cenozoic rocks in the footwall overlain by isolated outcrops of andesite to the south. The south-bounding faults are misaligned and have a dog-leg geometry accommodated by through-going north-northwest—striking faults. The central and northern part of the basin is segmented by east-striking and south-dipping normal faults that are antithetic to the north-dipping master faults.

Fault Kinematics of the Bettles Well Valley Half-Graben

Fault-slip lineations related to three episodes of extension (Fig. 2.18) are recorded in the damage zone of east and north-northwest—striking faults that form the boundaries of the Bettles Well Valley half-graben. A total of 252 fault-slip measurements were separated into the three generations of slip by 25 superposed slickenlines recognized at six stations. The fault-slip data was collected in Paleozoic siliciclastic and carbonate metasediments, late Oligocene ignimbrites of the Yerington sequence, and the early Miocene andesite at 27 stations that lie along the southern, eastern and western boundaries of the Bettles Well Valley half-graben.

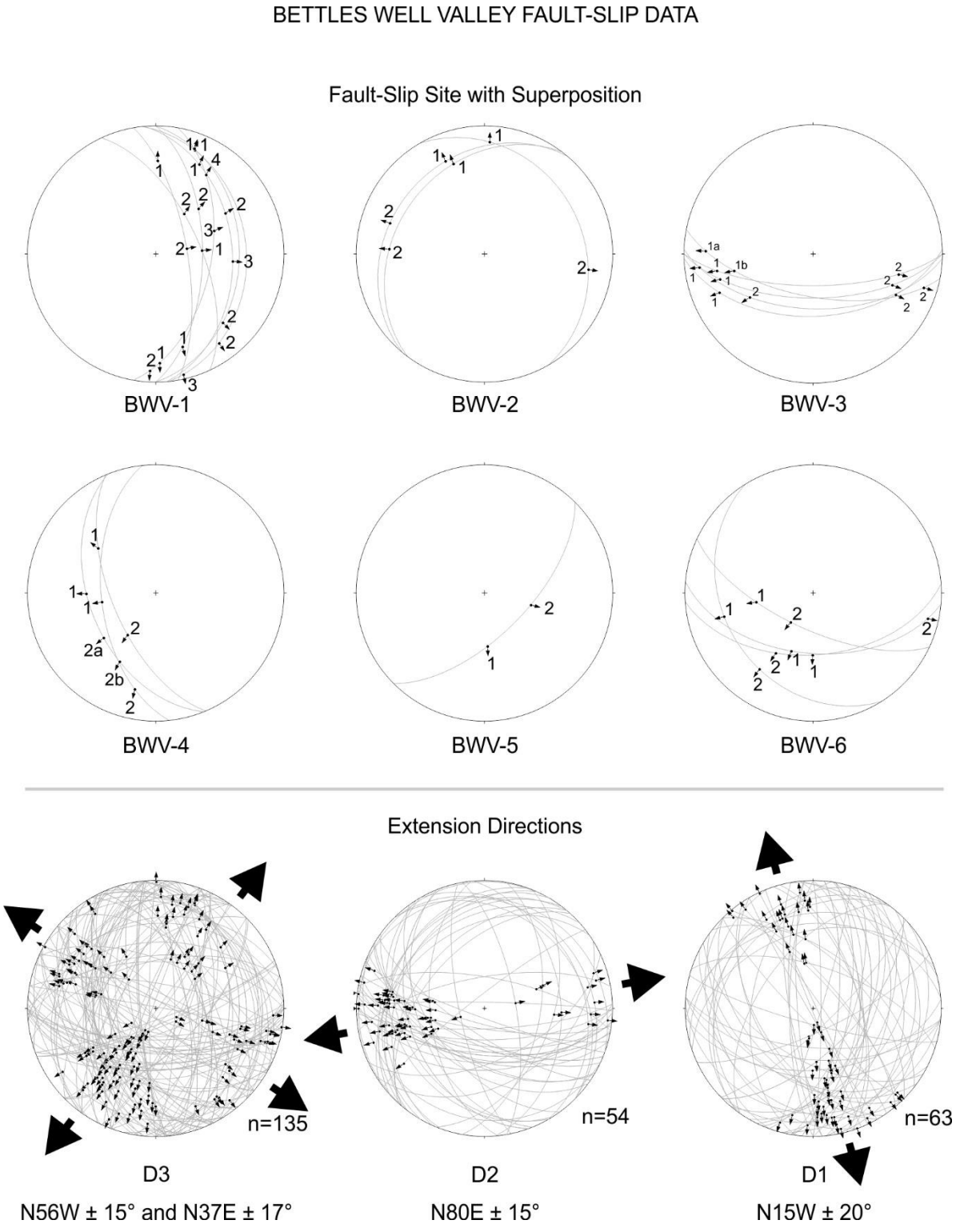

Figure 2.18. Bettles Well Valley fault-slip data.

The youngest and contemporary extensional event (D3) consists of two extension directions (Fig. 2.18) oriented N56W ± 21° and N37E ± 17°. Simultaneous activity of west-northwest and north-northeast extension is demonstrated by mutually cross cutting slip lineations at stations BWV-1, BWV-4, and BWV-6. West-northwest and north-northeast trending slickenlines mutually cross at station BWV-1 whereas west-northwest crosses north-northeast once at station BWV-6, and north-northeast crosses west-northwest once at station BWV-4. Both sets of lineations are found at station BWV-3 but were not observed on common slip surface. A subset of 54 measurements are related to west-northwest extension and another 81 measurements are consistent with north-northeast extension.

The second extension direction (Fig. 2.18) consists of a single east-northeast trend (D2) oriented N80E ± 15°. East-northeast trending slip lineations are cross cut by lineations associated with west-northwest extension on five surfaces at station BWV-3 and by north-northeast lineations in six cases at stations BWV-1, BWV-3, BWV-4, and BWV-6. East-northeast extension consists of 55 fault-slip lineations.

North-south extension (Fig. 2.18) is the earliest late Cenozoic event recognized in the fault-slip data. The direction of extension is N15W ± 20° and is demonstrated by 62 measurements. Superposed fault-slip data at four stations demonstrate that north-south trending slickenlines are consistently cross cut by slip lineations related to D2 and D3 extension. East-northeast trending (D2) slip lineations cut north-south lineataions on five slip surfaces at stations BWV-1 and BWV-2. Fault-slip lineations attributed to west-northwest extension (D3) cut north-south lineations in two cases at stations BWV-5 and BWV-6, and slip lineations related to north-

northeast extension (D3) cut north-south lineations in three cases at stations BWV-1 and BWV-6.

Extension across the Bettles Well Valley Half-Graben

The Bettles Well Valley half-graben experienced 856±155 m to 1015±182 m of horizontal extension (Fig. 2.8). Extension occurred on the east-trending faults I, II, III, and IV that bound and cross the basin and were active in the late Oligocene and early Miocene given changes in stratal thickness recognized in outcrop and gravity studies (Oldow and Meinwald, 1992; Oldow and Dockery, 1993; Meinwald, 1982). The faults in this area are modeled at 60°±5°. Horizontal motion on these faults was directed N15W±20° as indicated by fault-slip analysis.

Extension was predominately accommodated on the north-dipping faults II and IV (Fig. 2.8) as indicated by the southward thickening wedges of late Oligocene and early Miocene strata (Fig. 2.17). Fault II dips north and forms a curved trace that ranges in strike from N60E to N80W. Vertical displacement on Fault II was 840 m as indicated by the maximum thickness of the late Oligocene and early Miocene rocks and resulted in 524±123 m of horizontal motion. Fault IV strikes N80E to N90E and experienced 714±166 m of horizontal movement as indicated by a 1200 m thick section of Oligo-Miocene basin-fill recognized in gravity surveys that indicates 1200 m of vertical displacement.

The south-dipping faults I and III acted as antithetic structures to the master faults (Figs. 2.8 and 2.17). Fault I has a strike of N90W and shows a variable amount of displacement between its eastern and western sides. Offsets and thickness changes of the Oligo-Miocene rocks indicates that the eastern half of Fault I has vertical displacement of 550 m that resulted in

332±95 m of horizontal movement whereas the western half shows only 75 m of vertical motion resulting in 45±13 m of horizontal extension. Fault III dips strikes approximately N70W and experienced about 360 m throw that resulted in 256±74 m of horizontal extension.

Northern Garfield Hills and Soda Springs Valley West

The northern Garfield Hills lie along the southern margin of Soda Springs Valley (Figs. 2.2 and 2.19) that forms an anomalous east-trending depression that is 10 to 15 km long, 6 km wide, and is bordered to the north by the Gillis Range. The Cenozoic stratigraphy in each of the bounding mountain ranges differs in age and lithologic composition and rests unconformably on Paleozoic to Mesozoic metasedimentary rocks and Mesozoic plutons (Ekren and Byers, 1985). Cenozoic rocks in the Gills range consist of the Yerington tuff sequence, early Miocene andesite, and late Miocene to Pliocene tuffs, sedimentary rocks, and basalt flows. The Yerington tuff sequence has an aggregate thickness of 1670 m but is most often on the order of hundreds of meters thick due to omission of stratigraphic units. The sequence predominate contains the Guild Mine member of the Mickey Pass tuff dated at 28.0 to 27.4 Ma (Ekren et al., 1980; Henry and John, 2013) and the Singatse Tuff dated at 27.2 Ma (Proffett, 1977) but also contains less widespread units such at the Blue Sphinx Tuff and Hu-Pwi Tuff dated at 24.3 Ma and 23.6 Ma, respectively (Dilles and Gans, 1995; Henry and John, 2013). Early Miocene rocks in the Gillis Range is mainly composed of lava flows dated at 22.5 to 15 Ma but interleaved ash flow tuffs dated at 19.2 and 18.1 Ma and volcaniclastic sedimentary rocks (Ekren and Byers, 1985). In contrast, Cenozoic strata in the northern Garfield Hills on the south side of the east-trending basin only consist of a 200 m thick section early Miocene andesite. The andesite sequence in

this part of the Mina-Dyer region is not divided into the lower and upper sequences seen in the Excelsior Mountains, Candelaria Hills, Monte Cristo Range, and Palmetto Mountains.

The margin between the northern Margin Hills and Soda Springs Valley west is occupied by an east-striking fault that forms the southern boundary of Soda Springs Valley west separates bedrock from the present-day basin (Hardyman and Oldow, 1991). The south-bounding fault dips north and is crossed by north-northwest—striking faults that run along Soda Spring Valley, the eastern Garfield Hills, and extend northward across the Gillis Range (Ekren and Byers, 1985). A series of east-northeast—striking normal faults cross the northern Garfield Hills (Fig. 2.19) and juxtapose early Miocene andesite with pre-Cenozoic rocks (Oldow and Steuer, 1985).

The Case for a Half-Graben in Soda Springs Valley West

Gravity models of the east-trending Soda Springs Valley by Wetterauer (unpublished data 1980) indicate that the basin has an asymmetric geometry and increases depth southward across the basin axis. The maximum depth of the basin varies from 1000 to 2000 m deep depending on which stratigraphic units fill the basin and lies along the east-striking fault the separates bedrock in the Garfield Hills from Soda Springs Valley to the north. The preferred model (Fig. 2.20) suggests that the basin is 1500 m and is predominately filled with early Miocene andesite, lahars, and sedimentary rocks underlain by a thin layer of Yerington sequence tuffs, and overlain by a thin prismatic wedge of Quaternary alluvium. Variations on this basic model all give depth results in the 1500 to 2000 m range (Keller, 1998) except for the unlikely case that the half-graben is entirely filled with alluvium in which case the basin could be as shallow as 1000 m. Excessive outcrop of late Oligocene to early Miocene rocks exposed along the margins of Soda Spring Valley indicate that it is unlikely that the basin only contains

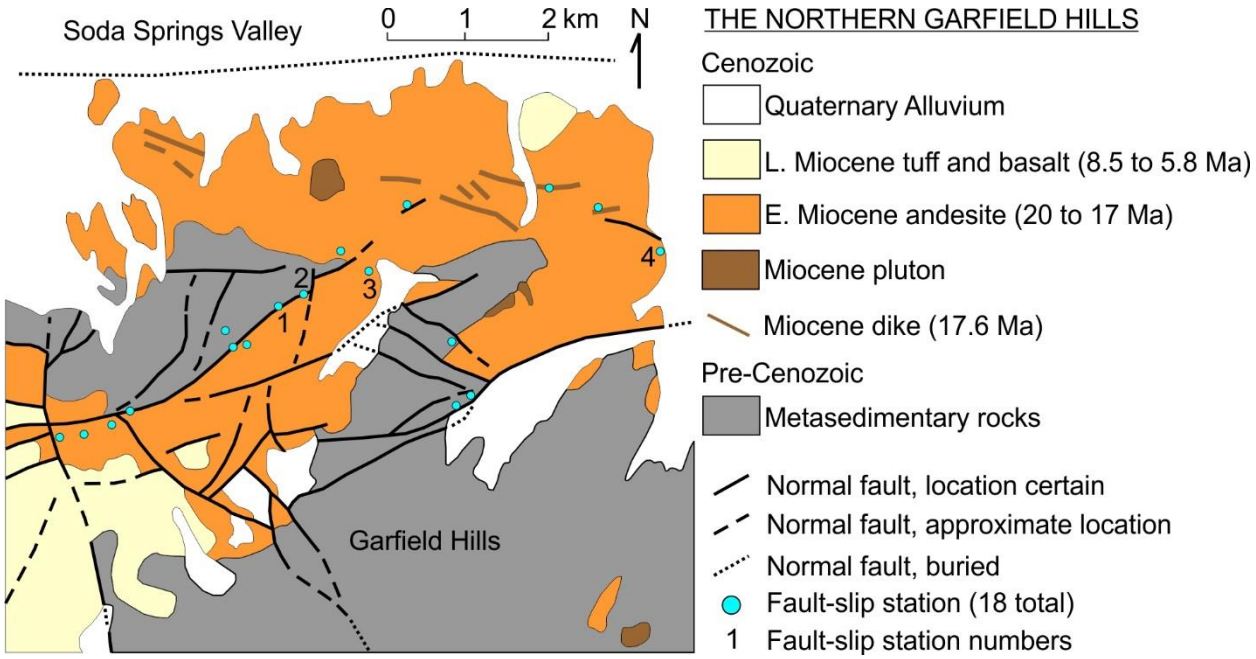

Figure 2.19. Geologic Map of the northern Garfield Hills. Modified from Hardyman and and Oldow (1991).

alluvium. Aside from the abundance of Oligo-Miocene rocks surround the basin, the master wouldn't be able to form 1 km deep basin under current extension direction. The gravity study suggests that the basin has an east-west length of 10 to 15 km where the basin is terminated by north-northwest—striking faults (Keller, 1998) exhibiting the same orthogonal fault geometry seen in Bettles Well Valley (Meinwald, 1982).

Fault Kinematics of the Northern Garfield Hills Half-Graben

Fault-slip data (Fig. 2.21) was collected along east to east-northeast—striking faults that cross the northern Garfield Hills along the southern flank of Soda Springs Valley because the proposed half-graben is itself buried beneath Quaternary alluvium. The northern Garfield Hills lie in the footwall of the master fault of the Soda Spring Valley half-graben and potentially lies

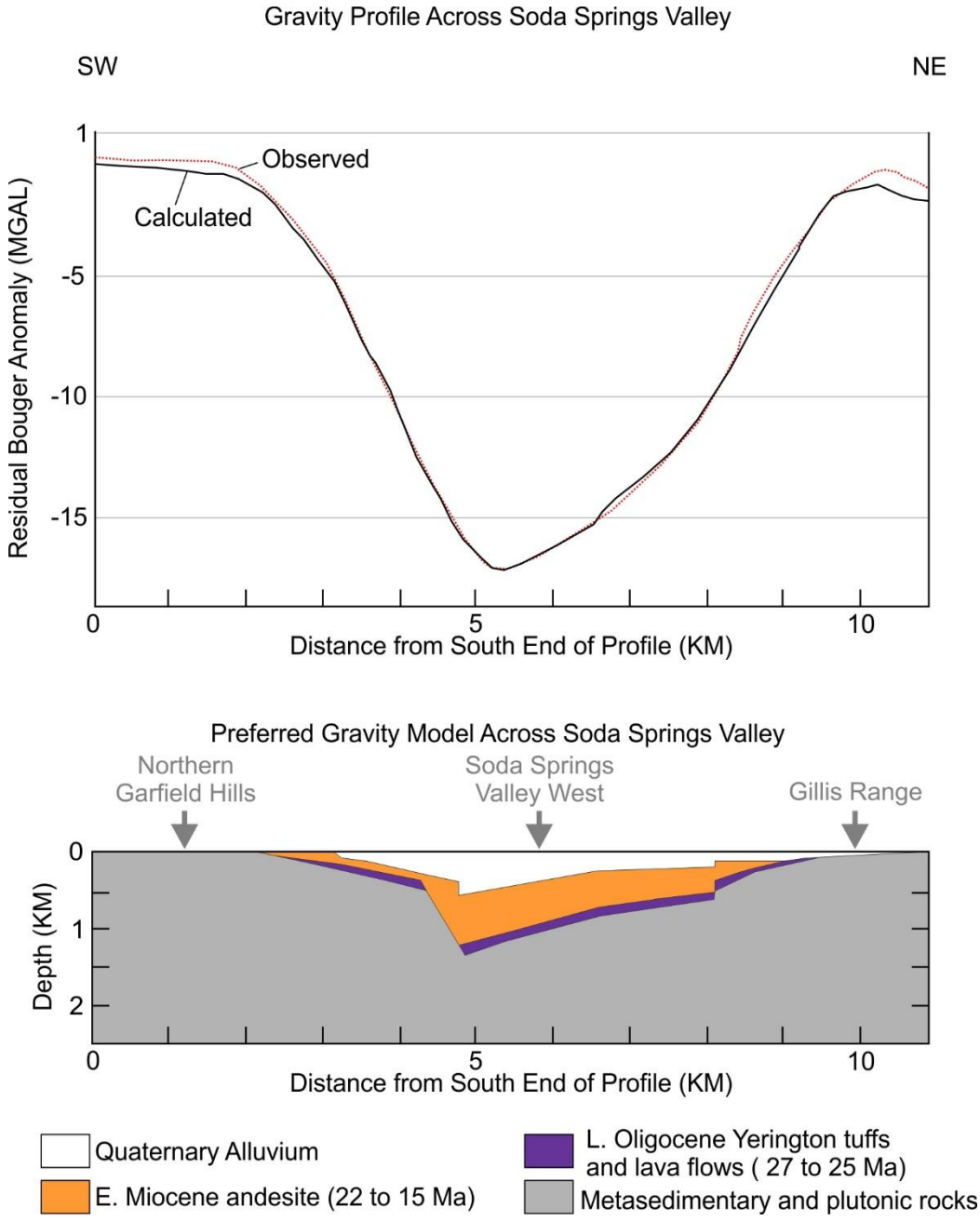

Figure 2.20. Gravity model of the northern Garfield Hills and Soda Springs Valley west. Modified from Wetterauer (unpublished data 1980) and Keller (1998).

within its damage zone as seen in other fault systems that preserve kinematic indicators at distances as far as 1 km from the main fault strand (Ferranti et al., 2009). A total of 183 fault-

slip measurements were collected at eighteen stations (Fig. 2.19) in Mesozoic metasedimentary rocks and early Miocene andesite. Seventeen cross cutting slickenlines observed at four stations (Fig. 2.21) divide the fault-slip data into three generations.

Contemporary extension (D3) is oriented N62W ± 17° and has a secondary extensional axis oriented N37E ± 17° (Fig. 2.21). The two extension directions operate simultaneously as demonstrated by mutually cross cutting relationships at stations GH-2 and GH-4. West-northwest trending lineations cut across north-northeast lineations on three occasions whereas the opposite situation occurs on two surfaces. Slickenlines attributed to the two extension directions lie in close proximity to each other at stations GH-1 and GH-3 but were not observed in contact on a shared slip surface. West-northwest extension consists of 28 measurements and north-northeast extension is composed of 66 lineations.

The second extensional event (D2) consists of a single extension direction oriented N80E ± 10° (Fig. 2.21). Slickenlines associated with east-northeast extension are crossed by west-northwest and north-northeast trending lineations of D3 extension on two instances at station GH-3. A total of 34 slip lineations comprise east-northeast extension.

The oldest extensional event (Fig. 2.21) recognized is north-south extension (D1) and is oriented N15W ± 15°. Slickenlines associated with north-south extension are cross cut by east-northeast trending (D2) lineations at station GH-3, and by west-northwest and north-northeast slip lineations at stations GH-1, GH-2, GH-3, and GH-4. North-south lineations are crossed by fault-slip lineations attributed to west-northwest extension (D3) on two instances and by north-northeast trending lineations in seven cases. A total of 55 fault-slip measurements are associated with north-south extension.

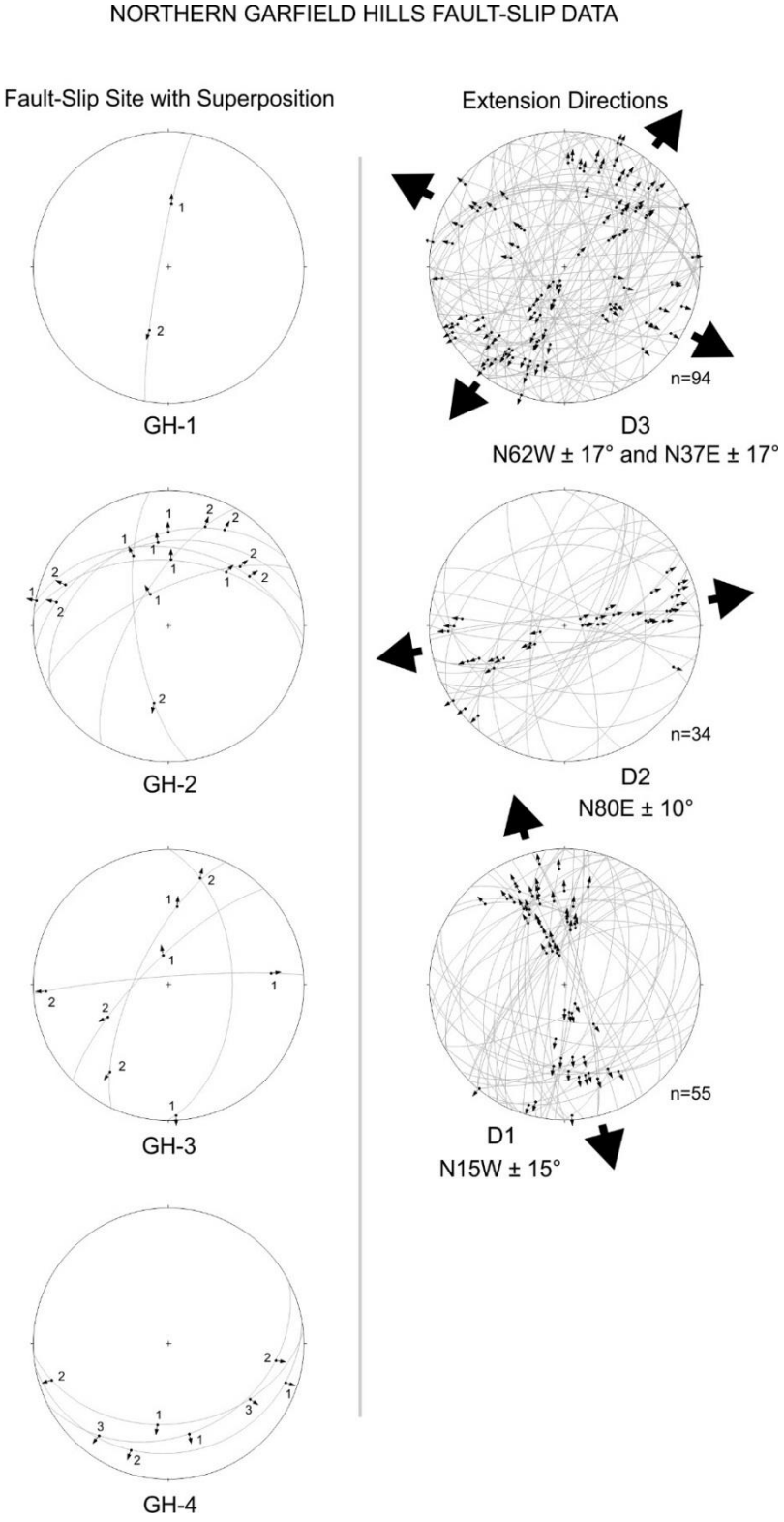

Figure 3.21. Northern Garfield Hills fault-slip data.

Extension across the Northern Garfield Hills Half-Graben

Horizontal extension across the northern Garfield Hills half-graben was at least 671±48 m (Fig. 2.8). The asymmetric geometry recognized in gravity anomalies (Wetterauer, unpublished data 1980) indicates that most of the extension was accommodated by the master fault that forms the southern margin of the basin. The master fault strikes N70W to N80W and dips 60°±5° north (Keller, 1998). A minimum estimate of throw of 1000 m resulted in at least 671±48 m of horizontal motion under extension oriented N15W ± 15°. Only the master fault was recognized by the gravity survey but the possible presence less pronounced synthetic and antithetic faults that lie below the resolution of gravity data could indicate that Extension across the basin is underestimated. No such structures are recognized, of course, but it is not beyond the realm of possibility considering that each of the other east-trending half-grabens preserve many synthetic and antithetic faults.

DISCUSSION

The Mina-Dyer region (Fig. 2.2) experienced a period of low-magnitude north-south extension recognized by development of east-northeast and west-northwest—trending half-grabens (Fig. 2.4) containing late Oligocene to early Miocene synextensional basin-fill. Although the half-grabens on an individual basins are 500 to 1500 m deep, extension across the region was low-magnitude as indicated by thin, extensive deposits of late Oligocene and early Miocene strata that occupy the areas between half-grabens and show no sign of synextensional deposition. Fault kinematic data preserved in fault zones of the half-grabens, basin geometry, stratal geometry and east-trending dike swarms and hypabyssal plutons indicate that the basins formed under north-south extension. Formation of the late Oligocene and early Miocene half-

grabens created low-relief topography that controlled the thickness and spatial distribution of late Oligocene and early Miocene rocks of the ignimbrite flare-up and subsequent andesite volcanism.

Geometry of Late Oligocene and Early Miocene Half-Grabens

Synextensional deposition of late Oligocene to early Miocene strata within the east-northeast, east-west, and west-northwest—trending half-grabens (Figs. 2.4, 2.5, 2.9, 2.11, 2.14, 2.17, and 2.20) is indicated by across-fault changes in thickness, asymmetric stratal wedges, and upward decreasing dips within the stratigraphic section. Late Oligocene to early Miocene basin-fill in all six half-grabens dips south indicating the asymmetric basin geometry and in two basins locally dips north due to changes in basin polarity. Gravity surveys conducted in three of the six half-grabens show an asymmetric basin geometry. The basin-fill in each area forms asymmetric stratal wedges (Figs. 2.6, 2.12, 2.15, 2.17, and 2.20) that mimic the asymmetric geometry of the half-grabens and thicken into basin-bounding master faults that strike east-northeast, east-west and west-northwest. The asymmetric geometry of the basin-fill results in fanning-stratal geometries resulting from upward decreases in dip that show angular discordance of 10° to 30° between the base of the wedge and the top. Individual tuffs, lava flows and lahars increase thickness southward across-strike into their basin-bounding master faults. In contrast, age-equivalent rocks deposited outside the basins sit relatively flatly and are typically 100 to 200 m thick showing no sign of synextensional deposition.

The half-grabens had discontinuous basin-axes (Fig. 2.2) segmented by north-northeast to north-northwest—striking faults indicated by across-fault basin depth and thickness changes in the late Oligocene and early Miocene stratigraphy. Transfer faults that bound the half-grabens

are recognized by the late Oligocene and early Miocene rocks abruptly changing thickness and stratal geometry along basin axes (Figs. 2.12 and 2.15). Synextensional rocks within the half-grabens form tilted, asymmetric stratal wedges that are 500 to 1500 m thick whereas aqe-equivalent strata outside the basins rest flatly on the pre-Cenozoic substrate and are only 100 to 200 m thick. In many cases, entire stratigraphic units are omitted are omitted across north-northeast and north-northwest—striking faults. Transfer faults also crossed the center of the half-grabens as indicated by dog-legs in the master fault geometry and reversals in basin polarity (Figs. 2.5, 2.6, 2.14, and 2.15).

The transfer faults bounded and segmented the late Oligocene and early Miocene half-grabens causing a dog-leg geometry in the system of basins (Figs. 2.2, 2.11, and 2.17). The late Oligocene and early Miocene half-grabens are separated by 10 to 20 km steps (Fig. 2.2) to north or south along transfer faults. Many of the of the late Oligocene and early Miocene transfer faults are active today with right-lateral motion but the half-graben axes do not consistently step to the right across the transfer faults indicating that the dog-legs in the half-graben axes are part of the original basin geometry and not necessarily the result of younger displacement on reactivated structures. Although most of the late Oligocene and early Miocene transfer faults were reactivated by younger extension, some were not reactivated are remain buried by late Miocene to Pliocene strata. The discontinuous geometry of the half-graben axes and dog-legs that were part of the late Oligocene to early Miocene basin geometry indicating that the half-grabens are unsuitable to use as displacement markers for modern right-lateral strike-slip faults of the Walker Lane.

The variation in basin axes and transfer fault trends can be attributed to late Miocene to recent vertical-axis rotation (Fig. 2.4). Half-grabens within the rotational domain have east to west-northwest trends that differ by 20° to 30° from east-northeast—trending basins that were not rotated. The half-grabens in the rotational domain have east to east-northeast trends originally and transfer faults that were oriented north-south to north-northwest. Likewise, transfer faults that were rotated strike north to north-northeast whereas those that lie outside the rotational domain strike north-northwest.

North-South Extension

The late Oligocene and early Miocene half-grabens formed under north-south extension as indicated by basin geometry, stratal patterns, dike orientations, and fault-slip data (Figs. 2.4, 2.7, 2.10, 2.13, 2.16, 2.18, and 2.21). Synextensional strata that thicken to the north and south within the half-grabens indicate that east-northeast and west-northwest—striking basin-bounding faults had a significant component of dip-slip motion. However, stratal tilts only record the dip-slip component of displacement and not the strike-slip component of motion and therefore it is fault dip-parallel slip lineations that truly demonstrate normal displacement on the east-northeast and west-northwest—trending faults. Cross-cutting slickenlines within the damage zones of the basin-bounding faults indicate that dip-slip motion is the oldest recorded history of displacement on the east-northeast and west-northwest—striking faults. Dip-slip motion along these faults during deposition of late Oligocene and early Miocene rocks would have allowed the asymmetric geometry of the half-grabens and basin-fill to form. Absolute timing of north-south extension and half-graben formation is best demonstrated in the Palmetto Mountains where synextensional strata accumulated in a west-northwest—trending basin from 22 to 16.6 Ma and was in turn

overlapped by thin, flat-lying layers of post-extensional rocks at 16.1 to 15 Ma. North-south fault-slip lineations are restricted to the early Miocene synextensional andesite and Paleozoic metasediments and Mesozoic pluton indicating that north-south extension was on-going in the early Miocene and ceased by the mid-Miocene. Other five half-grabens see the same sequence of extension directions and NS extension is the oldest in each case. Presence of late Oligocene tuffs synextensionally deposited within the east-northeast and west-northwest—trending half-grabens indicates that north-south extension started as early as 27.4 Ma. North-south extension is consistent with the emplacement of east-west—trending hypabyssal plutons and dikes dated at ~17.4 Ma across the Mina-Dyer region. In the Palmetto Mountains, the east-trending dikes and pluton were emplaced during half-graben development as indicated by hydrothermal alteration of the basin-fill and intrusive rocks that were then unconformably overlain by a thin layer of unaltered, post-extensional andesite.

Space-Time Patterns of Half-Graben Subsidence and Magmatism

Formation of the half-grabens (Fig. 2.22) coincided with synextensional deposition of volcanic and sedimentary rocks indicating that development of the late Oligocene and early Miocene half-grabens represent a structural component of ignimbrite flare-up and subsequent andesite volcanism in the Mina-Dyer region. Extension started with onset of ignimbrite volcanism as indicated by late Oligocene strata that form the base of the synextensional stratigraphy. Extension didn't started significantly before ignimbrite volcanism or there would be thick sedimentary deposits within the basins. In ranges where base of basin-fill is exposed, volcanic rocks sit directly on pre-Cenozoic rocks and sedimentary deposition becomes dominant much later in early Miocene. Extension continued after the ignimbrite flare-up into early

Miocene andesite deposition and even into the waning stages of volcanism as sedimentary deposition dominated late andesite time. Extension ended by the mid-Miocene when the Gilbert andesite buried several of the half-grabens under thin layers of lava flows. Half-grabens buried by the Gilbert andesite are recognized in the Palmetto Mountains and Candelaria Hills but may be more widespread given the difficulty in differentiating two andesite successions in many areas.

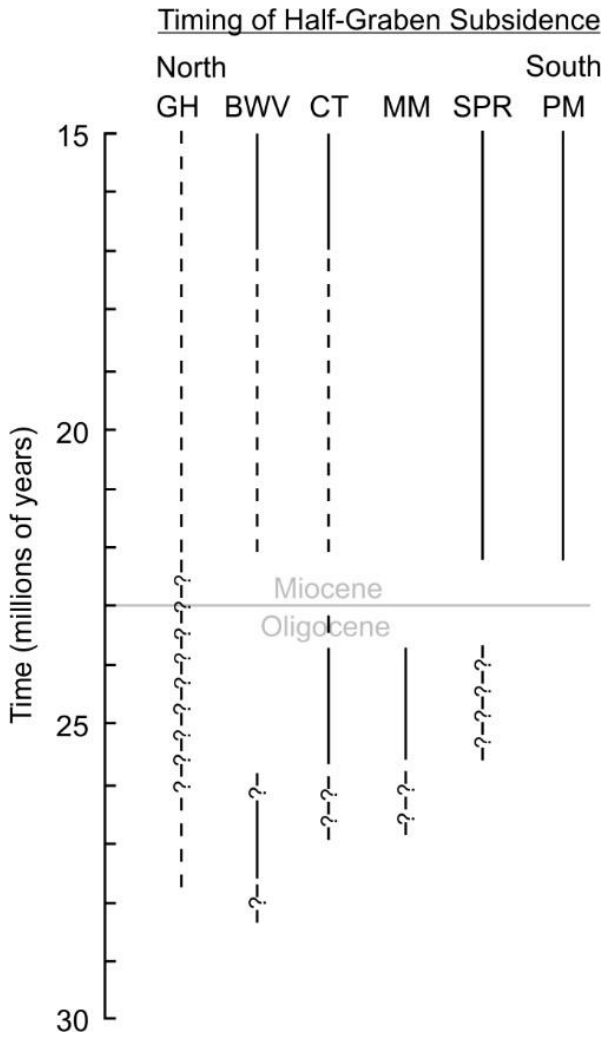

Figure 2.22. Timing of late Oliocene and early Miocene half-graben subsidence. Solids lines show the basin was certainly subsiding, dashed lines show the basin was likely subsiding, and dashed lines with questions marks show basins that where subsidence was unlikely.

The thickness and spatial distribution of late Oligocene and early Miocene rocks indicates that extension and subsidence in the half-grabens occurred asynchronously (Figs. 2.2, 2.5, 2.9, 2.11, 2.14, 2.17, and 2.20). Not all basins are the same age so that some are only early Miocene, only late Oligocene, or late Oligocene to early Miocene. The Miller Mountain half-graben (Fig. 2.11) is only late Oligocene in age and was sealed by the Candelaria Junction Tuff. The Palmetto Mountains half-graben (Fig. 2.5) is only early Miocene in age was sealed by the Gilbert andesite. The Garfield Hills and Silver Peak half-grabens (Figs. 2.10 and 2.20) are predominately filled with early Miocene synextensional strata although minor amounts of extension may have occurred in the late Oligocene as well. Half-grabens in the Candelaria Hills and Bettles Well Valley (Figs. 2.14 and 2.17) contain synextensional deposits that range in age from late Oligocene to early Miocene. Earliest extension occurred in basins (Fig. 2.22) containing the Yerington tuff sequence which appear to have started a couple million year earlier than basins containing the Candelaria tuff sequence although extension could have started at the same time depending on the age of the undated tuffs and older andesite at the base of the Candelaria sequence (and possibly below Yerington and Royston Hills tuffs too). Extension in these basins continued into the early Miocene as indicated by synextensional deposits of andesite but at Miller Mountain extension ended in late Oligocene. With continuation of extension in early Miocene new basins formed that contain only early Miocene rocks. Finally all extension ended by mid-Miocene.

Unconformities in the Candelaria Hills and Bettles Well Valley (Figs. 2.14 and 2.17) suggest that there may be two periods of extension and basins subsidence. Two distinct periods of basin subsidence are demonstrated by basins that contain only Miocene andesite such as the

Palmetto Mountains and Silver Peak half-grabens and the late Oligocene ignimbrite-containing Miller Mountain half-graben that differ in age and geographic location. Formation of angular unconformities at the interface of the Oligocene and Miocene sections and the lack of synextensional units indicates the absence of deposition and basin subsidence for at least 1 to 2 million years around the Oligocene-Miocene boundary. In Bettles Well Valley (Fig. 2.17), the intervening period of inactivity could have lasted for 4 to 5 million years. The angular unconformity between Oligocene and Miocene units is best observed in the Candelaria Hills and Bettles Well Valley where the angular discordance between the two sections is 15° to 25°. These areas demonstrate that enough time passed between deposition of the ignimbrites and the andesite to allow for erosion of the older sequence as evidenced by the scouring of channels into the tuffs that were later filled in with volcaniclastic sedimentary rocks. In Candelaria (Figs. 2.14), the Oligocene tuffs are folded into gentle east-west—trending folds and are overlain by flat-lying andesite. The hinges of anticlines were beveled by erosion which allowed the younger andesite to rest on many units of the older tuff stratigraphy throughout the region. The base of the overlying andesite sequence is mainly lava flows but locally is characterized by channel-filling breccia that occupy scours in the Oligocene tuffs (Speed and Cogbill, 1979). The presence of basin-fill tuff clasts in the breccias indicate the tuffs were being actively eroded before andesite deposition and therefore indicates a lack of basin subsidence directly before andesite deposition. In Bettles Well Valley, the andesite section rests on the Yerington tuff sequence and the Bettles Lava indicating the formation of a profound angular unconformity prior to the early Miocene.

The compositional change from silicic to andesitic volcanism correlates to the two periods of late Oligocene and early Miocene half-graben development. The temporal shift from a more mature magma source to a more primitive source occurred across throughout the Mina-Dyer region during the break in basin subsidence as indicated by consistent ages of silicic and intermediate composition rocks in the half-grabens. The lack of calderas and prevalence of silicic and intermediate intrusive rocks suggests that the rocks are locally sourced from fissure vents (Ekren and Byers, 1976) and leaky faults (Kerstetter et al., in prep), and is consistent with a widespread change in magma composition.

Low-Magnitude Extension and Paleotopography

North-south extension covered an area of 15,000 km^2 given the spatial distribution, thickness and stratal geometry of late Oligocene and early Miocene strata (Fig. 2.2) but was low-magnitude and restricted to the east-northeast and west-northwest—trending half-grabens (Figs. 2.4 and 2.23) so that many parts of the Mina-Dyer region did not experience extension. A total of 1 to 2 km of extension (Fig. 2.23) was accommodated by formation of east-northeast and west-northwest—trending half-grabens. Individual half-grabens are 0.5 to 1.5 km deep and experienced 400 to 1000 m of north-south extension indicated by magnitudes of displacement of late Oligocene and early Miocene growth faults. The half-grabens are separated by 10 to 25 km (Fig. 2.4) where thin, flat-lying deposits of late Oligocene to early Miocene rocks and a lack of growth faults indicate that areas outside the basins experience little, if any, north-south extension. East-northeast and west-northwest—trending fault systems in the intervening areas between the half-grabens equally offset all late Oligocene and early Miocene strata indicating that the faults postdate deposition and are unrelated to north-south extension.

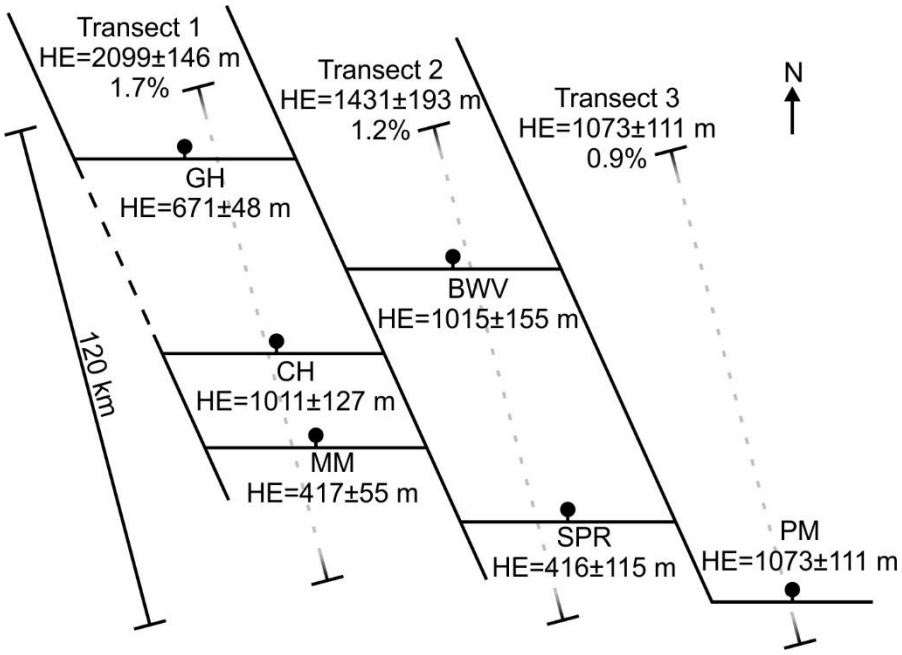

Figure 2.23. Rectlinear model of late Oliocene and early Miocene half-graben system, and total horizontal extension.

The spatial distribution of late Oligocene and early Miocene strata (Figs. 2.2 and 2.3) indicate that the low-magnitude of extension formed low-relief, long wavelength topography punctuated by broad, elevated areas. Topography around most of the half-grabens was subdued as indicated by late Oligocene and early Miocene rocks being deposited inside and outside the basins despite the changes in thickness of growth strata. Late Oligocene tuffs in particular form extensive deposits that cover areas of 1,500 to 2,000 km^2 although the Yerington, Candelaria and Royston Hills tuff sequences are spatially segregated indicating that broad elevated regions were capable of separating 100 to 200 m thick tuff successions. Likewise, the early Miocene andesite is widely distributed across the region and sits on each of the three late Oligocene tuff successions.

The margins of the elevated areas correspond to the master faults and transfer faults of a few late Oligocene and early Miocene half-grabens (Fig. 2.2) indicating that the elevated parts of the paleotopography mimicked the dog-leg geometry of the half-grabens. The near absence of Yerington and Candelaria tuffs in the Excelsior Range, Garfield Hills and Pilot Mountains indicate a 50 km long, east-trending topographic that separated Yerington tuffs to the north from Candelaria tuffs to the south. The paleotopographic high decreased width from 25 km in the Excelsior Mountains and Garfield Hills to 10 to 15 km in the Pilot Mountains across north-northwest—trending transfer faults between the Garfield Hills and Bettles Well Valley half-grabens. The spatial distribution of the Yerington sequence in the Gillis Range, Gabbs Valley Range and Bettles Well Valley indicates that the northern margin of the Excelsior-Pilot Mountains trend has a dog-leg geometry controlled by master faults and transfer faults of the northern Garfield Hills half-graben and the Bettles Well Valley half-graben. The southern margin of elevated region was fairly linear and was bounded by the antecedent to the Excelsior fault along the southern flank of the present-day Excelsior Mountains and by a buttress unconformity along the south flank of the Pilot Mountains. The transition from structural control to a buttress unconformity along the south flank of the Excelsior Mountains and Pilot Mountains indicates that the antecedent to the Excelsior fault did not extend eastward past the north-northwest—trending transfer faults in Soda Springs Valley and that there is a complicated relationship between extension, deposition, and paleotopography. Similar to the Excelsior Mountains and Pilot Mountains, near absence of late Oligocene Candelaria tuffs and early Miocene andesite south of the northern Palmetto Mountains and central Silver Peak Range indicate the presence of a west-northwest—trending elevated area that coincides with the

southern edges of the Palmetto Mountains and Silver Peak half-grabens. Separation of the Yerington and Candelaria sequences from Royston Hills tuffs in the Cedar Mountains, Royston Hills, and Jackson Wash indicates the presence of the north-trending elevated area along the present-day Clayton Ridge and west flank of the Cedar Mountains. Synextensional deposits of early Miocene andesite indicate that the Clayton Ridge fault system was active during north-south extension and controlled stratigraphic omission of the andesite succession (Kerstetter et al., in prep) but it is uncertain whether or not the paleotopographic area bordering the Cedar Mountains had structural control.

CONCLUSIONS

The Mina-Dyer region experienced a period of late Oligocene to early Miocene north-south extension that formed a series of east-northeast, east-west, and west-northwest—trending half-grabens. The half-grabens controlled the spatial distribution and thickness of late Oligocene and early Miocene volcanic and sedimentary rocks. Synextensional deposition within and around the half-grabens is indicated by late Oligocene and early Miocene strata that form asymmetric stratal wedges within the basins, fanning stratal patterns, and show across-fault changes in thickness. Basin geometry, stratal patterns, orientations of dikes that intrude the basin-fill, and fault-slip data all indicate that the late Oligocene and early Miocene half-grabens formed under north-south extension. Absolute timing of north-south extension is indicated by restriction of north-south slip lineations to late Oligocene, early Miocene and older rocks, whereas mid-Miocene to recent strata do not record north-south slip. Formation of the half-grabens during late Oligocene and early Miocene magmatism indicates that the easterly trending basins represent a structural component of the ignimbrite flare-up and subsequent andesitic

volcanism. Changes in the age of the graben-fill indicate that extension occurred asynchronously throughout the Mina-Dyer regin during magmatism. Despite the prevalence of late Oligocene and early Miocene half-grabens, extension was low-magnitude (1 to 2%) and much of the area between the basins did not see active faulting. The spatial distribution of the late Oligocene to early Miocene strata indicates that the region was characterized by low-relief, long-wavelength topography that controlled the spatial distribution of late Oligocene tuff sequences.

REFERENCES

Albers, J.P., and Stewart, J.H., 1972, Geology and mineral deposits of Esmeralda County, Nevada, Nevada Bureau of Mines and Geology Bulletin, v. 78, 80 p.

Andrew, J.E., and Walker, J.D., 2009, Reconstructing late Cenozoic deformation in central Panamint Valley, California: Evolution of slip partitioning in the Walker Lane, Geosphere, v. 5, no. 3, p. 172-198, doi:10.1130/GES00178.1.

Bachman, 1978, Pliocene-Pleistocene break-up of the Sierra Nevada-White-Inyo Mountains block and formation of Owens Valley, Geology, v. 6, no. 8, p. 461-463.

Bally, A. W., Price, R. A., Roberts, D. G., and Osmaston, M. F., 1982, Musings over sedimentary basin evolution [and Discussion], Philosophical Transactions of the Royal Society of London. Series A, Mathematical and Physical Sciences, v. 305, no. 1489, p. 325-338.

Beeson, J. W., Johnson, S. Y., and Goldfinger, C., 2017, The transtensional offshore portion of the northern San Andreas fault: Fault zone geometry, late Pleistocene to Holocene sediment deposition, shallow deformation patterns and asymmetric basin growth, Geosphere, v. 13, no. 4, p. 1173-1206.

Best, M.G., 1988, Early Miocene change in direction of least principal stress, southwestern United States: Conflicting inferences from dikes and metamorphic core-detachment fault terranes, Tectonics, v. 7, no. 2, p. 249-259.

Best, M.G., and Christiansen, E.H., 1991, Limited extension during peak Tertiary volcanism, Great Basin of Nevada and Utah, Journal of Geophysical Research, vol., 96, no. B8, p. 13509-13528.

Best, M.G., Barr, D.L., Christiansen, E.H., Gromme, S., Deino, A.L., and Tingey, D.G., 2009 The Great Basin altiplano during the middle Cenozoic ignimbrite flareup: insights from volcanic rocks, International Geology Review, v. 51, no. 7-8, p. 589-633, doi:10.1080/00206810902867690.

Best, M.G., Christiansen, E.H., de Silva, S., Lipman, P.W., 2016, Slab-rolback ignimbrite flareups in the southern Great Basin and other Cenozoic American arcs: A distinct style of arc volcanism, Geosphere, v. 12, no. 4, p. 1-39, doi:10.1130/GES01285.1.

Bonham, H.F., 1970, Geologic map and sections of a part of the Shoshone Mountains, Lander and Nye Counties, Nevada, Nevada Bureau of Mines and Geology Map 38, scale 1:62,500.

Buchanan, P.G., and McClay, K.R., 1991, Sandbox experiments of inverted listric and planar fault systems, Tectonophysics, vol. 188, no. 1-2, p. 97-115.

Burke, D.B., and McKee, E.H., 1979, Mid-Cenozoic volcano-tectonic trough in central Nevada, Geological Society of America Bulletin, v. 90 p. 181-184.

Cland, B., and Oldow, J.S., 2017, Late Cenozoic superposition of high-angle faults and low-angle detachment faults in the eastern Mina deflection, west-central Nevada, Geological Society of America Abstracts with Programs, v. 49, no. 6, doi: 10.1130/abs/2017AM-303511.

Colgan, J.P., Henry, C.D., 2009, Rapid middle Miocene collapse of the Mesozoic orogenic plateau in north-central Nevada, International Geology Review, v. 51, no. 9-11, p. 920-961, doi:10.1080/00206810903056731.

Coney, P.J., 1978, Mesozoic-Cenozoic Cordilleran plate tectonics, in Smith, R.B., and Eaton, G.P., eds., Cenozoic Tectonics and Regional Geophysics of the Western Cordillera: Geological Society of America Memoir 152, p. 33-50, doi:10.1130/MEM152-p33.

Cowie, P.A., and Scholz, C.H., 1992, Displacement-length scaling relationships for faults: data synthesis and discussion, Journal of Structural Geology, v. 14, no. 10, p. 1149-1156.

Crowder, D. F., Robinson, P. T., and Dahl, L. H., 1972, Geologic map of the Benton Quadrangle, Mono County, California and Esmeralda and Mineral Counties, Nevada, United States Geologic Survey Geologic Quadrangle Map 1013, scale 1:62,500.

Dahlstrom, C.D.A., 1969, Balanced cross sections, Canadian Journal of Earth Sciences, vol. 6, no. 4, p. 743-757.

Delaney, P. T., Pollard, D. D., Ziony, J. I., and McKee, E. H., 1986, Field relations between dikes and joints: Emplacement processes and paleostress analysis, Journal of Geophysical Research, v. 91, no. B5, p. 4920 – 4938.

Diamond, D.S., 1990, Structural and sedimentological evolution of an extensional orogen, Silver Peak Range, and adjacent area, west-central Nevada [Ph.D. thesis]: Los Angeles, University of California-Los Angeles, 360 p.

Diamond, D.S., and Ingersoll, R.V., 2002, Structural and sedimentological evolution of a Miocene supradetachment basin, Silver Peak Range and adjacent areas, west-central Nevada, International Geology Review, v. 44, p. 588-623.

Dickinson, W.R., 2006, Geotectonic Evolution of the Great Basin, Geosphere, v. 2, no. 7, p. 353-368, doi:10.1130/GES00054.1.

Dilles, J.H., and Gans, P.G., 1995, The chronology of Cenozoic volcanism and deformation in the Yerington area, western Basin and Range and Walker Lane, Geological Society of America Bulletin, vol. 107, no. 4, p. 474-486.

Dockery, H.A., 1982, Cenozoic Stratigraphy and Extensional Faulting in the Southern Gabbs Valley Range, West-Central Nevada [M.S. Thesis]: Houston, Rice University, 89 p.

Dokka, R.K., and Travis, C.J., 1990, Role of the Eastern California Shear Zone in accommodating Pacific-North American plate motion, Geophysical Research Letters, v. 17, no. 9, p. 1323-1326.

Dover, J.H., 1962, Geology of the northern Palmetto Mountains, Esmeralda County, Nevada (M.S. thesis) Seattle, University of Washington, 50 p.

Dubyoski, P., Andrew, T., and Lee, J., 2016, Tuff-filled paleovalleys dextrally offset across the Benton Springs fault, central Walker Lane, Nevada, Geological Society of America Abstracts with Programs, v. 48, no. 7, doi:10.1130/abs/2016AM-283180.

Dunham, J.P., 2016 Reorganization and superposition of late Eocene to Holocene extension and late Cenozoic displacement field conservation on a kinematically linked array of basin-bounding faults, north-central Great Basin (Ph.D. dissertation): Richardson, The University of Texas at Dallas, 116 p.

Dunn, S. B., Oldow, J. S., and Mueller, N. J., 2015, Late Cenozoic displacement transfer in the eastern Sylvania Moutain fault system and Lida Valley pull-apart basin, southwestern Nevada, based on three-dimensional gravity depth inversion and forward models, Geosphere, vol. 11, no. 5, p. 1565-1589.

Ekren, E.B., and Byers, Jr., F.M., 1976, Ash-flow fissure vent in west-central Nevada: Geology, v. 4, p. 247-251, doi: 1130/0091-7613 (1976).

Ekren, E. B., and Byers, Jr., F.M., 1985a, Geologic map of Gabbs Mountain, Mount Ferguson, Luning, and Sunrise Flat quadrangles, Mineral and Nye Counties, Nevada: US Geological Survey miscellaneous investigations series map I-1577, scale 1:48,000.

Ekren, E. B., and Byers, Jr., F.M., 1985b, Geologic map of the Win Wan Flat, Kinkaid NW, and Indian Head Peak quadrangles, Mineral County, Nevada: US Geological Survey miscellaneous investigations series map I-1578, scale 1:48,000.

Ekren, E.B., Byers, Jr., F.M., Hardyman, R.F., Marvin, R.F., and Silverman, M.L., 1980, Stratigraphy, preliminary petrology, and some structural features of Tertiary volcanic rocks in the Gabbs Valley and Gillis Ranges, Mineral County, Nevada, USGS Bulletin 1464, 60 p.

Elias, E.A., 2005, Structural control of Late Miocene to Pliocene volcanic and volcaniclastic deposition during upper-plate fragmentation in the Silver Peak Extensional Complex, west-central Great Basin [M.S. thesis]: Moscow, University of Idaho, 68 p.

Ellis, P.G., and McClay, K.R., 1987, Listric extensional fault systems—results of analogue model experiments, Basin Research, vol. 1, no. 1, p. 55-70.

Faulds, J. E., and Varga, R.J., 1998, The role of accommodation zones and transfer zones in the regional segmentation of extended terranes *in* Faulds, J.E., and Stewart, J.H., eds., Accommodate zones and transfer zones: The regional segmentation of the Basin and Range Province: Geological Society of America Special Paper 323, p. 1-46.

Faulds, J.E., Henry, C.D., and Hinz, N.H., 2005, Kinematics of the northern Walker Lane: An incipient transform fault along the Pacific-North American plate boundary, Geological Society of America Bulletin, v. 33, no. 6, p. 505-508.

Ferguson, H.G., 1927, The Gilbert district, Nevada, U.S. Geological Survey Bulletin 795-F, p. 125-145.

Ferguson, H.G., and Muller, S.W., 1949, Structural geology of the Hawthorne and Tonopah quadrangles, Nevada: U.S. Geological Survey Profession Paper 216, 53 p.

Ferranti, L., Oldow, J. S., Geissman, J. W., and Nell, M. M., 2009, Flattening strain during coordinated slip on a curved fault array, Rhodes Salt Marsh extensional basin, central Walker Lane, west-central Nevada *in* Late Cenozoic structure and evolution of the Great Basin-Sierra Nevada transition: Geological Society of America Special Paper 447, p. 189 – 213, doi: 10.1130/2009.2447(11).

Garside, L.J., 1979, Geologic map of the Camp Douglas quadrangle, Nevada, Nevada Bureau of Mines and Geology Map 63, scale 1:24,000.

Gamond, J. F., 1987, Bridge structures as sense of displacement criteria in brittle fault zones, Journal of Structural Geology, vol. 9, no. 5, p. 609-620.

Garfunkel, Z., and Bartov, Y., 1977, The tectonics of the Suez rift, Geological Survey of Israel Bulletin, vol. 71, p. 1-41.

Gephart, J.W., 1990, Stress and the direction of slip on fault planes, Tectonics, v. 9, no. 4, p. 845-858.

Gibbs, A.D., 1983, Balanced cross-section construction from seismic section in areas of extensional tectonics, Journal of Structural Geology, v. 5, no. 2, p. 153-160.

Gibbs, A. D., 1984, Structural evolution of extensional basin margins, Journal of the Geological Society, v. 141, p. 609-620.

Gilully, J., and Masursky, H., 1965, Geology of the Cortez quadrangle, Nevada: US Geological Survey Bulletin 1175, 117 p.

Gonsior, Z. J., and Dilles, J. H., 2008, Timing and evolution of the Cenozoic extensional normal faulting and magmatism in the southern Tobin Range, Nevada, Geosphere, Vol. 4, no. 4, p. 687-712.

Hamblin, W.K., 1965, Origin of "reverse drag" on the downthrown side of normal faults, Geological Society of America Bulletin, v. 76, p. 1145-1164.

Hancock, P. L., and Barka, A. A., 1987, Kinematics indicators on active normal faults in western Turkey, Journal of Structural Geology, vol. 9, no. 5, p. 573-584.

Hardyman, R.F., and Oldow, J.S., 1991, Tertiary tectonic framework and Cenozoic history of the central Walker Lane, Nevada, Geology and ore deposits of the Great Basin: Geological Society of Nevada Symposium Proceedings, v. 1, p. 279-301.

Henry, C.D., 2008, Ash-flow tuffs and paleovalleys in northeastern Nevada: Implications for Eocene paleogeography and extension in the Sevier hinterland, northern Great Basin: Geosphere, v. 4, no. 1, p. 1-35, doi: 10.1130/GES00122.1

Henry, C.D., and Faulds, J.E., 2010, Ash-flow tuffs in the Nine Hill, Nevada, Paleovalley and implications for tectonism and volcanism of the western Great Basin, Geosphere, v. 6, no. 4, p. 339-369.

Henry, C.D., and John, D.A., 2013, Magmatism, ash-flow tuffs, and calderas of the ignimbrite flare-up in the western Nevada volcanic field, Great Basin, USA, Geosphere, vol. 9, no. 4, p. 951-1008.

Henry, C.D., and Perkins, M.E., 2001, Sierra Nevada-Basin and Range transition near Reno, Nevada: Two-stage development at 12 and 3 Ma, Geology, v. 29, no. 8, p. 719-722.

Henry, C.D., Faulds, J.E., dePolo, C.M., and David, D.A., 2004, Geologic map of the Dogskin Mountain Quadrangle, Washoe County, Nevada, Nevada Bureau of Mines and Geology Map 148, scale 1:24,000.

Henry, C.D., McGrew, A.J., Colgan, J.P., Snoke, A.W., and Brueseke, M.E., 2011, Timing, distribution, amount, and style of Cenozoic extension in the northern Great Basin, *in* Lee, J., and Evans, J.P., *eds*., Geologic Field Trips to the Basin and Range, Rocky Mountains, Snake River Plain, and Terranes of the U.S. Cordillera: Geological Society of America Field Guide 21, p. 27-66, doi:10.1130/2011.0021(02).

Henry, C. D., Hinz, N. H., Faulds, J. E., Colgan, J. P., John, D. A., Brooks, E., R., Cassel, E. J., Garside, L. J., Davis, D. A., and Castor, S. B., 2012, Eocene-early Miocene

paleotopography of the Sierra Nevada-Great Basin-Nevadaplano based on widespread ash-flow tuffs and paleovalleys, Geosphere, vol. 8, no. 1, p. 1-27.

Janecke, S. U., Hammond, B. F., Snee, L. W., and Geissman, J. W., 1997, Rapid extension in an Eocene volcanic arc: structure and paleogeography of an intra-arc half-graben in central Idaho, Geological Society of America Bulletin, v. 109, no. 3, p. 253-267.

John, D.A., Henry, C.D., and Colgan, J.P., 2008, Magmatic and tectonic evolution of the Caetano caldera, north-central Nevada: A tilted, mid-Tertiary eruptive center and source of the Caetano Tuff, Geosphere, v. 4, no. 1, p. 75-106.

Katopody, D.T., Oldow, J.S., Mueller, N.J., Nix, C., and Kerstetter, S.R., in review, Fault geometry, kinematics, and evolution of the Palmetto Mountain displacement transfer system, southern Walker Lane, Geosphere (submitted Spring 2018).

Keller, R.O., 1998, Late Tertiary tectonic evolution of the central Walker Lane, west-central Nevada and California [Ph.D. Thesis]: Houston, Rice University, 164 p.

Leeder, M.R., and Gawthorpe, R.L., 1987, Sedimentary models for extensional tilt-block/half-graben basins, Geological Society of London Special Publications, v. 28, no. 1, p. 139-152.

Lipman, P.W., Prostka,H.J., and Christiansen, R.L., 1972, Cenozoic volcanism and plate tectonic evolution of the western United States: Part 1. Early and middle Cenozoic: Philosophical Transactions of the Royal Society of London, ser.A, v. 271, p. 217-248, doi: 10.1098/rsta.1972.0008.

Locke, A., Billingsley, P., and Mayo, E.B., 1940, Sierra Nevada tectonic pattern, Geological Society of America Bulletin, v. 51, no. 4, p. 513-539.

McClay, K.R., and Scott, A.D., 1991, Experimental models of hangingwall deformation in ramp-flat listric extensional fault systems, Tectonophysics, vol. 188, no. 1-2, p. 85-96.

McQuarrie, N., and Wernicke, B.P., 2005, An animated tectonic reconstruction of southwestern North American since 36 Ma: Geosphere, v. 1, p. 147-172, doi: 10.1130/GES00016.1.

Marrett, R. A., and Allmendinger, R. W., 1990, Kinematic analysis of fault-slip data: Journal of Structural Geology, v. 12, p. 973-986.

Marvin, R. H., Speed, R. C., and Cogbill, A. H., 1977, K-Ar ages of Tertiary igneous and sedimentary rocks of the Mina-Candelaria region, Nevada: Isochron/West, v. 18, p. 9-12.

Masursky, H., 1960, Welded tuffs in the northern Toiyabe Range, Nevada: U.S. Geological Survey Professional Paper 400-B, p. B281-B283.

Meinwald, J., 1982, Extensional Faulting in the Mina Region Study of an Oligocene Basin, West-Central Nevada [M.S. Thesis]: Houston, Rice University, 164 p.

Morley, 1989, Extension, detachments, and sedimentation in continental rifts (with particular reference to eat Africa), Tectonics, v. 8, no. 6, p. 1175-1192.

Morley, C. K., Nelson, R. A., Patton, T. L., and Munn, S. G., 1990, Transfer zone in the East African rift system and their relevance to hydrocarbon exploration in rifts, The American Association of Petroleum Geologists Bulletin, v. 74, no. 8, p. 1234-1253.

Mueller, N., Oldow, J.S., Katopody, D., Gibson, K., Pham, B., McBride, K., Shilpakar, P., and Aguilar, R., 2016, Pliocene reorganization of eastern California shear zone kinematics documented in the Cucomungo Canyon restraining bend of the Furnace Creek-Fish Lake Valley fault zone, northern Death Valley and southern Fish Lake Valley, California, western Great Basin, Geological Society of America Abstracts with Programs, v. 48, no. 4, doi: 10.1130/abs/2016CD-274477.

Ng, M., and Oldow, J.S., 2017, Geometry of superposed low-angle detachment and high-angle faults in the western Silver Peak Range and northern Fish Lake Valley, Nevada, Geological Society of America Abstracts with Programs, v. 49, no. 6, doi: 10.1130/abs/2017AM-306721.

Noble, D.C., 1972, Some observations on the Cenozoic volcano-tectonic evolution of the Great Basin, western United States: Earth and Planetary Science Letters, v. 17, p.142-150, doi:10.1016/0012-821X(72)90269-5.

Oldow J. S. and Dockery, H. A., 1993, Geologic map of the Mina Quadrangle, Mineral County, Nevada, Nevada Bureau of Mines and Geology Field Studies Map 6, scale 1:24,000.

Oldow J. S. and Meinwald, J. N., 1992, Geologic map of the Bettles Well Quadrangle, Mineral County, Nevada, Nevada Bureau of Mines and Geology Field Studies Map 1, scale 1:24,000.

Oldow J. S. and Steuer, M. R., 1985, Preliminary geologic map of the Mable Mountain Quadrangle, Mineral County, Nevada, United States Geological Survey Map MF-1486, scale 1:24,000.

Oldow, J.S., and Geissman, J.W., 2013, Evolution of a late Miocene to contemporary displacement transfer system between the northern Furnace Creek and southern Fish Lake Valley fault zones and the central Walker Lane, southwest Nevada, Geological Society of America Abstracts with Programs, v. 45, no. 7, p. 224.

Oldow, J.S., Kohler, G., and Donelick, R.A., 1994, Late Cenozoic extensional transfer in the Walker Lane strike-slip belt, Nevada, Geology, v. 22, p. 637-640.

Oldow, J.S., Payne, J.D., Prestia, V.I., McClelland, W.C., and Ferranti, L., 2003, Stratigraphic and structural evolution of the Silver Peak extensional complex, western Great Basin, U.S.A. *in* Fall Field Trip Guidebook Special Publication 38, p. 51-73.

Oldow, J. S., Geissman, J. W., and Stockli, D. F., 2008, Evolution and strain reorganization within the late Neogene structural stepovers linking the central Walker Lane and the northern Eastern California shear zone, western Great Basin, International Geology Review, vol. 50, no. 3, p. 270-290.

Oldow, J.S., Elias, E.A., Ferranti, L., McClelland, W.C., and McIntosh, W.C., 2009 Late Miocene to Pliocene synextensional deposition in fault-bounded basins within the upper plate of the western Silver Peak-Lone Mountain extensional complex, west-central Nevada *in* Oldow, J.S., and Cashman, P.H., eds., Late Cenozoic structure and evolution of the Great Basin-Sierra Nevada transition: Geological Society of America Special Paper 447, p. 275-312.

Oldow, J.S., Katopody, D.T., Kerstetter, S.R., and Mueller, N.J., 2016, Regional setting, geometry, and structure of the northern Fish Lake Valley basin, American Lithium Corporation Technical Report, http://www.americanlithiumcorp.com/assets/docs/reports/ALC-Report.pdf

Petit, J. P., 1987, Criteria for sense of movement on fault surfaces in brittle rocks, Journal of Structural Geology, vol. 9, no. 5, p. 597-608.

Petronis, M. S., Geissman, J. W., Oldow, J. S., and McIntosh, W. C., 2009, Late Miocene to Pliocene vertical-axis rotation attending development of the Silver Peak-Lone Mountain displacement transfer zone, west-central Nevada in Oldow, J.S., and Cashman, P.H., eds., Late Cenozoic structure and evolution of the Great Basin-Sierra Nevada transition: Geological Society of America Special Paper 447, p. 215-253, doi: 10.1130/2009.2447(12).

Proffett, J.M., 1977, Cenozoic geology of the Yerington district, Nevada, and implications for the nature and origin of Basin and Range faulting, Geological Society of America Bulletin, vol. 88, no. 2, p. 247-266.

Proffett, J.M., and Proffet, B.H., 1976, Stratigraphy of the Tertiary Ash-flow tuffs in the Yerington District, Nevada, Nevada Bureau of Mines and Geology Report 27, 28 p.

Ratcliffe, N. M., Burton, W. C., D'Angelo, R. M., and Costair, J. K., 1986, Low-angle extensional faulting, reactivated mylonites, and seismic reflection geometry of the Newark basin margin in eastern Pennsylvania, Geology, v. 14, p. 776 – 770.

Robinson, P.T., McKee, E.H., and Moiola, R.J., 1968, Cenozoic volcanism and sedimentation, Silver Peak region and adjacent California *in* Geological Society of America Memoirs, v. 116, p. 577-612.

Robinson, P.T., Stewart, J.H., Moiola, R.J., and Albers, J.P., 1976, Geologic map of the Rhyolite Ridge quadrangle, Esmeralda County, Nevada: U.S. Geological Survey, Geologic Quadrangle Map GQ-1325, scale 1:62,500.

Rosendahl, B.R., 1987, Architecture of continental rifts with special reference to East Africa, Annual Review of Earth and Planetary Sciences, v. 15, no. 1, p. 445-503.

Rosendahl, B. R., Reynolds, D. J., Lorber, P. M., Burgess, C. F., McGill, J, Scott, D., Lambiase, J. J., and Derksen, S. J., 1986, Structural expressions of rifting: lessons from Lake Tanganyika, Africa *in* Sedimentation in the African rifts: Geologic Society of London Special Publication no. 25, p. 29-43.

Ross, D.C., 1961, Geology and mineral deposits of Mineral County, Nevada, Nevada Bureau of Mines and Geology Bulletin, vol. 58, 112 p.

Ryall, A., and Priestley, K., 1975, Seismicity, secular strain, and maximum magnitude in the Excelsior Mountains area, western Nevada and eastern California, Geological Society of America Bulletin, v. 86, p. 1585-1592.

Schlische, R. W., 1992, Structural and stratigraphic development of the Newark extensional basin, eastern Northern America: Evidence for the growth of the basin and its bounding structures, Geological Society of America Bulletin, v. 104, p. 1246 – 1263.

Smith, R.L., 1960, Zones and zonal variations in welded ash-flows, U.S. Geological Survey Proffesional Paper 354-F, p. 149-159.

Snyder, W.S., Dickinson, W.R., and Silberman, M.L., 1976, Tectonic implications of space-time patterns of Cenozoic magmatism in the western United States, Earth and Planetary Science Letters, v. 32, p. 91-106.

Speed, R.C., and Cogbill, A.H., 1979a, Deep fault trough of Oligocene age, Candelaria Hills, Nevada: Summary, Geological Society of America Bulletin, v. 90, p. 145-148.

Speed, R.C., and Cogbill, A.H., 1979b, Candelaria and other left-oblique slip faults of the Candelaria region, Nevada, Geological Society of America Bulletin, v. 90, p. 149-163.

Stewart, J.H., 1979, Geologic map of Miller Mountain and Columbus quadrangles, Mineral and Esmeralda Counties, Nevada: U.S. Geological Survey, Open-File Report OF-79-1145, scale 1:24,000.

Stewart, J.H., Robinson, P.T., Albers, J.P., and Crowder, D.F., 1974, Geologic map of the Piper Peak quadrangle, Nevada-California: U.S. Geological Survey, Geologic Quadrangle Map GQ-1186, scale 1:62,500.

Stewart, J.H., Kelleher, P.C., and Zorich, E.A., 1994, Geologic map of the Monte Cristo Range area, Esmeralda and Mineral Counties, Nevada: U.S. Geological Survey, Miscellaneous Field Studies Map MF-2260, scale 1:62,500.

Stockli, D.F., Dumitru, T.A., McWilliams, M.O., and Farley, K.A., 2003, Cenozoic tectonic evolution of the White Mountains, California and Nevada, Geological Society of America Bulletin, v. 115, no. 7, p. 788-816.

Taylor, W.J., Bartley, J.M., Lux, D.R., Axen, G.J., 1989, Timing of Tertiary extension in the Railroad Valley-Pioche transect, Nevada: Constraints from $^{40}Ar/^{39}Ar$ ages of volcanic rocks, Journal of Geophysical Research, v. 94, no. 56, p. 7757-7774.

Tincher, C. R., and Stockli, D. F., 2009, Cenozoic volcanism and tectonics in the Queen Valley area, Esmeralda County, western Nevada Nevada *in* Oldow, J.S., and Cashman, P.H., eds., Late Cenozoic structure and evolution of the Great Basin-Sierra Nevada transition: Geological Society of America Special Paper 447, p. 255-274.

Twiss, R.J., and Unruh, J.R., 1998, Analysis of fault slip inversions: Do they constrain stress or strain rate?, Journal of Geophysical Research, v. 103, no. B6, p. 12205-12222.

Vreeland, J.H., and Berrong, B.H., 1979, Seismic exploration in Railroad Valley, Nevada, Rocky Mountain Association of Geologists 1979 Basin and Range Symposium, p. 556-569.

Wesnousky, S.G., 2005, Active faulting in the Walker Lane, Tectonics, v. 24, TC3009.

Whitebread, D.H., and Hardyman, R.F., 1988, Preliminary geologic map of part of the Cedar Mountains and Royston Hills, Esmeralda and Nye Counties, Nevada: U.S. Geological Survey, Open-File Report OF-87-613, scale 1:62,500.

Withjack, M.O., Islam, Q.T., and Pointe, P.R., 1995; Normal faults and their hanging-wall deformation: An experimental study, AAPG Bulletin, v. 79, no. 1, p. 1-18.

Worthington, J.E., 1992, Neogene structural and volcanic geology of the Gold Mountain-Slate Ridge area, Esmeralds County, Nevada [Ph.D. Dissertation]: Reno, The University of Nevada at Reno, 116 p.

Zoback, M. L., and Thompson, G. A., 1978, Basin and Range rifting in northern Nevada: clues from a mid-Miocene rift and its subsequent offsets, Geology, vol. 6, no. 2, p. 111-116.

Zoback, M. L., McKee, E. H., Blakely, R. J., and Thompson, G. A., 1994, The northern Nevada rift: regional tectono-magmatic relations and middle Miocene stress direction, Geological Society of America Bulletin, vol. 106, no. 3, p. 371-382.

BIOGRAPHICAL SKETCH

Scott Robertson Kerstetter was born in Richardson, Texas. Scott earned a Bachelor of Science in Geosciences from The University of Texas at Dallas in 2011. He started his graduate studies at The University of Texas at Dallas in 2012 under the advisement of Dr. John S. Oldow.

CURRICULUM VITAE

Scott Robertson Kerstetter

Education

The University of Texas at Dallas, *The Department of Geosciences*
2018 Doctor of Philosophy, Geosciences
2011 Bachelor of Science, Geosciences

Work Experience

Pioneer Natural Resources (Present)
Operations Geologist

Devon Energy Company (2017)
Geology Intern

Pioneer Natural Resources Company (2015)
Geology Intern

Gentry Petroleum Corporation/Dale Operating (2014)
Geology Intern

Teaching Experience

Structural Geology Lab (2016 – 2017)
Stratigraphy and Sedimentology Lab (2016 – 2017)

Selected Abstracts

Kerstetter, S.R., Katopody, D.T., and Oldow, J.S., 2016, Architecture, Kinematics, and Development of Widespread Late Oligocene to Early Miocene East-Northeast and West-Northwest Trending Extensional Basins during North-South Extension in the Central and Southern Walker Lane, Western Great Basin, American Geophysical Union, Fall General Assembly 2016, abstract id. T41E-2974.

Kerstetter, S.R., and Oldow, J.S., 2016, Synorogenic Deposition in an East-Northeast Trending Half-Graben during Late Oligocene to Mid-Miocene North-South Extension in West-Central Nevada, Geological Society of America Abstracts with Programs, v. 48, no. 7, doi: 10.1130/abs/2016AM-284921.

Kerstetter, S.R., Oldow, J.S., and Katopody, D.T., 2016, Mid-Miocene Synextensional Deposition during North-South Extension in a West-Northwest Trending Half-Graben in the Western Great Basin, Geological Society of America Abstracts with Programs, v. 48, no. 4, doi: 10.1130/abs/2016CD-274463.